Validation of the Gonioreflectometer

Hongsong Li
Kenneth E. Torrance

PCG-03-2 May 21, 2003

Abstract

This report describes a series of experiments conducted in the Light Measurement Laboratory of the Program of Computer Graphics in the summer of 1999 to validate the Gonioreflectometer. The Gonioreflectometer is an automated device to measure the BRDF (Bidirectional Reflectance Distribution Function) of a flat test sample. The sample is illuminated and reflected light collected at multiple preset angles of illumination and/or reflection. Light detection is at 1024 spectral bands over the visible wavelength range.

The validation experiments described herein include stray light, polarization, and detector noise and linearity tests. Further tests determined the light source and detector footprints, the instrument solid angles, and the instrument signature (i.e., instrument response when scanning the incident beam without a test sample). All parts of the instrument (including the light source, the positioning mechanism, and the detector) were carefully studied.

Many of the experiments were to explain an unexpected difficulty that was discovered: the spectral bias of recent BRDF measurements (i.e., after Foo's thesis [**1**] was completed). Extensive work showed that the error comes from the chromatic aberrations of the light source, the nonlinear response of the detector, and the background noise measurements.

Chapter 7 recommends a new method to obtain reflectance measurements with better accuracy, and which avoids the spectral bias of the light source. BRDFs are measured relative to a white reference material (Spectralon). Such a procedure is known as a

relative reflectance method, and is the preferred method for reflectance samples that are strongly diffusing.

Absolute reflectance measurements are still possible with the Gonioreflectometer, however, and may be preferred for reflectance samples with strong specular, or mirror-like, reflection behavior. For such materials, the peak reflected signal and the incident source signal might be close in magnitude. A special measurement procedure is recommended for such surfaces, and is discussed in Chapter 6.

Several samples were measured. Strongly specular reflecting materials were measured with the absolute reflectance technique (Chapter 6). The materials were a smooth gold mirror, a smooth black plastic, and a smooth blue plastic. Materials with strong directional-diffuse reflection were measured using the new relative reflectance method (Chapter 7). The materials included metals (rough steel Q-panel; two aluminum coated ground glass surfaces), nonmetals (white Spectralon), and paints (Ford metallic gray; Krylon blue; Bristol light gray).

The appendix of the report presents an alignment procedure for the Gonioreflectometer.

Table of Contents:

List of Figure Captions:

List of Table Captions:

Chapter 1

Introduction

During 1999, work was carried out to validate an optical instrument, known generically as a Gonioreflectometer, which resides in the Light Measurement Laboratory of the Program of Computer Graphics at Cornell University. The Gonioreflectometer measures the directional reflectance of a flat sample surface for visible light. Measurements are carried out for various directions of the incident light, and for various arbitrary directions of the reflected light. The visible wavelength spectrum is resolved up to 1024 wavelengths. The resulting measurements, using either absolute or relative measurement procedures, yield what is called the Bidirectional Reflectance Distribution Function (hereafter, BRDF). The present report describes a series of related experiments, recommended measurement methods, and alignment procedures.

Historically, the core instrument was donated by Eastman Kodak Company via Larry Iwan [Cornell BS'60 (EP), MS'64 (Aero)]. The donated instrument was a two-axis goniometer for holding and rotating a test sample. Sing-Choong Foo [Cornell BS'93 (EP), MEng'95 (EP), MS'97 (Arch)] added a light source, a detector, and a third axis of rotation, modifying it into an efficient, flexible, computer-controlled, and automated BRDF measurement instrument. Subsequently, Steve Westin and Eric Lafortune improved the hardware and control software. However, further work was needed for quantitative measurements. Extensive experiments were carried out by the present lead author to make sure the instrument was able to produce accurate BRDF measurements.

The first of these efforts was to duplicate Foo's measurements; results are presented in Chapter 2. Between Foo's original measurements and the present duplication, many parts of the instrument, including the solid angle of the light source and the preferred detector slit size, changed. Therefore, although the two sets of measurements were in qualitative agreement, there were quantitative differences.

The foregoing measurements and later tests revealed some problems. Among them, the most important was a spectral bias. It was observed that reflectance measurements were approximately 10% too low in magnitude at both short wavelengths (380~450nm) and long wavelengths (600nm~710nm). By extensive work, we concluded that the spectral bias comes from the error in direct light-source measurement, the nonlinear response of the detector, and the background noise measurements.

Each part of the system was systematically tested, as described in Chapters 3 to 5. For the detector (Chapter 3), we tested the background signal, the linearity, the spectrum response, the footprint, the polarization effects of the detector, and the influence of the detector slit on BRDF measurements. For the light source (Chapter 4), we examined the spectral bias by using two light sources; this turns out to be a defining experiment. We also measured the chromatic aberrations of the light source, the instrument signature, and the influence of light source and detector apertures on the instrument signature. Other possible sources of measurement error were also examined (Chapter 5), including stray light, intrinsic detector noise, polarizer effects, and a reciprocity confirmation.

In addition, as part of the testing, we measured the specular reflectance of a gold mirror and some smooth-surface plastics (which have a mirror reflection component). The positioning angular error of the Gonioreflectometer is discussed and an absolute method is proposed to improve the accuracy of the specular reflectance measurements (Chapter 6).

The absolute reflectance method may be preferred for reflecting surfaces with very-strong specular, or mirror-like, reflection behavior. For such materials, the peak reflected signal may be close in magnitude to the incident source signal; both are measured directly and the ratio calculated; subsequently, the rest of the reflected field is measured. On the other hand, when the peak reflected signal is small compared to the incident source signal, the absolute method can lead to large errors (uncertainties) in the reflected signal. This is typically the case for strongly-diffusing surfaces. For such surfaces, a relative method may be better, in which the reflected signal is measured relative to a white, diffuse reflectance standard (e.g., Spectralon).

In Sing-Choong Foo's thesis [1], he introduced methods for absolute and relative BRDF measurements. In Chapter 7, we recommend a new relative measurement method that is different from his relative method, in order to reduce the spectral bias. We applied this method on a somewhat specular, but diffusing sample (metallic paint), a less-specular, diffusing sample (Q-panel), and five diffuse samples (Spectralon, Bristol Sample#4, Krylon paints, and two ground glass samples with aluminum coatings). The best results were obtained from the diffuse samples with high diffuse reflectance. We could reduce

the integrated error to within 1% in those cases. For the slightly-specular, but diffusing samples, with a significant mirror-reflection component, we had to scan the specular direction to find the maximum BRDF and the lateral shape of the specular lobe. The small solid angle of the light source and the associated angular positioning errors necessitated dense scanning of the specular component. By combining the diffuse measurement and the specular scanning measurement, we could obtain the whole BRDF with good integrated accuracy (1%).

In conclusion, we are now able to measure the BRDF efficiently. We can measure diffuse, specular, and diffuse-specular surfaces. Due to the diversity of surfaces in the real world, it is not realistic to use a single procedure to measure all surfaces. Tentative measurements must first be carried out to reveal the magnitude of the BRDF and the reflection pattern over the hemisphere. These measurements determine the proper exposure time and hemispherical sampling positions to obtain accurate BRDF measurements. In the Appendix (due to Stephen Westin), we present a standard procedure to align the light source, detector optics, and positioning mechanism. The alignment has great influence on the accuracy and repeatability of the instrument.

Chapter 2

Duplicating Sing-Choong Foo's Measurements

We repeated several of Sing-Choong Foo's measurements and present them in this chapter. We took care to follow Foo's procedures as closely as possible, but modifications to the instrument have changed some of the results. We explain these differences in each case.

For reference, the rotational axes of the Gonioreflectometer are shown in Figure 2.1.1 and Figure 2.1.2. The unprimed coordinates are in the stationary laboratory frame, while the primed coordinates are in the sample's reference frame. Generally, θ_1(the polar angle of reflection) is the angle of Motor1; θ_2(the azimuthal angle of reflection) is the angle of Motor2; θ_3 is the angle of Motor3 (the angle between the incident light beam and $\hat{z}$). θ_3 together with θ_2 determine the polar angle of incidence. [Chapter 3.2 of Foo's thesis]

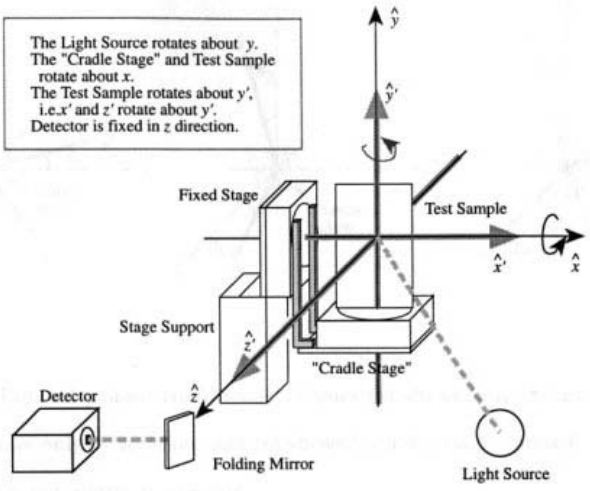

Figure 2.1.1: Coordinates setup of the Gonioreflectometer. All stages and motors are at home position (i.e. $\theta_1 = \theta_2 = \theta_3 = 0°$). [Foo's thesis Figure 3.1]

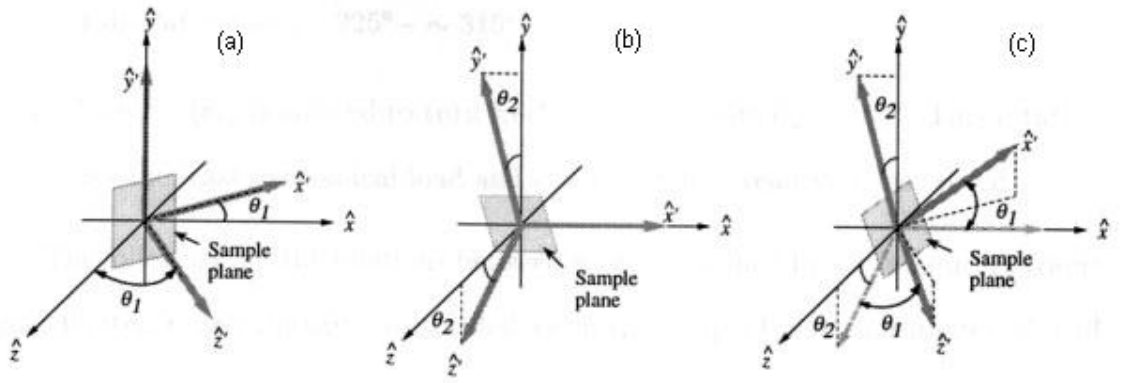

Figure 2.1.2: (a) shows the rotation of θ_2; (b) shows the rotation of θ_2; (c) shows the rotation of both θ_1 and θ_2. [Foo's thesis Figure 3.2]

In the following sections, we describe and discuss our replications of some of Foo's measurements: instrument signature (Section 2.1); specular measurements for a smooth blue plastic (Section 2.2); BRDF of Spectralon (Section 2.3); and BRDF of a blue latex paint (Section 2.4)

2.1 Measurements of the instrument signature: scanning of the incident beam in the absence of a test sample, θ_3=178 to180° (03/08/1999)

2.1.1 Background

The instrument signature is measured by scanning the incident beam in the absence of a test sample. (An alternative definition of instrument signature is to use a mirror test sample, scan the specular beam reflected from the mirror test sample, and use that as a proxy for the incident beam.) The signature curve comes from the convolution of the detector aperture with the source beam, so called "aperture convolution." (Apertures are sketched in Figure 4.3.1 and Figure 4.3.2 and will be discussed later.) Foo measured the

instrument signature, as presented in Figure 9.1 of his thesis and Figure 2.1.2 here. The same experiment was repeated and the duplicated result is presented in Figure 2.1.3.

2.1.2 Procedures

The experimental setup is shown in Figure 2.1.1. No sample was mounted during the measurement. In this procedure, the light source is directly aimed toward the detector via the folding mirror. The instrument signature is measured by scanning the incident light source beam across the detector, by rotating Motor 3 or equivalently θ_3.

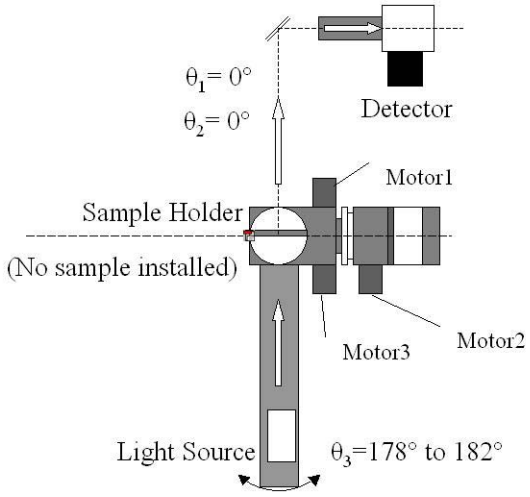

Figure 2.1.1: Experimental setup as viewed from above

a. Turn the light source on, wait to let the system reach steady state;
b. Rotate control motors, make θ_1=0°, θ_2=0°, θ_3=180° (Under these conditions the detector views the light source by looking directly through the nominal sample location);
c. Measure the direct signal at s polarization;
d. Measure the direct signal at p polarization;

e. Rotate Motor 3 from 178° to 182°, 0.1° per step, record the direct signal, exposure time is 1, at s polarization;

f. Repeat step e at p polarization;

g. Measurement the background signal at exposure time 1;

h. Ratio the measurements in e and c, and f and d, and average.

2.1.3 Measurement results

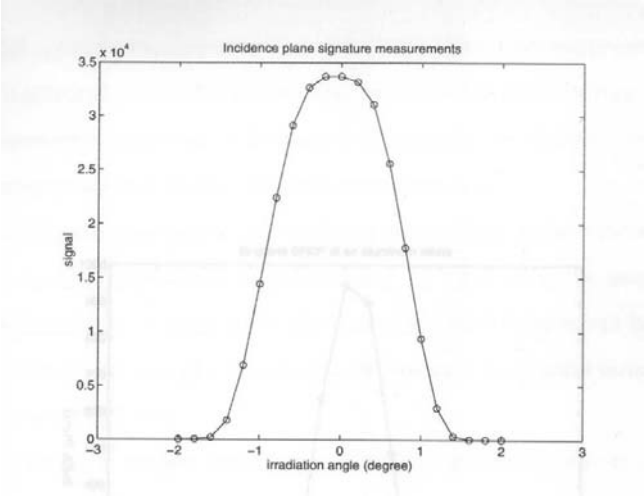

Figure 2.1.2: The signature as measured by Foo with the light source moving from θ_3=178° to 182°, without a test sample. λ=650nm. The broadened peak shows the effect of aperture convolution since the detector has a finite aperture (of about 1° in width) as it crosses the incident beam (which has a width of about 2°). [Foo's thesis Figure 9.1]

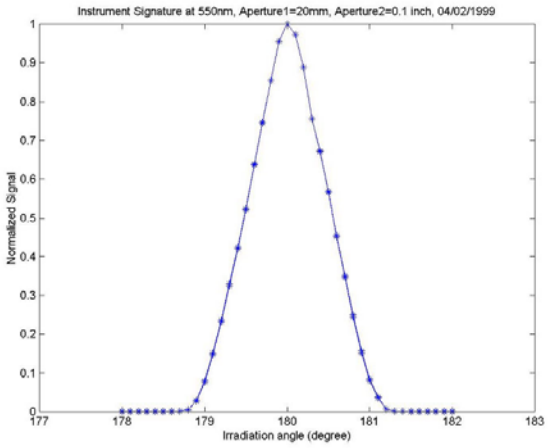

Figure 2.1.3: Duplicated measurements at λ=500nm, normalized curve. The detector aperture is about 1° as it crosses the incident beam (also about 1° in width).

2.1.4 Comments

The new instrument signature is different from Foo's early measurement. The difference is mainly due to better matching of source and detector solid angles. The detector solid angle is determined by the diameter of the iris between the polarizer and the achromatic doublet of the detector assembly (shown in Figure 4.3.1). The light source solid angle is determined by the diameter of the iris between the Nikkor lens and the aspheric lens of the light source (shown in Figure 4.3.2). The new measurement shows the instrument signature when the detector aperture is 20mm and the light source aperture is 2.5mm (0.1 inch). The nearly triangular shape of the signature in Figure 2.1.3 implies that the solid angles of the detector and light source are very close in size.

Another later experiment showed that the instrument signature is strongly related to the detector aperture (Aperture1) and the light source aperture (Aperture2). Please refer to Section 4.3, *Influence of light source and detector apertures on instrument signature and BRDF measurements of Spectralon at 0/45 (04/02/1999)*.

The ordinate in Figure 2.1.3 is the normalized polarization-averaged incident light. Actually, this measurement is not sensitive to polarization, so a fast check can be made. It is acceptable to measure only the incident light at one polarization and to normalize it without subtracting the background signal. The results should be the same.

It is recommended that the instrument signature be measured and recorded whenever the detector aperture or the light source aperture is changed.

2.1.5 Matlab Script

```
%This function is used to plot Instrument Signature
%The 123 file is Sig.123
%The exposure time is 1.
%by Hongsong Li
%04/02/1999
clear
% Reads the raw data files with measurements and exposure times of the
% background, the direct source, and the measurements.
[exposure_b,background]    = readfile(['Bkg.dat']);
[exposure_u,direct_v]      = readfile(['Directv.dat']);
[exposure_n,direct_h]      = readfile(['Directh.dat']);
[exposure_v,measurement_v] = readfile(['Measv.dat']);
[exposure_h,measurement_h] = readfile(['Meash.dat']);

%load vhbias[1024]
load vhbias.mat

%Locate signal data of 650nm
sample550=517;

%Get average direct signal of vertical and horizonal polarization
temp=(direct_v(sample550)/vhbias(sample550)+direct_h(sample550))/2.0-
background(sample550,1)
%Get Normalized Signal of Different Angles
for i=1:41,
    y(i)=((measurement_h(sample550,i)+measurement_v(sample550,i)/vhbias(sample55
0))/2.0-background(sample550,1));
    y(i)=y(i)/temp;
end;

%plot the Instrument Signature
x=[178:0.1:182]
plot(x,y,'*-'), hold on
axis([177,183,0,1])
xlabel 'Irradiation angle (degree)'
ylabel 'Normalized Signal'
title 'Instrument Signature at 550nm, Aperture1=20mm, Aperture2=0.1 inch,

04/02/1999'
```

2.2 Specular reflectance of a blue plastic at an incidence angle of 45°, over visible wavelengths (03/25/1999)

2.2.1 Background

In Foo's thesis, he presented specular reflectance measurements for a 5-inch by 5-inch square blue plastic sample. The measurements were obtained with both the Gonioreflectometer and an Optronics OL740-75M specular reflectometer, at an incidence angle of 45°. The sample is smooth, shiny, and very stable. The results are shown in Figure 2.2.2. The specular reflectance at 45° was measured again with the Gonioreflectometer on March 25, 1999 using the setup shown in Figure 2.2.1. The duplicated results are presented in Figure 2.2.3.

2.2.2 Procedures

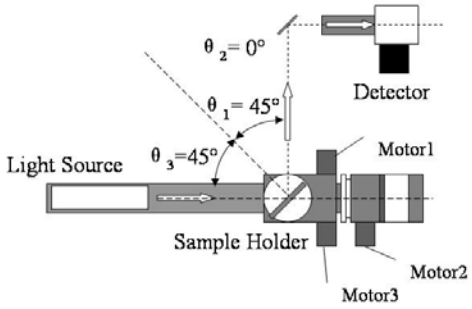

Figure 2.2.1 Experimental setup as viewed from above

a. Measure the background noise, save the data into bkg.dat;

b. Turn Motor 3 to $\theta_3 = 180°$, take the sample off the sample mount;

c. Put a polarizer in front of the light source, set its polarization direction to vertical; set the polarizer in front of the detector to vertical; measure the s polarization direct signal, exposure time is 10; save the data into Directv.dat;

d. Put the blue plastic on the sample mount;

e. Turn the Motor 3 to $\theta_3 = 90°$;

f. Turn the Motor 1 to $\theta_1 = 45°$;

g. Measure the s polarization reflection signal, save the data into plast_v.dat;

h. Set the polarizer in front of the light source to horizontal; set the polarizer in front of the detector to horizontal; measure the p polarization reflection signal, exposure time is 10; save the data into plast_h.dat;

i. Turn Motor 3 to $\theta_3 = 180°$;

j. Turn Motor 1 to $\theta_1 = 0°$;

k. Take the sample off the sample mount;

l. Measure the p polarization direct signal, save the data into Directh.dat.

2.2.3 Measurement results

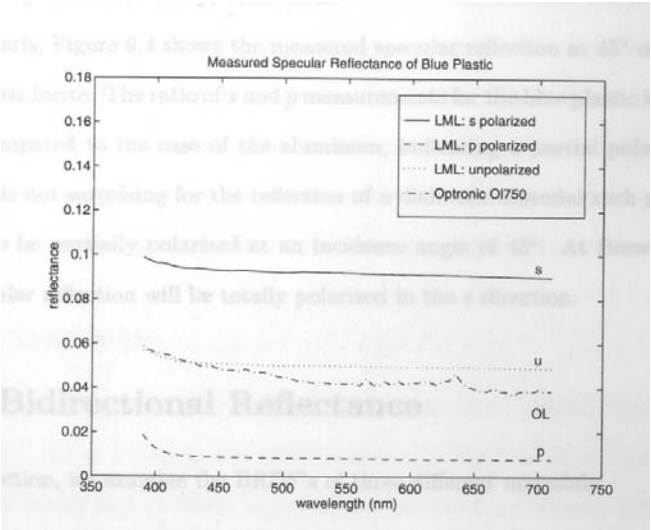

Figure 2.2.2: Comparison of polarized specular reflection of a blue plastic at an incidence angle of 45°, as measured by Foo with the Optronics OL740-75M specular reflectometer and the Gonioreflectometer. The measurements made by the Optronics OL740-75M have not been adjusted for polarization bias in that instrument. [Foo's thesis Fig. 9.4]

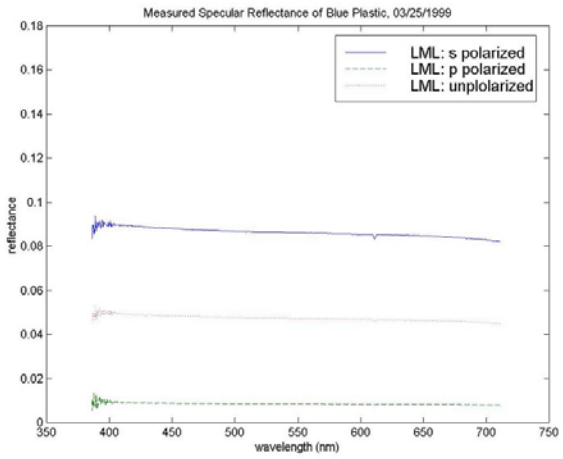

Figure 2.2.3: Specular reflectance of blue plastic, as measured with the Gonioreflectometer (3/25/1999)

2.2.4 Comments

The duplicated measurement is close to, but slightly lower than, Foo's measurement. The average difference is about 5-8%, which is at the design level of repeatability of the instrument. No significant differences are observed, except that the duplicated measurement has a stronger signal noise at short wavelengths. Compared to the magnitude of the specular reflectance, the magnitude of the noise is negligible.

For plastic, the specular component of reflection arises from mirror reflection at the smooth, polished surface of the plastic. The amount of mirror reflection depends on the index of refraction of the plastic. For a dielectric material like the blue plastic, the index of refraction is about 1.48, and is nearly constant over the visible wavelength range. Since the index is constant, the specular reflectance is also nearly constant over the visible wavelength range (see Figure 2.2.2 and Figure 2.2.3). The diffuse color of the plastic arises from sub-surface scattering within the plastic, and is of such a low radiance in the specular direction that it essentially does not appear in the figures.

2.2.5 Matlab Script

```
%This function is used to plot Specular reflection of blue plastic
%polarized specular relection of a blue plastics at an incidence
%angle of 45 degree, measured with our Gonioreflectometer
%A polarizer is inserted in front of the light source to obtain polarized
%incidence light, both in s and p directions.
%theta_1=45 theta_3=90
%This graph is used to compare with Foo's Fig.  9.4
%1999.03.25

clear
% Reads the raw data files with measurements and exposure times of the
% background, the direct source, and the measurements.
[exposure_b,background]    = readfile(['Bkg.dat']);

[exposure_u,direct_v]      = readfile(['Directv.dat']);
[exposure_n,direct_h]      = readfile(['Directh.dat']);

[exposure_v,measurement_v] = readfile(['plast_v.dat']);
[exposure_h,measurement_h] = readfile(['plast_h.dat']);

for i=1:1024,
      yv(i)= ((measurement_v(i)-background(i,3))/exposure_v)/(direct_v(i)-background(i,1));
      yh(i)= ((measurement_h(i)-background(i,3))/exposure_h)/(direct_h(i)-background(i,1));
end;

x=[386:(325/1023):711];
plot(x,yv,'-',x,yh,'--',x,0.5*(yv+yh),':')
legend('LML: s polarized','LML: p polarized','LML: unplolarized')
axis([350 750 0 0.18])
title 'Measured Specular Reflectance of Blue Plastic, 03/25/1999'
xlabel 'wavelength (nm)'
ylabel 'reflectance'
```

2.3 BRDF measurements of Spectralon (03/08/1999)

2.3.1 Background

The Spectralon reflectance material is a thermoplastic resin that can be machined into a wide variety of shapes for the construction of optical components. In the Light Measurement Lab at Cornell, we have a 5-inch by 5-inch square Spectralon sample and a small Spectralon sample that is used as a reference surface with the Optronics OL-750 reflectometer. The Spectralon reflectance material has the highest diffuse reflectance of any known material or coating over the UV-VIS-NIR region of the spectrum. The hemispherical reflectance is generally larger than 99% over the range from 400-1500 nm and is larger than 95% from 250-2500 nm. Surface or subsurface contamination may lower the reflectance at the extreme upper and lower ends of the spectral range. The material is also very Lambertian (i.e., ideal diffuse) at wavelengths from 0.257 μm to 10.6μm.

Foo carried out incidence-plane BRDF measurements of a Spectralon reference sample and the results were presented in his thesis. There were two experiments:

a. BRDF measurements of Spectralon over the visible spectrum at normal incidence (θ_i=0°, φ_i=0°) and a fixed angle of reflection (θ_r=45°, φ_r=180);
b. BRDF measurements of Spectralon in the incidence plane, at one wavelength (633nm), at two fixed angles of incidence (30° and 60°), and at various angles of reflection (-90° to 90°).

Similar BRDF measurements were carried out by the manufacturer of the Spectralon sample (Labsphere) [2] and by RIT [3] on other Spectralon samples. Their results were plotted with Foo's results in his thesis, to verify that the Gonioreflectometer produced correct measurements.

The two experiments above were duplicated here and the results are presented.

2.3.2 Procedures

A. BRDF measurements of Spectralon at 0/45 over the visible wavelength range

a. Measure the background noise signal, save the data into bkg.dat;

b. Turn the Motor 3 to $\theta_3 = 180°$, take the sample off the sample mount;

c. Set the polarizer in front of the detector to vertical position, and measure the s polarization direct signal, save the data into Directv.dat;

d. Set the polarizer in front of the detector to horizontal position, and measure the p polarization direct signal, save the data into Directh.dat;

e. Turn the Motor 3 to $\theta_3 = 45°$;

f. Turn the Motor 1 to $\theta_1 = 45°$;

g. Put the Spectralon sample on the sample mount;

h. Set the polarizer in front of the detector to vertical position, and measure the s polarization reflection signal, exposure time is 500, save the data into Meas_v.dat;

i. Set the polarizer in front of the detector to horizontal position, and measure the p polarization reflection signal, exposure time is 500, save the data into Meas_h.dat.

Procedure A produced BRDF measurements of Spectralon at 0/45. The experimental setup is shown in Figure 2.3.1. The measured results appear in Figure 2.3.4.

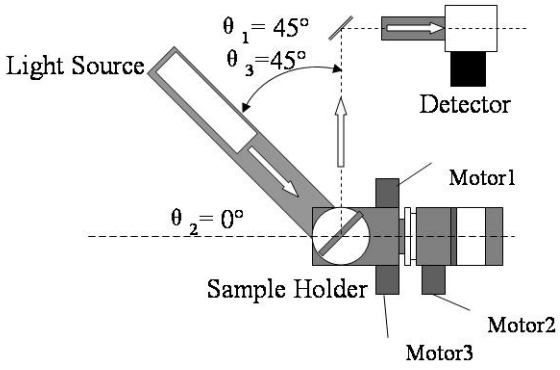

Figure 2.3.1: Experimental setup as viewed from above; BRDF measurements for the Spectralon at 0/45 (normal incidence; 45° reflection angle).

B. BRDF measurements of Spectralon in the incidence plane at θ_i = 30° or θ_i = 60°, incident light source of p polarization, 633nm wavelength

a. Measure the background noise, save the data into bkg.dat;

b. Turn Motor 3 to $\theta_3 = 180°$, $\theta_1 = 0°$, take the sample off the sample mount;

c. Put a polarizer in front of the light source, set its polarization direction to horizontal, set the polarizer in front of the detector to horizontal, and measure the p polarization direct signal, save the data into Directh.dat;

d. Put the Spectralon sample on the sample mount;

e. Set the polarizer in front of the detector to vertical, and measure the s polarization reflection signal in the incidence plane, save the data into Measv.dat, exposure time is 500;

f. Set the polarizer in front of the detector to horizontal, and measure the p polarization reflection signal in the incidence plane, save the data into Meash.dat, exposure time is 500.

Procedure B produced BRDF measurements of Spectralon in the incidence plane. Figure 2.3.2 shows the experimental setup. To keep θ_i=30°, the angle between the light source arm and the normal of the sample is kept at 30°. Similar procedures are used for θ_i=60°. The angle of reflection is varied by rotating the light source arm and the sample. The measured results appear in Figure 2.3.6 and Figure 2.3.8.

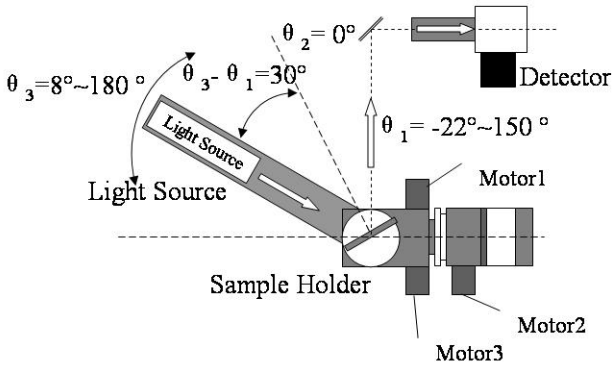

Figure 2.3.2: Experimental setup as viewed from above; BRDF measurements of Spectralon in the incidence plane; shown for θ_i = 30°.

2.3.3 Measurement results

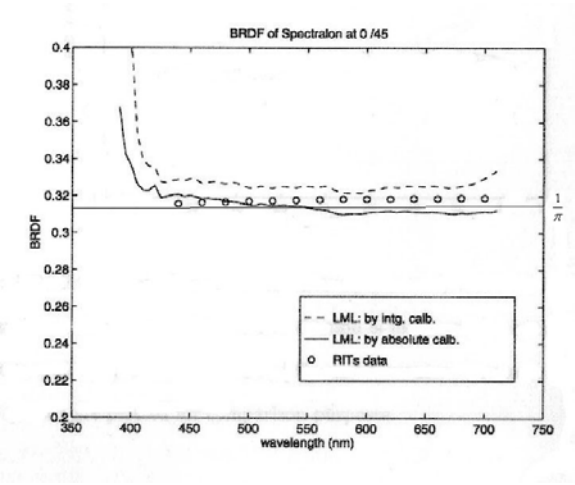

Figure 2.3.3: Measured BRDF (unpolarized) by Foo of the Spectralon sample with source incident at θ_r=0°, φ_r=0°, and view direction at θ_r=45°, φ_r=180°. BRDFs obtained by absolute calibration (abs.) and diffuse reference calibration (intg.) are shown. For the detail of these calibration methods, refer to Chapter 8 of Foo's thesis. Measured data published by RIT are plotted as circles. [Foo's thesis Fig. 9.5]

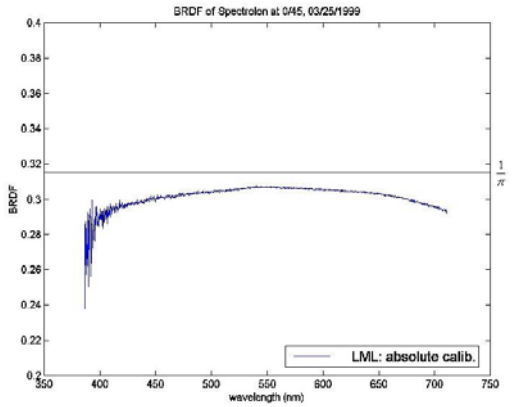

Figure 2.3.4: Duplicated measurements of Foo's thesis Fig. 9.5; BRDF measurements of the Spectralon sample at 0/45

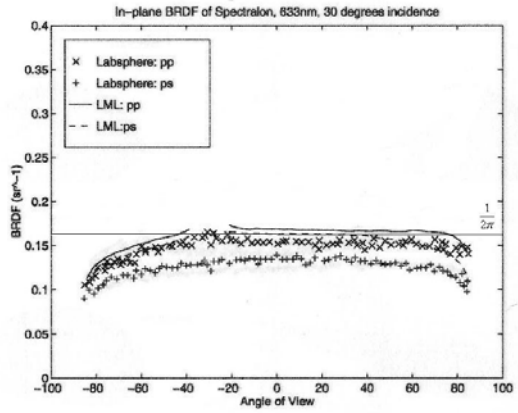

Figure 2.3.5: BRDF of the Spectralon sample as measured by Foo in the incidence plane with $\theta_i = 30°$ for an incident light source of *p* polarization, 633nm wavelength. The reflection is measured for both *s* and *p* polarizations. Data published by Labsphere [2], and measurements made by the Gonioreflectometer (LML) are plotted for comparison purposes. [Foo's thesis Fig. 9.6]

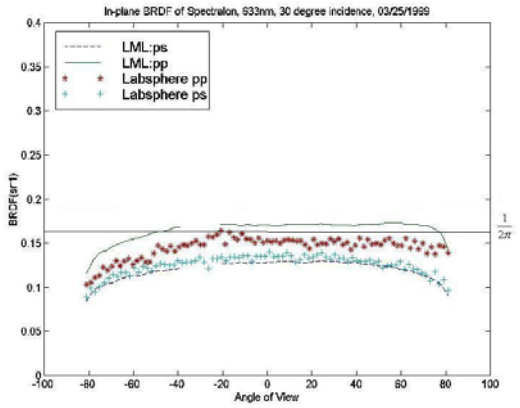

Figure 2.3.6: Duplicated measurement of Foo's thesis Fig.9.6; BRDF measurements of the Spectralon sample in the incidence plane at $\theta_i = 30°$; λ=633nm

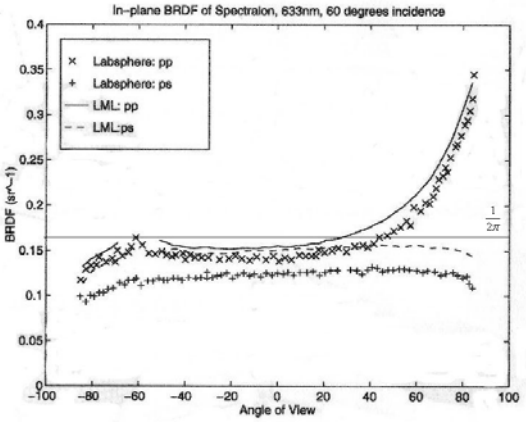

Figure 2.3.7: BRDF of the Spectralon sample as measured by Foo in the incidence plane with $\theta_i = 60°$ for an incident light source with *p* polarization, 633nm wavelength. The reflection is measured for both *s* and *p* polarizations. Data published by Labsphere [2], and measurements made by the Gonioreflectometer (LML) are plotted. [Foo's thesis Fig. 9.7]

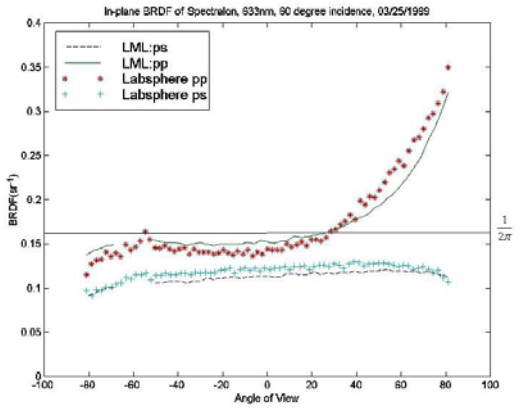

Figure 2.3.8: Duplicated measurement of Foo's thesis Fig. 9.7; BRDF measurements of the Spectralon sample in the incidence plane at $\theta_i = 60°$; λ=633nm

2.3.4 Comments

For reference purposes, in Figure 2.3.3 to Figure 2.3.8 horizontal lines are shown which correspond to ideal diffuse reflection from a perfect, white, 100% reflecting surface. The BRDF for such a surface is $1/\pi$, and for the polarization components, $1/2\pi$.

Figure 2.3.3 and Figure 2.3.4 illustrate the apparent differences among Foo's result, the RIT result, and the presently duplicated results for 0/45 BRDF data. The 0/45 directional BRDF data can, of course, fall above or below the reference line of $1/\pi$ if the surface is not ideal diffuse. The RIT measurements in Figure 2.3.3 appear to be the most plausible because the Spectralon sample is expected to have a neutral spectral reflectance, and that behavior is shown by the RIT data. Foo used two calibration methods, absolute calibration and integrated calibration. For both calibration methods, his results are close to the RIT results, except at short wavelengths (380 to 420nm). The presently duplicated measurements, Figure 2.3.4, use the integrated calibration method to obtain the BRDF. The duplicated result shows that reflectance measurements were approximately 10% too low, at both short wavelengths (380~450nm) and long wavelengths (600nm~710nm).

In Section 4.1, the spectral bias of the BRDF measurements is discussed in detail. The new results reveal magnitude and spectral errors, which led to the present extensive study of the spectral bias and angular error of the Gonioreflectometer. The final recommended measurement method, described in Chapter 7, corrects for those errors.

Figure 2.3.5 and Figure 2.3.7 show Foo's BRDF measurements of the Spectralon sample vs. angle of reflection in the incidence plane, for θ_i = 30° and 60°, respectively. Data published by Labsphere are also plotted, as are the $1/2\pi$ reference lines for an ideal, white, diffuse surface.

Figure 2.3.6 and Figure 2.3.8 show the presently duplicated measurements and the Labsphere data, for θ_i = 30° and 60°, respectively. The duplicated measurements are in better agreement with the Labsphere data than Foo's measurements, for both angles of incidence. The reflectance measurements at ps polarization were improved significantly.

One possible source of discrepancies in the present measurements is changes in the sample itself. Though carefully kept, the surface of a Spectralon sample can be contaminated. The manufacturer recommends that the surfaces be cleaned and the high reflectance be restored by sanding the surface. After sanding our 5-inch Spectralon sample, we found that the diffuse reflectance was increased by 1%. Keeping the sample in the cabinet in the laboratory is highly recommended. Another way to clean the

Spectralon sample is to heat the sample in a vacuum oven. This operation can remove the dust absorbed into the subsurface. We have not taken this step.

Another possible source of discrepancies is the surface roughness of the Spectralon sample. Our sample may have a smaller surface roughness. The smoother surface can make the *pp* curve in the present measurement (Figure 2.3.6 and Figure 2.3.8) higher than Labsphere's result.

In summary, the present measurements suggest a spectral bias in the current instrument (Figure 2.3.4), but reasonably good directional measurements (Figure 2.3.6 and Figure 2.3.8), when data are compared with reference measurements. The latter conclusion regarding directional measurements may be considered as general; nevertheless, the directional measurements were carried out at a wavelength of 633nm, a region where the effects of the spectral bias are minimal.

2.3.5 Matlab Script

A. BRDF measurements of Spectralon at 0/45, over the visible wavelength range

```
%This function is used to plot bidirectional reflectance of
%Spectralon at an incidence angle of 0 degree, measured with
%our Gonioreflectometer
%theta_i = 0
%theta_r = 45
%This graph is used to compare with Foo's Fig. 9.5
%1999.02.25

clear
% Reads the raw data files with measurements and exposure times of the
% background, the direct source, and the measurements.
[exposure_b,background]    = readfile(['bkg.dat']);
[exposure_u,direct_v]      = readfile(['directv.dat']);
[exposure_n,direct_h]      = readfile(['directh.dat']);
[exposure_v,measurement_v] = readfile(['meas_v.dat']);
[exposure_h,measurement_h] = readfile(['meas_h.dat']);

%load vhbias[1024]
load vhbias.mat

%Solid Angle
SolidAngle = 5.537e-004

%Calculate the bidirectional reflectance
for i=1:1024,
      V0(i)= 0.5*((direct_v(i)-background(i,1))/vhbias(i)+(direct_h(i)-background(i,1)));
  Vn(i)= 0.5*((measurement_v(i)-background(i,6))/(vhbias(i)*exposure_v)+(measurement_h(i)-
background(i,6))/exposure_h);
  fr(i)=Vn(i)/(V0(i)*SolidAngle);
end;

%plot
x=[386:(325/1023):711]
plot(x,fr,'-')
legend('LML: absolute calib.',4)
axis([350 750 0.2 0.4])
title 'BRDF of Spectrolon at 0/45, 03/25/1999'
xlabel 'wavelength (nm)'
ylabel 'BRDF'
```

B. BRDF measurements of Spectralon in the incidence plane at either θ_i = 30° or θ_i = 60°, incidence light source of p polarization, 633nm wavelength

```
%This function is used to plot BRDF of Spectralon
%at an incidence angle of 30 degree, measured with
%our Gonioreflectometer.
%A polarizer is inserted in front of the light source to obtain p
%polarized incidence light.
%wavelength = 633nm
```

```
%theta_i = 30
%theta_r ranges from -81 to 81
%This graph is used to compare with Foo's Fig. 9.6
%Its 123 file is fig96.123
%1999.03.25

clear

% Reads the raw data files with measurements and exposure times of the
% background, the direct source, and the measurements.
[exposure_b,background]    = readfile(['bkg.dat']);
[exposure_p,direct_p]      = readfile(['directh.dat']);
[exposure_v,measurement_v] = readfile(['measvp.dat']);
[exposure_h,measurement_h] = readfile(['meashp.dat']);

%load vhbias[1024]
load vhbias.mat
load Spectralon_labsphere.mat

%Solid Angle
SolidAngle = 3.5735e-004

%Locate signal data of 633nm
wv633=778

%Calculate the BRDF in both p and s polarization
%To deal with the hole in the curve,
%I divided the curve into two pieces
for i=1:15,
      ps1(i)= ((measurement_v(wv633,i)-background(wv633,6))/exposure_v(i))/(direct_p(wv633)-
background(wv633,6))/cos(pi/6)/SolidAngle;
      pp1(i)= ((measurement_h(wv633,i)-background(wv633,6))/exposure_v(i))/(direct_p(wv633)-
background(wv633,6))/cos(pi/6)/SolidAngle;
end;
for i=1:35,
      ps2(i)= ((measurement_v(wv633,i+15)-background(wv633,6))/exposure_v(i))/(direct_p(wv633)-
background(wv633,6))/cos(pi/6)/SolidAngle;
      pp2(i)= ((measurement_h(wv633,i+15)-background(wv633,6))/exposure_v(i))/(direct_p(wv633)-
background(wv633,6))/cos(pi/6)/SolidAngle;
end;

%plot
x1=[-81:3:-39];
x2=[-21:3:81];
x3=[-81:(162/86):81];
x4=[-81:(162/83):81];
plot(x1,ps1,'--',x1,pp1,'-',x3,Lpp_corrected,'*',x4,Lps_corrected,'+'), hold on
legend('LML:ps','LML:pp','Labsphere pp','Labsphere ps',2),hold on
plot(x2,ps2,'--',x2,pp2,'-');
axis([-100 100 0 0.4]);
xlabel 'Angle of View';
ylabel 'BRDF(sr^-1)';
title 'In-plane BRDF of Spectralon, 633nm, 30 degree incidence, 03/25/1999';
```

2.4 BRDF measurements of blue latex paint in the incidence plane (03/23/1999)

2.4.1 Background

The in-plane BRDF of a blue latex paint sample (Pratt & Lambert, Vapex Interior Wall Base I, color #1243 Cal. III.) was measured. The paint ages with time. Therefore, we expect that the optical properties can change. Although the present BRDF measurements are expected to differ from Foo's, the results turn out to be reasonably close.

The blue latex paint sample is a wood panel with blue paint applied to it. The BRDF of the blue latex paint was measured by Foo at incidence angles of θ_i = 55°, 65° and 75° in the incidence plane, while the angle of reflection θ_r varied from -63° to 81°, with λ=550nm (as shown in Figure 9.10 of Foo's thesis and Figure 2.4.2 here). Moreover, the BRDF of the blue latex paint at different wavelengths, λ=450, 550, 650nm, was also obtained, in the incidence plane at θ_i =75° (as shown in Fig. 9.11 of Foo's thesis and Figure 2.4.4 here). The aforementioned measurements were duplicated for this report and are shown in Figure 2.4.3 and Figure 2.4.5.

2.4.2 Procedures

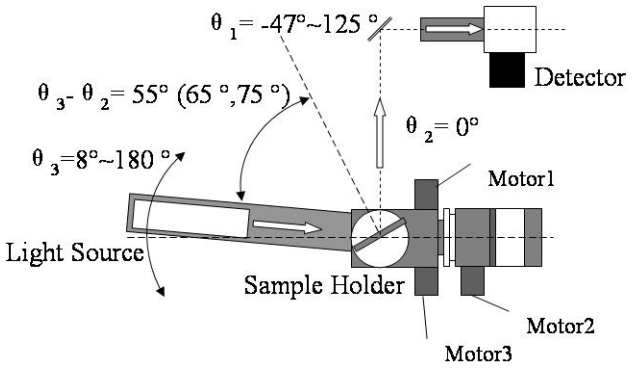

Figure 2.4.1: Experimental setup as viewed from above

a. Measure the background noise, save the data into bkg.dat;

b. Turn the Motor 3 to $\theta_3 = 180°$, take the sample off the sample mount;

c. Set the polarizer in front of the detector to vertical, and measure the s polarization direct signal, save the data into Directv.dat;

d. Set the polarizer in front of the detector to horizontal, measure the p polarization direct signal, save the data into Directh.dat;

e. Put the blue latex paint sample on the sample mount;

f. Set the polarizer in front of the detector to vertical; measure the s polarization reflection signal for incidence angle 55°, in the incidence plane, with 500 units exposure time; save the data into Meas55v.dat;

g. Set the polarizer in front of the detector to horizontal; measure the p polarization reflection signal for incidence angle 55°, in the incidence plane, with 500 units exposure time; save the data into Meas55h.dat;

h. Repeat step 5 and 6, measure the polarized reflection signal in both polarization for incidence angle 65° and 75°; the measurement results are stored in Meas65h.dat, Meas65v.dat, Meas75h.dat, Meas75h.dat.

2.4.3 Measurement results

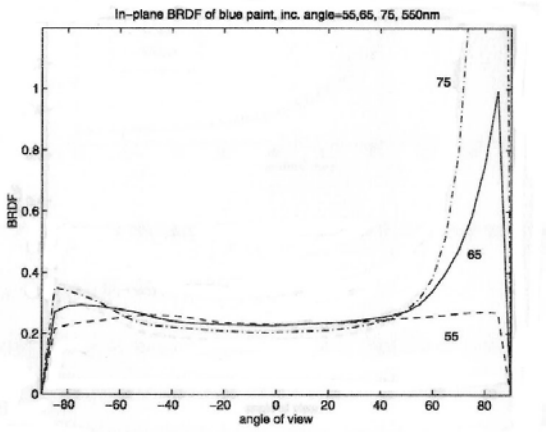

Figure 2.4.2: BRDF of the blue latex paint as measured by Foo in the incidence plane; θ_i = 55°, 65°, 75°; λ=550nm. The forward scattering increases as the incidence angle increases. [Figure 9.10 of Foo's thesis]

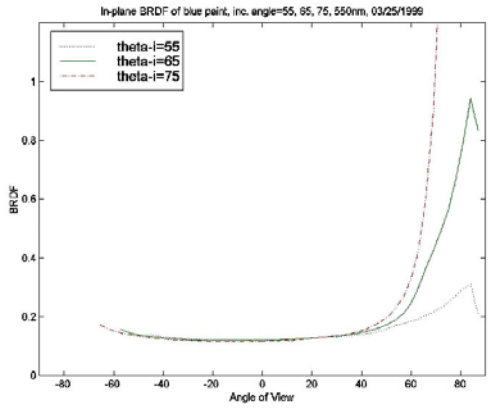

Figure 2.4.3: Duplicated measurement. BRDF of the blue latex paint in the incidence plane; θ_i = 55°, 65°, 75°; λ=550nm

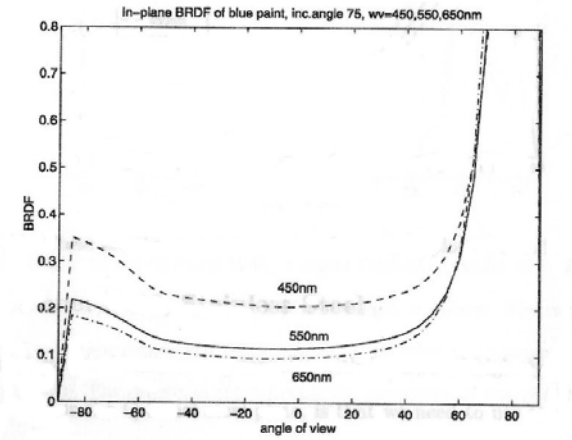

Figure 2.4.4: BRDF of the blue paint as measured by Foo in the incidence plane at θ_i = 75; λ=450, 550, 650nm. The forward scattering increases as wavelength increases but the diffuse part is dominated by the "color" of the paint. [Figure 9.11 of Foo's thesis]

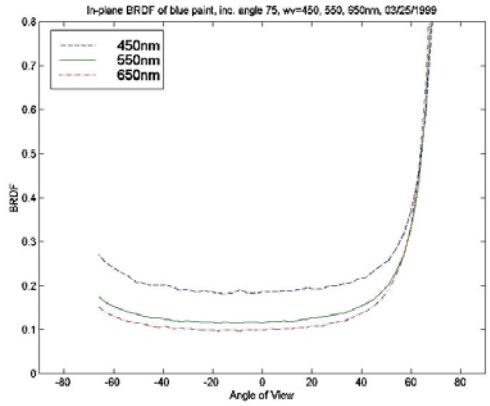

Figure 2.4.5: Duplicated measurement. BRDF of the blue latex paint in the incidence plane at θ_i =75°; λ=450, 550, 650nm

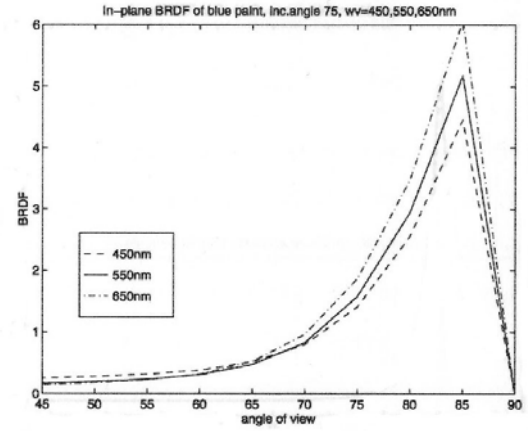

Figure 2.4.6: Figure 9.12 of Foo's thesis; same as Figure 2.4.4 here but on an expanded vertical scale

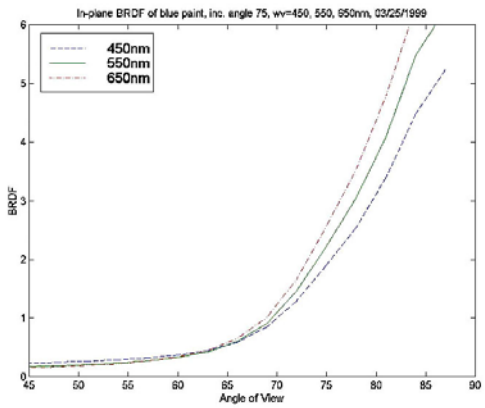

Figure 2.4.7: Duplicated measurement; same as Figure 2.4.5 here but on an expanded vertical scale.

2.4.4 Comments

The duplicated measurements of the directional reflectance of the blue paint sample are close to Foo's measurements. The agreement is reasonable, since the latex paint BRDF can change slightly with time, and can vary over the surface.

Foo obtained measurements at grazing angles of reflection by adding extra optics. The maximum reflection angle in the duplicated measurements is generally less than 87°.

2.4.5 Matlab Script

```
%This function is used to plot measured BRDF of the blue latex
%paint at theta_i = 55□, 65□, 75□, in the incidence plane.
%theta_r = -63~81□
%wavelength = 550nm
%This graph is used to compare with Foo's Fig.  9.10
%Its 123 file is Blue55.123,Blue65.123,Blue75.123.
%1999.03.25

clear

% Reads the raw data files with measurements and exposure times of the
% background, the direct source, and the measurements.
[exposure_b,background]    = readfile(['bkg.dat']);
[exposure_dv,direct_v]     = readfile(['directv.dat']);
[exposure_dh,direct_h]     = readfile(['directh.dat']);
[exposure55_v,measure55_v] = readfile(['meas55v.dat']);
[exposure55_h,measure55_h] = readfile(['meas55h.dat']);
[exposure65_v,measure65_v] = readfile(['meas65v.dat']);
[exposure65_h,measure65_h] = readfile(['meas65h.dat']);
[exposure75_v,measure75_v] = readfile(['meas75v.dat']);
[exposure75_h,measure75_h] = readfile(['meas75h.dat']);

%load vhbias[1024]
load vhbias.mat

%Locate signal data of 650nm
wv550=517

%Solid Angle
SolidAngel = 3.5735e-004

%Calculate unpolarized direct signal
Direct=0.5*((direct_v(wv550)-background(wv550,1))/(vhbias(wv550))+(direct_h(wv550)-
background(wv550,1)))

%Calculate unpolarized measurement signal
%To deal with the hole in the curve,
%I divided the curve into two pieces
for i=1:7,
  Vn55_1(i)=0.5*((measure55_v(wv550,i)-background(wv550,6))/(vhbias(wv550)*
exposure55_v(i))+(measure55_h(wv550,i)-background(wv550,6))/exposure55_h(i));
  Vn55_1(i)=Vn55_1(i)/Direct/cos(55*pi/180)/SolidAngel;
end;

for i=1:45,
  Vn55_2(i)=0.5*((measure55_v(wv550,i+7)-background(wv550,6))/(vhbias(wv550)*
exposure55_v(i+7))+(measure55_h(wv550,i+7)-background(wv550,6))/exposure55_h(i+7));
  Vn55_2(i)=Vn55_2(i)/Direct/cos(55*pi/180)/SolidAngel;
end;


for i=1:3,
```

```
  Vn65_1(i)=0.5*((measure65_v(wv550,i)-background(wv550,6))/(vhbias(wv550)*
exposure65_v(i))+(measure65_h(wv550,i)-background(wv550,6))/exposure65_h(i));
  Vn65_1(i)=Vn65_1(i)/Direct/cos(65*pi/180)/SolidAngel;
end;

for i=1:49,
  Vn65_2(i)=0.5*((measure65_v(wv550,i+3)-background(wv550,6))/(vhbias(wv550)*
exposure65_v(i+3))+(measure65_h(wv550,i+3)-background(wv550,6))/exposure65_h(i+3));
  Vn65_2(i)=Vn65_2(i)/Direct/cos(65*pi/180)/SolidAngel;
end;


for i=1:52,
  Vn75(i)=0.5*((measure75_v(wv550,i)-background(wv550,6))/(vhbias(wv550)*
exposure75_v(i))+(measure75_h(wv550,i)-background(wv550,6))/exposure75_h(i));
  Vn75(i)=Vn75(i)/Direct/cos(75*pi/180)/SolidAngel;
end;

%plot
x55_1=[-81:3:-63]
x55_2=[-45:3:87]
x65_1=[-81:3:-75]
x65_2=[-57:3:87]
x75=[-66:3:87]

plot(x55_1,Vn55_1,':',x65_1,Vn65_1,'-')
plot(x55_2,Vn55_2,':',x65_2,Vn65_2,'-',x75,Vn75,'-.')
legend('theta-i=55','theta-i=65','theta-i=75',2)

xlabel 'Angle of View'
ylabel 'BRDF'
title 'In-plane BRDF of blue paint, inc. angle=55, 65, 75, 550nm, 03/25/1999'
axis([-90,90,0,1.2])
```

Chapter 3:

Validation of the Gonioreflectometer: The Detector

Foo's thesis describes the detailed design of the Gonioreflectometer, including the light source, the sample positioning mechanism, and the detector. However, the lately discovered spectral bias cannot be explained by his thesis. Therefore, a series of experiments was designed and carried out to systematically test each part of the Gonioreflectometer. In chapters 3 to 5, we present these experiments and discuss the results.

Chapter 3 focuses on the detector. We tested the background noise (Section 3.1), the linearity of the detector response (Section 3.2 and Section 3.3), the spectrum response (Section 3.4), the footprint (Section 3.5), the polarization bias (Section 3.6), and the influence of the slit size (Section 3.7). These experiments provide information on the characteristics of the Gonio detector. First, the thermoelectric cooling device needs more than 30 minutes to allow the detector to reach a steady low temperature. Second, the detector response to the incident light intensity is linear within the dynamic range of the detector, except at very low intensities (about 20 counts). Third, the optimal size of the detector slit is 0.28mm. These facts help us to identify the source of the experimental uncertainties and to improve the measurement procedures.

Chapter 4 focuses on the light source. The BRDF of Spectralon was measured with the Gonio light source and with an integrating sphere light source (Section 4.1 and Section

4.2). The spectral bias of the BRDF measurements is demonstrated and the Gonio light source is proved to be a primary source of the error. The influence of the light source and detector apertures was studied and the instrument signature was obtained (Section 4.3). The detector aperture refers to the diameter of the iris located in the detector assembly between the polarizer and the achromatic doublet (see Figure 4.3.1). The light source aperture refers to the diameter of the iris located in the light source assembly between the Nikkor lens and the aspheric lens (see Figure 4.3.2). These two apertures were set empirically so that the solid angle of the light source would match that of the detector, to achieve maximum angular resolution of the reflected light fields. We also examined the chromatic aberrations of the light source (Section 4.4). The chromatic aberrations of the light source refer to a spectrally non-uniform focusing, so that radiation of different wavelengths has different foci. Only slight chromatic aberrations are observed when the solid angle of the light source matches that of the detector.

Chapter 5 summarizes miscellaneous further tests. Other possible sources of measurement error, including stray light, intrinsic detector noise (Section 5.1), polarizer properties (Section 5.2), and reciprocity (Section 5.3), were examined carefully. We believe these factors have no significant influence on BRDF measurements.

Those readers interested only in the proposed measurement method, and the measurements results, may proceed directly to Chapter 7. Other readers may wish to pursue the issues of the detector, light source, and other tests that follow hereafter.

3.1 Background signal of the detector (07/25/1999)

3.1.1 Background

In this section, we study the background signal of the Gonio detector. We are able to measure the background signal of the Gonio detector either (a) at 1, 3, 10, 50, 100, 500, and 1000 units of exposure time automatically using the "Gonio" program (called the "standard-seven-exposure-method") or (b) manually at any selected exposure time (called the "manual method"). One unit of exposure time is 20ms. During the background signal measurements, the detector is blocked off by putting a light shutter in front of the detector housing so that no external light energy is received by the detector. Thus, the signal reading depends only on the background noise of the detector.

Since the background signal is mainly due to thermal noise in the detector, a low working temperature of the detector can reduce the background noise level. A thermoelectric cooling device is built into the detector, and is designed to maintain a constant temperature during measurements after thermal equilibrium has been reached. A driver board in the control computer controls the cooling device. The thermoelectric cooling device is initialized and starts to cool whenever the 'Gonio' program is launched.

In nearly every experiment, the background signal was measured and was used for data processing. We make the following assumptions:

a. The background signal at any exposure time consists of a constant offset, a so-called dark current, and an exposure-time-dependent noise signal.
b. The dark current is not exposure time dependent.

To justify these assumptions, an experiment was carried out on July 25, 1999. The purpose was to examine the stability of the background signal of the Gonio detector. When the 'Gonio' program was launched (i.e., the thermoelectric cooling device was started), we set the clock to zero. Subsequently, we took background signal measurements at running times after zero of 1, 2, 5, 7, 10, 16, 20, 25, 30, 55, 75, 100, 120, 185, 245, 295, 420, 1485, and 1665 minutes (yes, 1.25 days!). Altogether 19 measurements were made. For each measurement, we took two readings of the background signal using, first, the "standard-seven-exposure-method" and then, second, the "manual method" with a 500 unit exposure time. In theory, the detector should display a stable background signal after temperature equilibrium is reached, when using the thermoelectric cooler.

3.1.2 Measurement results

A. Time stability of the Gonio detector

For each exposure, we have signal readings from 1024 detector elements, with the elements spanning the visible wavelength range. These 1024 readings of the background signal are averaged to obtain a mean value of the background signal. For the "standard-seven-exposure-method" and the "manual method," we have one exposure-time in common, namely, 500 units of exposure time. The mean background signals for the two methods, at 500 units of exposure time, are shown in Figure 3.1.1 versus running time.

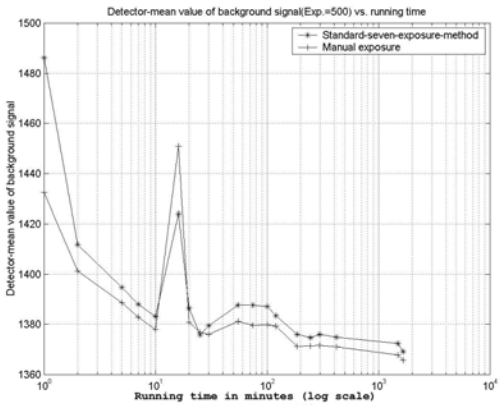

Figure 3.1.1: Detector-mean background signal vs. running time, by both "standard-seven-exposure-method" and "manual measurements." 500 units of exposure time. Y axis is logarithmic.

For the automatic "standard-seven-exposure-method," we also have mean values of the background signal for each of the seven exposure times; that is, we have seven mean values for the 1024-element detector. The seven mean values are graphed vs. running time in Figure 3.1.2. Each curve corresponds to a particular exposure time.

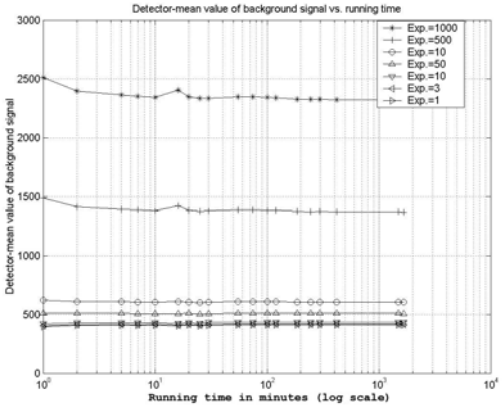

Figure 3.1.2: Detector-mean background signal for the seven exposure times. The second curve from the top is shown on an expanded vertical scale in Figure 3.1.1.

For each of the seven curves in Figure 3.1.2, we calculated the mean value over the running time, and normalized each curve by that mean. Figure 3.1.3 displays an overlay of the seven normalized curves.

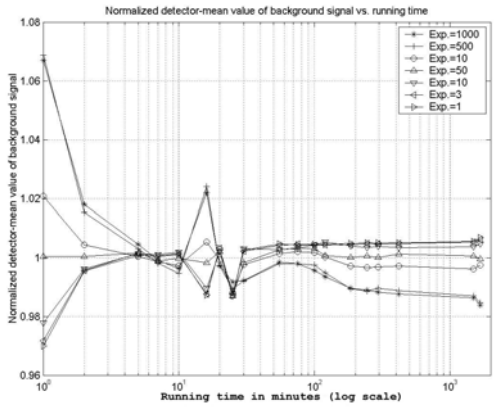

Figure 3.1.3: Normalized detector-mean background signals for the seven exposure times

B. Dark current of the Gonio detector

We did not expect the dark current to be time dependent, that is, to depend on exposure time. Therefore, based on the assumptions mentioned in Section 3.1.1, we tried to obtain the dark current by a linear regression of the background signals at different exposure times. A linear regression was conducted using $y=a+bx$, where a is the dark current, b is the slope, and x is the exposure time.

We chose the measurement at 420 minutes of running time to study the variation of dark current with wavelength. At that time, we expect a steady thermal state in the detector. For the "standard-seven-exposure-method," we graphed the detector-mean readings versus exposure time. The data were plotted together with a straight line defined by the linear model $y=a+bx$ (where a is the dark current, b is the slope, x is the exposure time), as in Figure 3.1.4. a and b are obtained by linear regression. With the expanded axes used in Figure 3.1.5, it is apparent that the measured background signal at low exposure

times (less than 20 units of exposure time) is lower than the linear regression correlation. At low levels of background signal, the signal is slightly nonlinear.

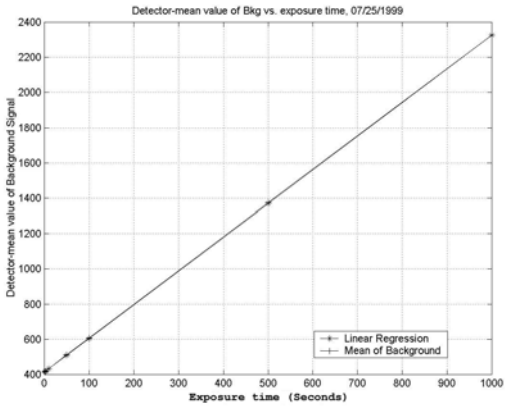

Figure 3.1.4: Detector-mean background signal vs. exposure time. Running time is 420 minutes.

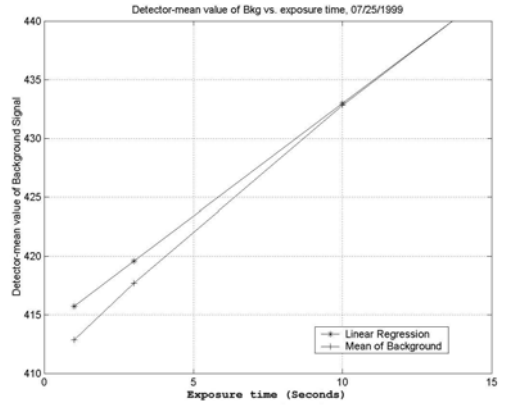

Figure 3.1.5: Detector-mean background signal vs. exposure time (expanded scales). Running time is 420 minutes.

We repeated the foregoing for each detector element. That is, we carried out a linear regression for each detector element. This provides the regression coefficients *a* and *b* as a function of wavelength. The intercepts "*a*" obtained by linear regression are plotted in Figure 3.1.6. Also shown are the actual readings of the background signal at 1 unit exposure time, for comparison. Note that the projected intercepts are higher than the

measured background signal at 1 unit exposure time, due to the nonlinear behavior of the actual signal at zero exposure time.

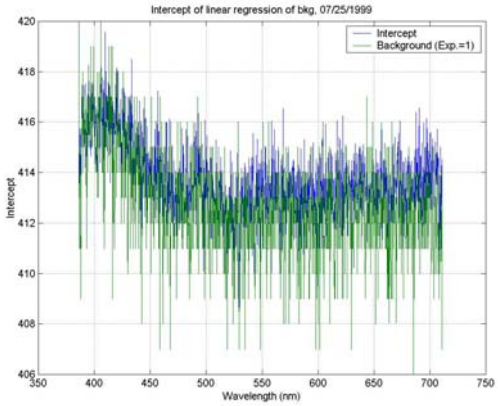

Figure 3.1.6: Comparison of the linear regression intercepts and the measured background measurement at 1 unit exposure time. Running time is 420 minutes.

Next, we studied the time variation of the dark current. For each running time, we calculated the detector-mean values of the linear regression intercept *a* (the dark current) and the slope *b*. The resulting intercepts and slopes are shown in Figure 3.1.7 and Figure 3.1.8, respectively.

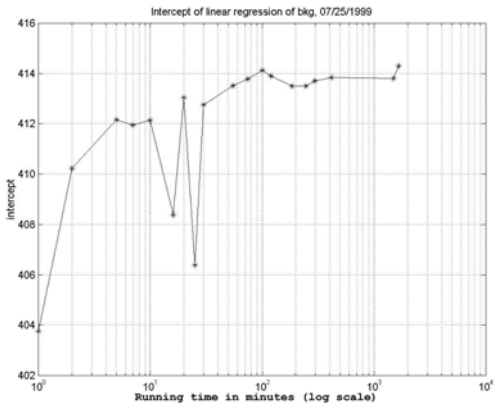

Figure 3.1.7: Intercept of linear regression, the detector-mean dark current vs. running time

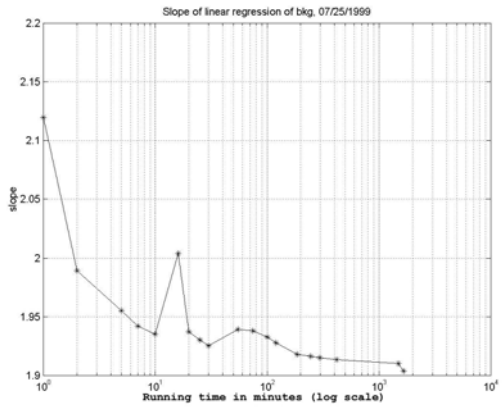

Figure 3.1.8: Slope of linear regression of background signal vs. running time

Although the intercept *a* is assumed to be constant over time, it increases slightly with time and converges to a value of approximately 414. Further, *b* converges to approximately 1.91. After about 30 minutes of running time, *a* and *b* are within 0.5% and 1.5%, respectively, of their asymptotic values.

3.1.3 Comments

From Figure 3.1.1 to Figure 3.1.8, most of the measured data follow smooth trends except near the running time of about 16 minutes. A possible reason for the abnormality is an unknown wrong operation in data entry, data storage, etc.

From Figure 3.1.1, the process of cooling down the detector is clear. The background signal slowly converges to a fixed value as the detector-temperature approaches an equilibrium. The time variation is partly due to the reduction in the dark current as the detector cools. The detector needs about half an hour to reach a steady state. Thus, no measurements should be carried out until a half hour after launching the 'Gonio' program.

Figure 3.1.1 shows that the signal readings of the background signal by the "manual method" were always slightly lower than with the "standard-seven-exposure-method." The phenomenon is unexpected because essentially there should be no difference between the two exposure methods, except that one was measured manually and the other was measured automatically. The consecutive measurement of the background signal by the "seven exposure time method" may bias the measurements. However, the differences in the background signal obtained by the two methods are small, being less than 0.5% for running times longer than 2 minutes.

Another interesting phenomenon is in Figure 3.1.2 and Figure 3.1.3. It seems that the automatically measured background signals at different exposure times have slightly different trends over running time. With the time passing by, the background signal at long exposure times decreased and the background signal at short exposure times increased. Both of these temporal effects are small, however; the total variation for running times larger than 2 minutes is less than about 2%. There are two possibilities for these changes. One is that the assumed constant offset, or dark current, increases over the running time. The other is that the slope of the exposure-time-dependent signal vs. exposure time decreases over time. Both of these effects are apparent in Figure 3.1.7 and Figure 3.1.8, respectively.

However, there is another paradox. The dark current obtained by linear regression is larger than the measured background signal at 1 unit exposure time. Thus, the linearity

of the exposure-time-dependent signal vs. exposure time is under question. The detector-mean values of background signal vs. exposure time are plotted in Figure 3.1.4 and Figure 3.1.5. It appears that a very slight non-linearity, say, several counts, happens at short exposure times (less than 20 units of exposure time).

In conclusion, there are two recommendations. First, in the case of measurements over a short period of running time, the manually measured background signal is preferred to the automatic background measurements. It is also more reliable to measure the background signal immediately after the reflected/direct signal measurement. Second, in the case of measurements made over a long running time, it is recommended to measure the background signal at the beginning of the measurements as well as at the end. The average of these two measurements should then be used for data processing.

3.2 Linearity of detector to exposure time and discussion of detector noise (07/08/1999)

3.2.1 Background

On July 8, 1999, an experiment was conducted to check the linearity of the detector response to exposure time. It is assumed that the signal reading at any exposure time consists of a background signal and a signal determined by the incident energy. With a fixed energy flux incident, the second signal should increase linearly with exposure time. The first half of this section focuses on this topic. Note that the background signal, often small, is also essentially linear in the exposure time. For details, refer to the previous section.

Furthermore, we observed that the signal noise is related to exposure time. This affects reflectance measurements made on samples with very low reflectance, where long exposure times may be required. The second half of this section focuses on the noise issue.

3.2.2 Procedure

First, the background signals at various exposure times were measured, with a light shutter installed in front of the detector housing. The 17 exposure times used were 1, 3, 5, 7, 9, 10, 30, 50, 70, 90, 100, 300, 500, 700, 900, 1000, and 3000 units of exposure time. One unit of exposure time is 20ms, so a 3000 unit exposure time corresponds to one minute.

Second, the voltage of the light source was set at 25Volt. The light source was aligned to directly illuminate the entrance optics of the detector. The incident light flux was measured at the same 17 exposure times.

Third, the voltage of the light source was reduced to 20Volt. The light source was aligned with the detector and the incident light flux was measured at the same 17 exposure times. Thus, for each exposure time, we have three measurements: background signal; direct light-source signal at 25 Volt; and direct light-source signal at 20 Volt.

3.2.3 Measurement results

A. Raw signals

The raw data for 17 exposures (1, 3, 5, 7, 9, 10, 30, 50, 70, 90, 100, 300, 500, 700, 900, 1000, 3000 units exposure time) are presented in Figure 3.2.1 to Figure 3.2.3

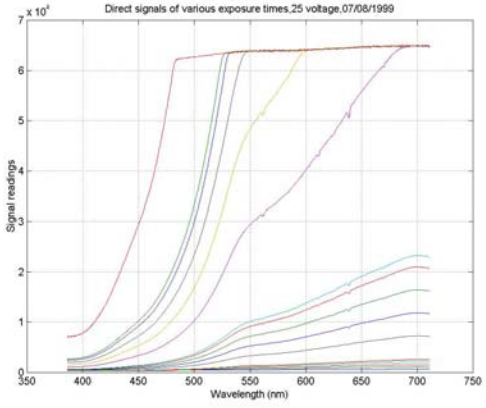

Figure 3.2.1: Direct light-source signal readings at various exposure times. The voltage of the light source was 25Volt

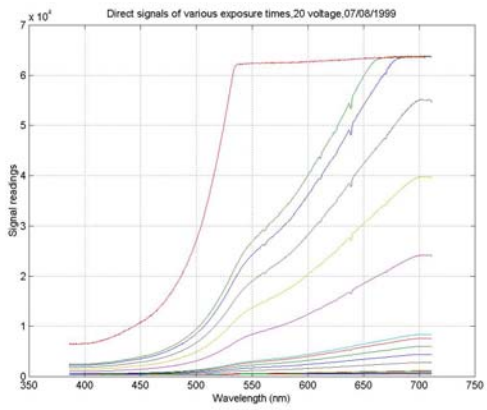

Figure 3.2.2: Direct light-source signal readings at various exposure times. The voltage of the light source was 20Volt

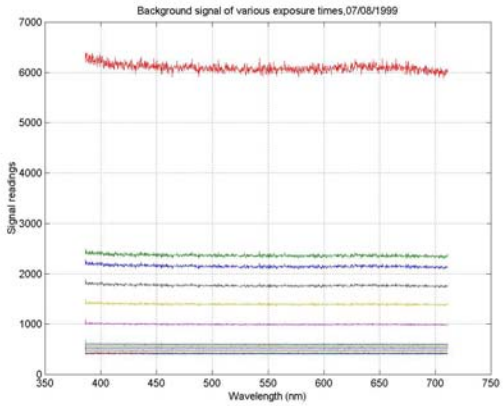

Figure 3.2.3: Background signal readings at various exposure times. The signal does not depend on the voltage of the light source.

B. The linearity of Gonio detector response to the exposure time

To check the linearity of the detector, we process the data as follows:

a. Subtract the background signal from the direct light-source signal readings, both with the same exposure time;

b. For each exposure time, calculate the sum of the signals obtained in the preceding step over all of the 1024 detector elements;

c. Normalize the 17 sums by the exposure time.

The result is shown in Figure 3.2.4.

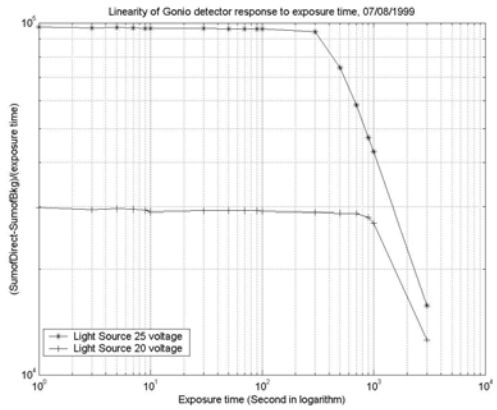

Figure 3.2.4: Linearity of Gonio detector response to exposure time

In theory, the ratios from step (3) should be constant, because the detector has a linear response to the incident light. In Figure 3.2.4, the drop at the right end of the two curves is due to saturation of the detector. Saturation appears when the signals plateau, as they do near the top of Figure 3.2.1 and Figure 3.2.2. Except for the saturated region, the level curves in Figure 3.2.4 establish that the detector response is basically linear with exposure time, at least to about 1%.

We next examine the variation of the detector response across the 1024 detector elements. Figure 3.2.4 applied for the sum of signals from all the detector outputs. To proceed, we take several selected elements in the detector array and repeat the foregoing data processing procedure.

We expect the most variations at the short wavelength end, where the incident light is weakest. Therefore, we chose detector elements number 1, 100, 200, 300 and 400 for examination. The performance of the five elements is displayed in Figure 3.2.5 to Figure

3.2.9. Again, the normalized ordinates are signal minus background, divided by exposure time.

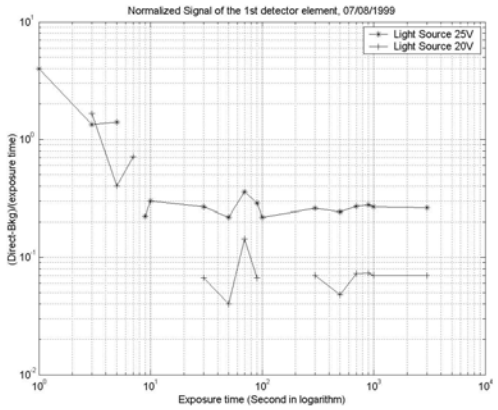

Figure 3.2.5: Linearity of 1st detector element with exposure time

Discontinuities in the curves are due to negative net values, when the measured signals are less than the background signals. Such behavior occurs at low light levels, when the source and background signals are each only a small number of counts. Since there are fluctuations in both the source and background signals with time and they are measured at different times, negative values can arise. For stronger source signals, as in Figure 3.2.7 to Figure 3.2.9, this anomalous behavior disappears.

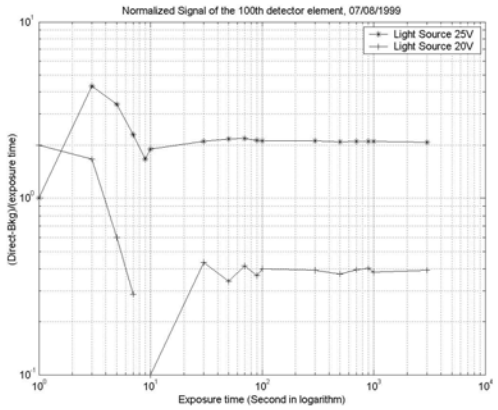

Figure 3.2.6: Signal Linearity of 100th detector element with exposure time

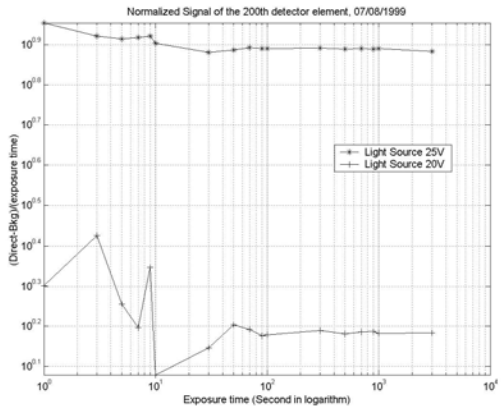

Figure 3.2.7: Signal Linearity of 200th detector element with exposure time

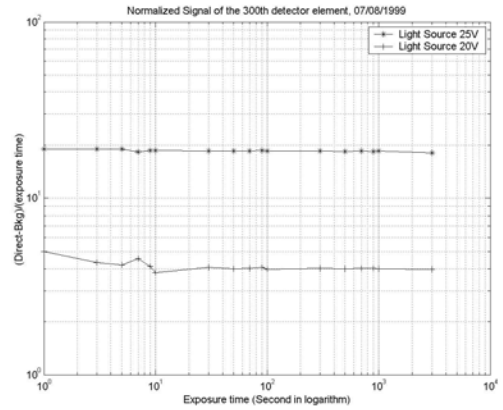

Figure 3.2.8: Signal Linearity of 300th detector element with exposure time

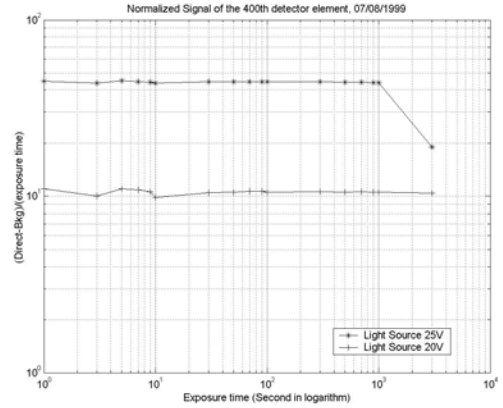

Figure 3.2.9: Signal Linearity of 400th detector element with exposure time

C. The relation between signal fluctuation and signal level

The preceding paragraphs suggest that large relative errors (due to signal fluctuations) can arise at low signal levels (below approximately 100 counts). The fluctuations come mainly from thermal noise in the detector. Since the thermoelectric cooling device keeps the detector at a low temperature, the magnitude of the thermal noise in the detector is of the order of about 10 counts. Therefore, the error due to the fluctuations can become excessive at low signal levels.

We processed the data of the previous section to obtain estimates of the fluctuation error versus signal count. We took the signal count data (signal minus background) for all 1024 detector elements, for the 17 exposure times used (1024*17=17408 data points). We normalized the signal count data by the exposure time (to eliminate the linear dependence). At each integer value of signal count, we averaged the foregoing normalized signal count data, and calculated the maximum deviation. We carried out this procedure on the measurements made with two light source voltages: 25 Volts and 20 Volts.

The maximum deviations at each integer signal count (signal minus background) are graphed in Figure 3.2.10 and Figure 3.2.11. A 90% upper bound, which is a loose limit, is added to provide a smooth estimate of the maximum expected fluctuation in the signal readings versus signal count.

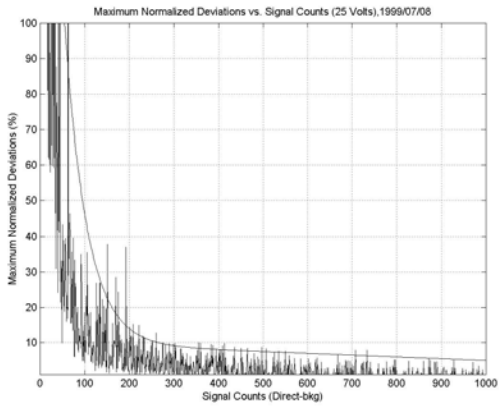

Figure 3.2.10: Maximum absolute deviations normalized by exposure time vs. signal level (number of counts). A 90% upper bound curve is included. The voltage of the light source was 25Volts.

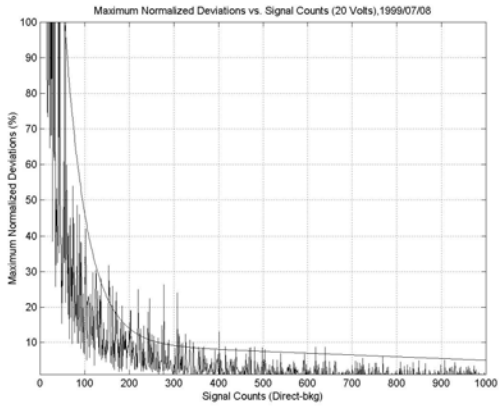

Figure 3.2.11: Maximum absolute deviations normalized by exposure time vs. signal level (number of counts). A 90% upper bound curve is included. The voltage of the light source was 20Volts.

3.2.4 Comments

Figure 3.2.4 shows that within most of the dynamic range of the detector, the response of the detector to exposure time is linear, at least to about 1%. However, Figure 3.2.5 and Figure 3.2.6 show that the signal readings of the detector at very low signal levels, and after subtracting the background signal, fluctuate. The fluctuations result because the source and background signals both fluctuate, and are not measured at precisely the same instant of time.

The relation of the maximum expected fluctuation in the exposure-time-normalized

signals was studied. Figure 3.2.10 and Figure 3.2.11 show that the maximum expected fluctuation decreases as the signal level increases. A loose 90% upper bound curve is included on the figures. In most cases, we expect that the fluctuations will be far less than the upper bound. (The generality of the figures is supported by considerable extra data obtained at lower light levels after attenuating the light source with filters. These results are not included here.) From the foregoing results, it is clear that the exposure time (or signal strength) is a very important issue for BRDF measurements, especially for samples with very low reflectance, like the Bristol Sample#1 [4]. The detector needs strong signals, which are much stronger than the background noise, to produce accurate measurements.

We also know that part of the errors of the BRDF measurement at 0/45 comes from insufficient exposure. For details, refer to Section 7.3. Longer exposure times can reduce the noise at short wavelengths.

3.2.5 Matlab Script

A. Code to generate Figure 3.2.4

```
clear
% Reads the raw data files with measurements and exposure times of the
% background, the direct source, and the measurements.
[exposure_b1,bkg1]   = readfile(['bkg.dat']);
[exposure_b,bkg(:,3)]   = readfile(['bkg005.dat']);
[exposure_b,bkg(:,4)]   = readfile(['bkg007.dat']);
[exposure_b,bkg(:,5)]   = readfile(['bkg009.dat']);
[exposure_b,bkg(:,7)]   = readfile(['bkg030.dat']);
[exposure_b,bkg(:,9)]   = readfile(['bkg070.dat']);
[exposure_b,bkg(:,10)]   = readfile(['bkg090.dat']);
[exposure_b,bkg(:,12)]   = readfile(['bkg300.dat']);
[exposure_b,bkg(:,14)]   = readfile(['bkg700.dat']);
[exposure_b,bkg(:,15)]   = readfile(['bkg900.dat']);
[exposure_b,bkg(:,17)]   = readfile(['bkg3k.dat']);
bkg(:,1)=bkg1(:,1);
bkg(:,2)=bkg1(:,2);
bkg(:,6)=bkg1(:,3);
bkg(:,8)=bkg1(:,4);
bkg(:,11)=bkg1(:,5);
bkg(:,13)=bkg1(:,6);
bkg(:,16)=bkg1(:,7);

[exposure,direct_1(:,1)]      = readfile(['Meas001_1.dat']);
[exposure,direct_1(:,2)]      = readfile(['Meas003_1.dat']);
[exposure,direct_1(:,3)]      = readfile(['Meas005_1.dat']);
[exposure,direct_1(:,4)]      = readfile(['Meas007_1.dat']);
[exposure,direct_1(:,5)]      = readfile(['Meas009_1.dat']);
[exposure,direct_1(:,6)]      = readfile(['Meas010_1.dat']);
[exposure,direct_1(:,7)]      = readfile(['Meas030_1.dat']);
[exposure,direct_1(:,8)]      = readfile(['Meas050_1.dat']);
[exposure,direct_1(:,9)]      = readfile(['Meas070_1.dat']);
[exposure,direct_1(:,10)]      = readfile(['Meas090_1.dat']);
[exposure,direct_1(:,11)]      = readfile(['Meas100_1.dat']);
[exposure,direct_1(:,12)]      = readfile(['Meas300_1.dat']);
[exposure,direct_1(:,13)]      = readfile(['Meas500_1.dat']);
[exposure,direct_1(:,14)]      = readfile(['Meas700_1.dat']);
[exposure,direct_1(:,15)]      = readfile(['Meas900_1.dat']);
[exposure,direct_1(:,16)]      = readfile(['Meas1k_1.dat']);
[exposure,direct_1(:,17)]      = readfile(['Meas3k_1.dat']);

[exposure,direct_2(:,1)]      = readfile(['Meas001_2.dat']);
[exposure,direct_2(:,2)]      = readfile(['Meas003_2.dat']);
[exposure,direct_2(:,3)]      = readfile(['Meas005_2.dat']);
[exposure,direct_2(:,4)]      = readfile(['Meas007_2.dat']);
[exposure,direct_2(:,5)]      = readfile(['Meas009_2.dat']);
[exposure,direct_2(:,6)]      = readfile(['Meas010_2.dat']);
[exposure,direct_2(:,7)]      = readfile(['Meas030_2.dat']);
[exposure,direct_2(:,8)]      = readfile(['Meas050_2.dat']);
[exposure,direct_2(:,9)]      = readfile(['Meas070_2.dat']);
[exposure,direct_2(:,10)]      = readfile(['Meas090_2.dat']);
[exposure,direct_2(:,11)]      = readfile(['Meas100_2.dat']);
[exposure,direct_2(:,12)]      = readfile(['Meas300_2.dat']);
```

```
[exposure,direct_2(:,13)]      = readfile(['Meas500_2.dat']);
[exposure,direct_2(:,14)]      = readfile(['Meas700_2.dat']);
[exposure,direct_2(:,15)]      = readfile(['Meas900_2.dat']);
[exposure,direct_2(:,16)]      = readfile(['Meas1k_2.dat']);
[exposure,direct_2(:,17)]      = readfile(['Meas3k_2.dat']);

x=[1 3 5 7 9 10 30 50 70 90 100 300 500 700 900 1000 3000 ];

for i=1:17,
   sum_bkg(i)=sum(bkg(:,i));
   sum_direct1(i)=(sum(direct_1(:,i))-sum_bkg(i))/x(i);
   sum_direct2(i)=(sum(direct_2(:,i))-sum_bkg(i))/x(i);
end;

loglog(x,sum_direct1,'*-',x,sum_direct2,'+-');
legend('Light Source 25 voltage','Light Source 20 voltage')
xlabel 'exposure time'
ylabel '(SumofDirect-SumofBkg)/(exposure time)'
title 'Linearity of Gonio detector response to exposure time,
07/08/1999'
%axis([0 12 16.3 16.8]);
```

B. Code to generate Figure 3.2.10 and Figure 3.2.11

```
clear
% Reads the raw data files with measurements and exposure times of the
% background, the direct source, and the measurements.
[exposure_b1,bkg1]   = readfile(['bkg.dat']);
[exposure_b,bkg(:,3)]   = readfile(['bkg005.dat']);
[exposure_b,bkg(:,4)]   = readfile(['bkg007.dat']);
[exposure_b,bkg(:,5)]   = readfile(['bkg009.dat']);
[exposure_b,bkg(:,7)]   = readfile(['bkg030.dat']);
[exposure_b,bkg(:,9)]   = readfile(['bkg070.dat']);
[exposure_b,bkg(:,10)]   = readfile(['bkg090.dat']);
[exposure_b,bkg(:,12)]   = readfile(['bkg300.dat']);
[exposure_b,bkg(:,14)]   = readfile(['bkg700.dat']);
[exposure_b,bkg(:,15)]   = readfile(['bkg900.dat']);
[exposure_b,bkg(:,17)]   = readfile(['bkg3k.dat']);
bkg(:,1)=bkg1(:,1);
bkg(:,2)=bkg1(:,2);
bkg(:,6)=bkg1(:,3);
bkg(:,8)=bkg1(:,4);
bkg(:,11)=bkg1(:,5);
bkg(:,13)=bkg1(:,6);
bkg(:,16)=bkg1(:,7);

[exposure,direct_1(:,1)]      = readfile(['Meas001_1.dat']);
[exposure,direct_1(:,2)]      = readfile(['Meas003_1.dat']);
[exposure,direct_1(:,3)]      = readfile(['Meas005_1.dat']);
[exposure,direct_1(:,4)]      = readfile(['Meas007_1.dat']);
[exposure,direct_1(:,5)]      = readfile(['Meas009_1.dat']);
[exposure,direct_1(:,6)]      = readfile(['Meas010_1.dat']);
[exposure,direct_1(:,7)]      = readfile(['Meas030_1.dat']);
[exposure,direct_1(:,8)]      = readfile(['Meas050_1.dat']);
[exposure,direct_1(:,9)]      = readfile(['Meas070_1.dat']);
[exposure,direct_1(:,10)]      = readfile(['Meas090_1.dat']);
```

```
[exposure,direct_1(:,11)]      = readfile(['Meas100_1.dat']);
[exposure,direct_1(:,12)]      = readfile(['Meas300_1.dat']);
[exposure,direct_1(:,13)]      = readfile(['Meas500_1.dat']);
[exposure,direct_1(:,14)]      = readfile(['Meas700_1.dat']);
[exposure,direct_1(:,15)]      = readfile(['Meas900_1.dat']);
[exposure,direct_1(:,16)]      = readfile(['Meas1k_1.dat']);
[exposure,direct_1(:,17)]      = readfile(['Meas3k_1.dat']);

[exposure,direct_2(:,1)]      = readfile(['Meas001_2.dat']);
[exposure,direct_2(:,2)]      = readfile(['Meas003_2.dat']);
[exposure,direct_2(:,3)]      = readfile(['Meas005_2.dat']);
[exposure,direct_2(:,4)]      = readfile(['Meas007_2.dat']);
[exposure,direct_2(:,5)]      = readfile(['Meas009_2.dat']);
[exposure,direct_2(:,6)]      = readfile(['Meas010_2.dat']);
[exposure,direct_2(:,7)]      = readfile(['Meas030_2.dat']);
[exposure,direct_2(:,8)]      = readfile(['Meas050_2.dat']);
[exposure,direct_2(:,9)]      = readfile(['Meas070_2.dat']);
[exposure,direct_2(:,10)]      = readfile(['Meas090_2.dat']);
[exposure,direct_2(:,11)]      = readfile(['Meas100_2.dat']);
[exposure,direct_2(:,12)]      = readfile(['Meas300_2.dat']);
[exposure,direct_2(:,13)]      = readfile(['Meas500_2.dat']);
[exposure,direct_2(:,14)]      = readfile(['Meas700_2.dat']);
[exposure,direct_2(:,15)]      = readfile(['Meas900_2.dat']);
[exposure,direct_2(:,16)]      = readfile(['Meas1k_2.dat']);
[exposure,direct_2(:,17)]      = readfile(['Meas3k_2.dat']);

x=[1 3 5 7 9 10 30 50 70 90 100 300 500 700 900 1000 3000 ];

Signal_1=direct_1-bkg;
Signal_2=direct_2-bkg;
max_signal1=max(max(Signal_1(:,1:10)));
max_signal2=max(max(Signal_2(:,1:10)));
Noise_1=zeros(max_signal1,1);
Noise_2=zeros(max_signal2,1);

for i=1:17,
   for j=1:1024,
      Normalized_1(j,i)=(direct_1(j,i)-bkg(j,i))/x(i);
      Normalized_2(j,i)=(direct_2(j,i)-bkg(j,i))/x(i);
   end;
end;

for i=1:1024,
   Mean_Normalized1(i)=mean(Normalized_1(i,1:10));
   for j=1:10,
      if Signal_1(i,j)>0
         if (abs(Normalized_1(i,j)-
Mean_Normalized1(i))/Mean_Normalized1(i))>Noise_1(Signal_1(i,j))
            Noise_1(Signal_1(i,j))=abs(Normalized_1(i,j)-
Mean_Normalized1(i))/Mean_Normalized1(i);
         end;
      end;
   end;
end;

for i=1:1024,
   Mean_Normalized2(i)=mean(Normalized_2(i,1:10));
```

```
   for j=1:10,
      if Signal_2(i,j)>0
         if (abs(Normalized_2(i,j)-
Mean_Normalized2(i))/Mean_Normalized2(i))>Noise_2(Signal_2(i,j))
            Noise_2(Signal_2(i,j))=abs(Normalized_2(i,j)-
Mean_Normalized2(i))/Mean_Normalized2(i);
         end;
      end;
   end;
end;

x1= [1:1:max_signal1];
x2= [1:1:max_signal2];

SignalCounts=    [0    25  50  75  100 150 200 250 300 350 400 450 500
600 700 800 900 1000 1200 1400 1600 1800 2000 2200 2400 2600 2800 3000
];
NoiseUpperBound= [1000 500 100 50  38  25  18  13  10   8   7   6   5
4   4   3.5 3   3    2.5  2    1.7  1.4  1.2  1    1    1    1    1 ];


plot(x1,Noise_1*100,'g',SignalCounts,NoiseUpperBound,'r');
axis([0 1000 0 100]);
title 'Maximum Normalized Difference vs. Signal Counts (25
Volts),1999/07/08'
ylabel 'Maximum Normalized Difference (%)'
xlabel 'Signal Counts(Direct-bkg)'

figure
plot(x2,Noise_2*100,'g',SignalCounts,NoiseUpperBound,'r');
axis([0 1000 0 100]);
title 'Maximum Normalized Difference vs. Signal Counts (20
Volts),1999/07/08'
ylabel 'Maximum Normalized Difference (%)'
xlabel 'Signal Counts(Direct-bkg)'
```

3.3 Linearity of detector to incident light intensity via transmittance measurements on neutral density filters

3.3.1 Transmittance measurements by OL-750 reflectometer and by Gonio detector + Gonio light source (07/30/1999)

A. Background

In the previous section, we studied the linearity of the Gonio detector response to exposure time. Here, we essentially repeat that experiment by varying the incident light intensity. To vary the light intensity, neutral density (ND) filters were placed at the output of the light source. A polarizer was placed before the detector. By measuring the transmitted and incident light intensities, and ratioing, we get the filter transmittance. The latter is then compared with values measured by another instrument.

The neutral density filters are intended to uniformly attenuate an incident beam of radiation without spectrally altering the distribution. Seven neutral density filters were used. Their names and nominal optical densities (OD) and transmittances are:

* Melles Griot 03FNQ002 optical density filter (ND filter OD=0.03, 93.32%)
* Melles Griot 03FNQ003 optical density filter (ND filter OD=0.1, 79.43%)
* Melles Griot 03FNQ007 optical density filter (ND filter OD=0.3, 50.12%)
* Melles Griot 03FNQ085 optical density filter (ND filter OD=0.5, 31.62%)
* Melles Griot 03FNQ015 optical density filter (ND filter OD=1, 10.00%)
* Melles Griot 03FNQ023 optical density filter (ND filter OD=2, 1.00%)
* Melles Griot 03FNQ027 optical density filter (ND filter OD=3, 0.1%)

The optical density, OD, is defined as $[-\log_{10}(\text{transmittance})]$.

The Gonioreflectometer was used to measure the spectral transmittance of the neutral density (ND) filters. The measurements can be used to indirectly check the response of the detector to the light intensity.

Other sources of transmittance data for the filters are available. First, from the manufacturer of the neutral density filters [5]. Second, from the report "Preliminary Calibration of the Photometrics PXL1300L CCD Camera" (1996) [6]. The OL-750 reflectometer in the Light Measurement Laboratory was used. The instrument setup, test procedure, and tabulated data for the filter transmittances are provided. Third, the measurements using the OL-750 reflectometer were repeated. The only difference is that the normal transmittance was measured. With that, the normal of the filters is aligned with the incident light direction, instead of at a small angle to the incident beam.

The four sets of data, from the Gonioreflectometer, from the manufacturer, from the old OL-750 measurements, and from the present OL-750 measurements, are plotted together in the results figures. Note that the ordinates in the resulting figures are greatly enlarged and cover only a small subset of the 0 to 100% transmittance range.

B. Procedure

The procedure for measuring the filter transmittance by the Gonioreflectometer is as follows:

a. Measure the background signal;

b. Turn on the light source of the Gonioreflectometer, measure the direct light-source signal, save the data as ‘dir_off0.dat’;
c. Add the neutral density filter with optical density 0.03, measure the transmitted signal, save the data as ‘dir_off1.dat’;
d. Add the neutral density filter with optical density 0.1, measure the transmitted signal, save the data as ‘dir_off2.dat’;
e. Add the neutral density filter with optical density 0.3, measure the transmitted signal, save the data as ‘dir_off3.dat’;
f. Add the neutral density filter with optical density 0.5 measure the transmitted signal, save the data as ‘dir_off4.dat’;
g. Add the neutral density filter with optical density 1, measure the transmitted signal, save the data as ‘dir_off5.dat’;
h. Add the neutral density filter with optical density 2, measure the transmitted signal, save the data as ‘dir_off6.dat’;
i. Add the neutral density filter with optical density 3, measure the transmitted signal, save the data as ‘dir_off7.dat’.

The procedure for using the OL-750 REFLECTOMETER for transmittance measurements is given in “Preliminary Calibration of the Photometrics PXL1300L CCD Camera.”[**6**]

C. Measurement results

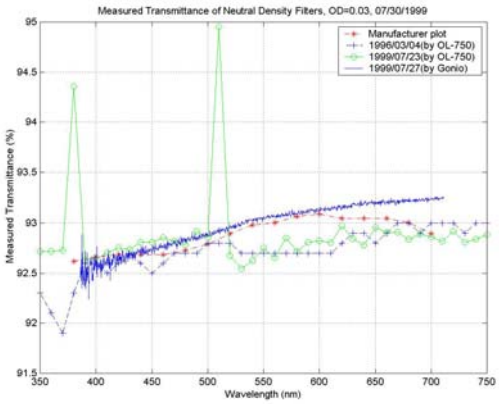

Figure 3.3.1: Comparison of measured transmittances for neutral density filter, OD=0.03

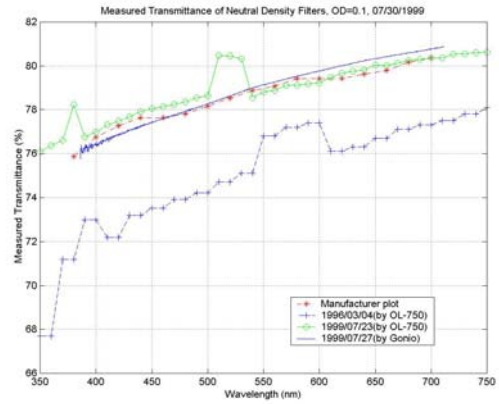

Figure 3.3.2: Comparison of measured transmittances for neutral density filter, OD=0.1

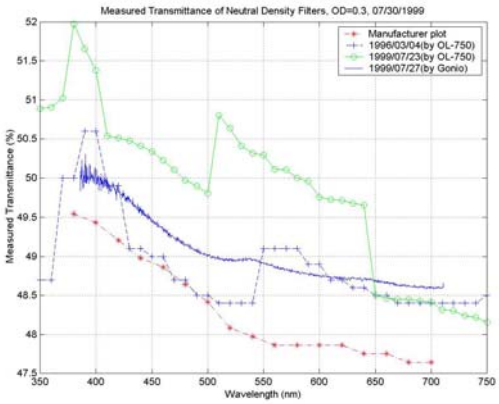

Figure 3.3.3: Comparison of measured transmittances for neutral density filter, OD=0.3

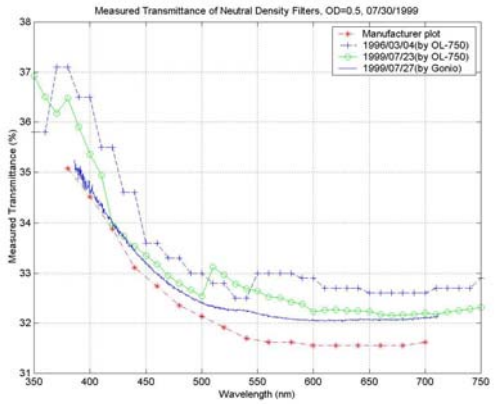

Figure 3.3.4: Comparison of measured transmittances for neutral density filter, OD=0.5

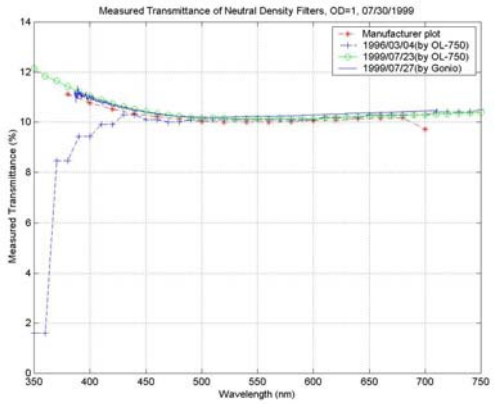

Figure 3.3.5: Comparison of measured transmittances for neutral density filter, OD=1

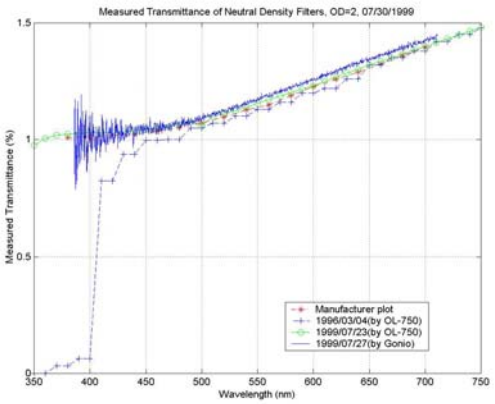

Figure 3.3.6: Comparison of measured transmittances for neutral density filter, OD=2

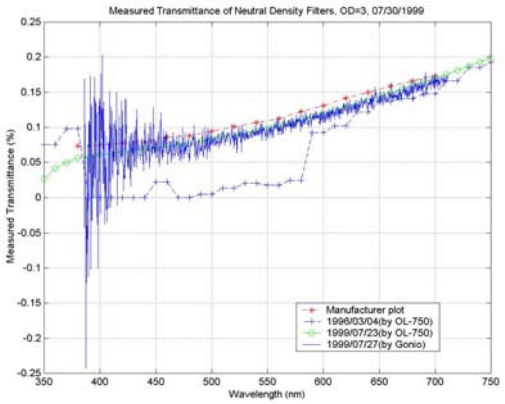

Figure 3.3.7: Comparison of measured transmittances for neutral density filter, OD=3

D. Comments

A comparison of the four sets of transmittance data indirectly establishes the linearity of the Gonio detector to incident light intensity. With the incident light intensity varying over three orders of magnitude, the spectral transmittances derived from the Gonio measurements show good agreement with the other measurements. Note that the neutral density filters are not perfectly neutral over the visible light range, only approximately neutral.

For some unknown reasons, the transmittance measurements of the OD=0.1, OD=0.3, and OD=0.5 filters have up to 5% error, compared with manufacturer's data. Most of the errors seem to be with the old (and new) OL-750 measurements. One possible source of error is the mismatch of the gratings. The max error always appears at certain wavelengths. Some discontinuities in the curves can be observed. However, not all of the filters show the same behaviors.

From Figure 3.3.6 and Figure 3.3.7, for the filters with the lowest transmittances, we observe strong noise in the Gonio measurements. It seems that the measurements of transmittance may be limited by the noise of the Gonio detector.

To improve the performance of the OL-750 reflectometer in measuring the reflectivity and transmittance at short wavelength, an extra reflection grating was added to the OL-750 monochromatic light source. The transmittance measurements at short wavelength were improved significantly, compared with the old measurements in 1996. This is the principal reason for the differences between the old and new measurements with the OL-750 instrument.

3.3.2 Transmittance measurements by Gonio detector + integrating sphere light source (07/27/2999)

A. Background

In the previous subsection, four sets of transmittance data were compared to indirectly establish the linearity of the Gonio detector to the incident light intensity. However, the transmittance measurements with the Gonioreflectometer had strong noise at short wavelengths, due to the low signal level of the light source. To eliminate any bias caused by the light source, while trying to establish the linearity of the detector, the transmittance measurements were repeated by using an integrating sphere light source (Labsphere US-080-SF) in place of the Gonio light source. The new measurements also indirectly establish the linearity of the Gonio detector.

The Labsphere US-080-SF integrating sphere light source was installed directly opposite to the Gonio detector assembly. The polarizer in front of the detector was removed during the experiment. By measuring the direct signal from the integrating sphere light source and the signal transmitted by the neutral density filters, we can obtain the spectral transmittances of the ND filters. However, we do not present our results in terms of transmittances. Instead, we compare the transmitted signals with the product of the direct signal from the integrating sphere light source and the transmittances measured by the OL-750 reflectometer. The later transmittance measurements were reliably measured in the previous subsection. If the response of the Gonio detector to incident light intensity is linear, the transmitted signal and the comparison product should be the same. Since we

exclude the Gonio light source and all polarizers, the results depend only on the detector response.

In the report "Preliminary Calibration of the Photometrics PXL1300L CCD Camera" (1996) [6], the instrument setup, test procedure and the measured data are presented for the transmittance measurements on the neutral density filters with the OL-750 instrument.

B. Procedure

Please refer to Subsection 0. In the present, the Gonio light source is replaced by the integrating sphere light source.

C. Measurement results

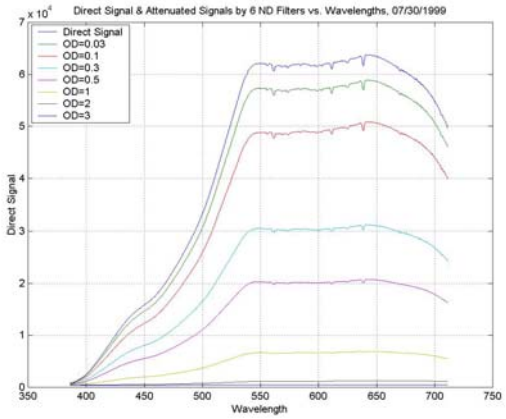

Figure 3.3.8: Source signal reading and signal readings after attenuation by various ND filters. Gonio detector and integrating sphere light source. The exposure time is held constant.

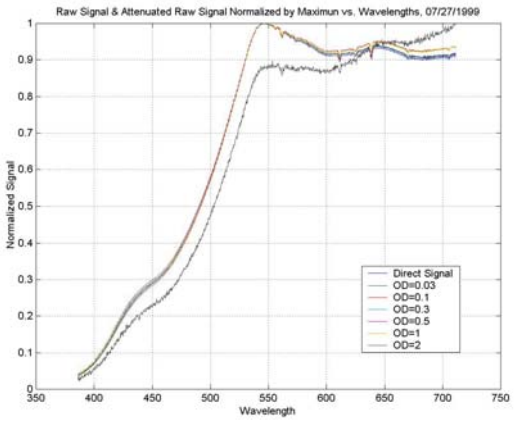

Figure 3.3.9: Source signal reading and ND filter attenuated signal readings each normalized by the curve maximum

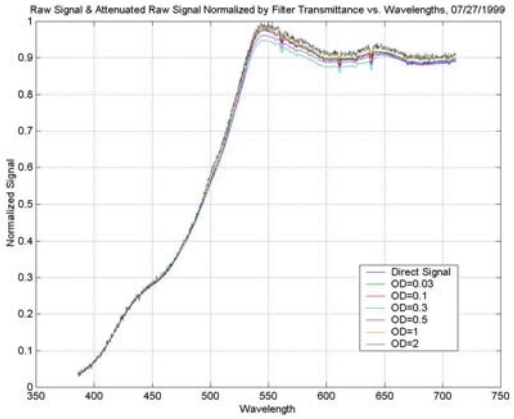

Figure 3.3.10: Source signal reading and ND filter attenuated signal readings. The latter are each normalized by the OL-750 reflectometer measured filter spectral transmittances

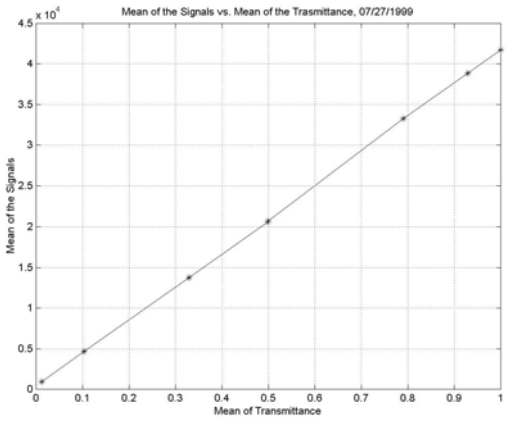

Figure 3.3.11: Wavelength averaged attenuated signal readings vs. wavelength averaged filter transmittances

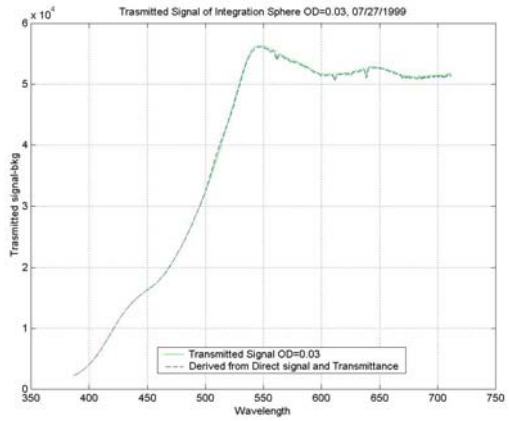

Figure 3.3.12: Comparison of the measured attenuated signals and the product of the source signal times the OL-750 measured transmittances, OD=0.03

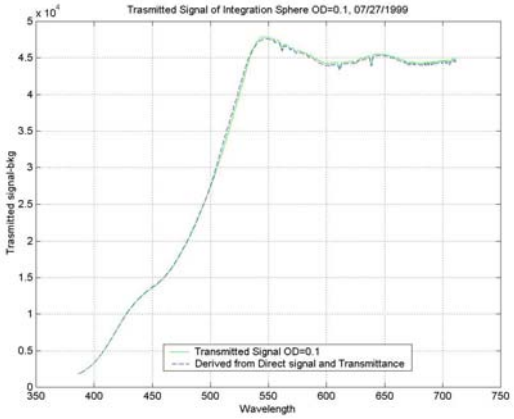

Figure 3.3.13: Comparison of the measured attenuated signals and the product of the source signal times the OL-750 measured transmittances, OD=0.1

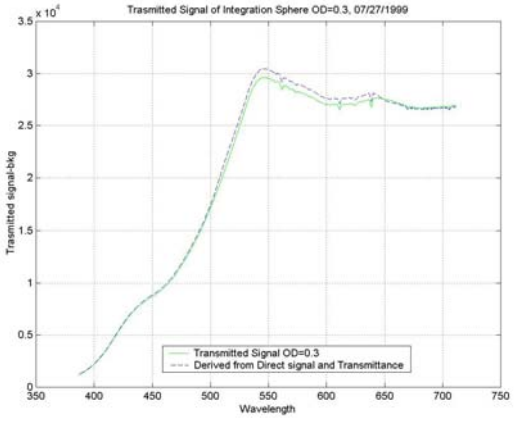

Figure 3.3.14: Comparison of the measured attenuated signals and the product of the source signal times the OL-750 measured transmittances, OD=0.3

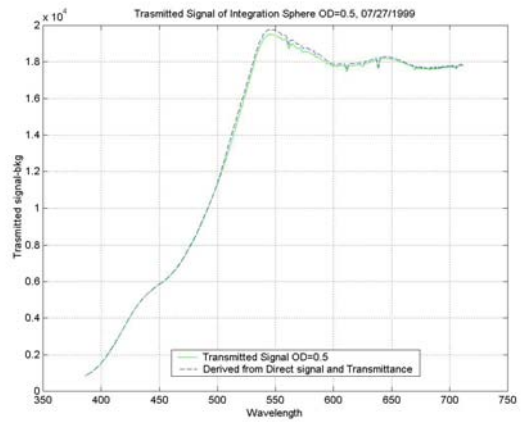

Figure 3.3.15: Comparison of the measured attenuated signals and the product of the source signal times the OL-750 measured transmittances, OD=0.5

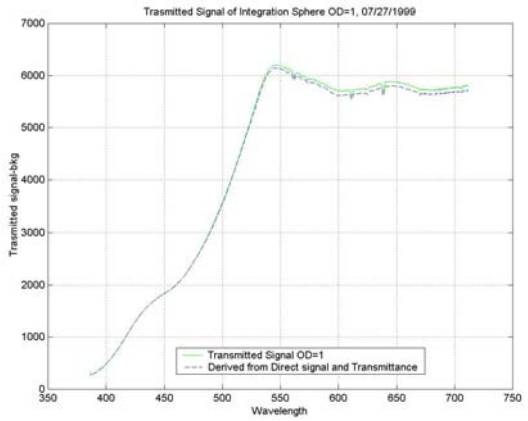

Figure 3.3.16: Comparison of the measured attenuated signals and the product of the source signal times the OL-750 measured transmittances, OD=1

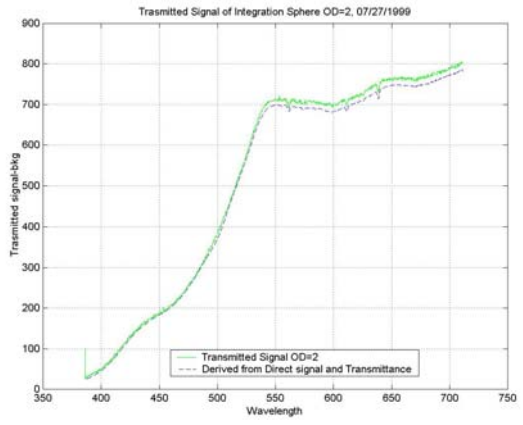

Figure 3.3.17: Comparison of the measured attenuated signals and the product of the source signal times the OL-750 measured transmittances, OD=2

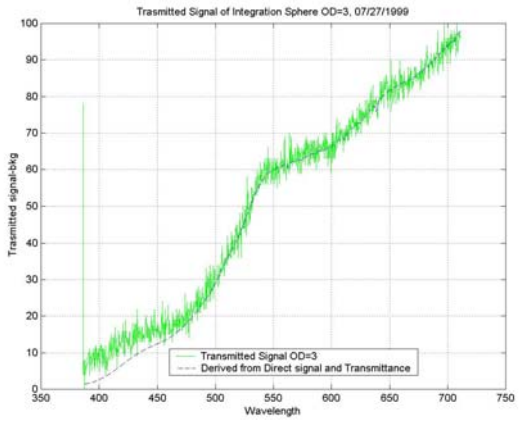

Figure 3.3.18: Comparison of the measured attenuated signals and the product of the source signal times the OL-750 measured transmittances, OD=3

D. Comments

Figure 3.3.11 shows that within the displayed dynamic range of the detector, the detector response is linear. Figure 3.3.12 to Figure 3.3.18 confirm this more precisely, assuming that the present OL-750 spectral transmittance measurements are reliable. The integrating sphere light source reduces the signal noise at short wavelengths. The linear range is from 20 to 60000 counts.

In Figure 3.3.18, the expected effect of the signal non-linearity at low signal levels is observed. The Gonio detector has a nonlinear response when the signals are below approximately 20 counts.

E. Matlab Script

```
clear
% Reads the raw data files with measurements and exposure times of the
% background, the direct source, and the measurements.
[exposure_b,bkg1]       = readfile(['Bkg10_2.dat']);

[exposure_b,directv(:,1)]       = readfile(['su0.dat']); %OD=0
[exposure_b,directv(:,2)]       = readfile(['su1.dat']); %OD=0.03
[exposure_b,directv(:,3)]       = readfile(['su2.dat']); %OD=0.1
[exposure_b,directv(:,4)]       = readfile(['su3.dat']); %OD=0.3
[exposure_b,directv(:,5)]       = readfile(['su4.dat']); %OD=0.5
[exposure_b,directv(:,6)]       = readfile(['su5.dat']); %OD=1
[exposure_b,directv(:,7)]       = readfile(['su6.dat']); %OD=2
[exposure_b,directv(:,8)]       = readfile(['su7.dat']); %OD=3

load nd990723

x = [386:(711-386)/1023:711];

for i=1:1024,
   Transmit_OD003(i)=(directv(i,1)-bkg1(i))*ND003_Transmittance2(i);
   Transmit_OD01(i)     =(directv(i,1)-kg1(i))*ND010_Transmittance2(i);
   Transmit_OD03(i)     =(directv(i,1)-kg1(i))*ND030_Transmittance2(i);
   Transmit_OD05(i)     =(directv(i,1)-kg1(i))*ND050_Transmittance2(i);
   Transmit_OD1(i)      =(directv(i,1)-kg1(i))*ND100_Transmittance2(i);
   Transmit_OD2(i)      =(directv(i,1)-kg1(i))*ND200_Transmittance2(i);
   Transmit_OD3(i)      =(directv(i,1)-kg1(i))*ND300_Transmittance2(i);
end;

plot(x,directv(:,2)-bkg1(i),'g-',x,Transmit_OD003,'b--');
legend('Transmitted Signal OD=0.03','Derived from Direct signal and
Transmittance')
title 'Trasmitted Signal of Integrating sphere OD=0.03, (1999/07/27)'
xlabel 'Wavelength'
ylabel 'Trasmitted signal-bkg'

figure
plot(x,directv(:,3)-bkg1(i),'g-',x,Transmit_OD01,'b--');
legend('Transmitted Signal OD=0.1','Derived from Direct signal and
Transmittance')
title 'Trasmitted Signal of Integrating sphere OD=0.1, (1999/07/27)'
xlabel 'Wavelength'
ylabel 'Trasmitted signal-bkg'

figure
plot(x,directv(:,4)-bkg1(i),'g-',x,Transmit_OD03,'b--');
legend('Transmitted Signal OD=0.3','Derived from Direct signal and
Transmittance')
title 'Trasmitted Signal of Integrating sphere OD=0.3, (1999/07/27)'
xlabel 'Wavelength'
ylabel 'Trasmitted signal-bkg'

figure
plot(x,directv(:,5)-bkg1(i),'g-',x,Transmit_OD05,'b--');
```

```
legend('Transmitted Signal OD=0.5','Derived from Direct signal and
Transmittance')
title 'Trasmitted Signal of Integrating sphere OD=0.5, (1999/07/27)'
xlabel 'Wavelength'
ylabel 'Trasmitted signal-bkg'

figure
plot(x,directv(:,6)-bkg1(i),'g-',x,Transmit_OD1,'b--');
legend('Transmitted Signal OD=1','Derived from Direct signal and
Transmittance')
title 'Trasmitted Signal of Integrating sphere OD=1, (1999/07/27)'
xlabel 'Wavelength'
ylabel 'Trasmitted signal-bkg'

figure
plot(x,directv(:,7)-bkg1(i),'g-',x,Transmit_OD2,'b--');
legend('Transmitted Signal OD=2','Derived from Direct signal and
Transmittance')
title 'Trasmitted Signal of Integrating sphere OD=2, (1999/07/27)'
xlabel 'Wavelength'
ylabel 'Trasmitted signal-bkg'

figure
plot(x,directv(:,8)-bkg1(i),'g-',x,Transmit_OD3,'b--');
legend('Transmitted Signal OD=3','Derived from Direct signal and
Transmittance')
title 'Trasmitted Signal of Integrating sphere OD=3, (1999/07/27)'
xlabel 'Wavelength'
ylabel 'Trasmitted signal-bkg'
```

3.4 Laser (spectral) check on Gonio detector elements (07/12/1999)

3.4.1 Background

The tests in this section address the spectral independence of the detector elements in the Gonio detector.

The Gonio detector consists of a folding mirror, a focusing lens and an Oriel Multispec II spectroradiometer. The latter spectroradiometer consists of a grating spectrograph and a 1024-pixel diode array detector. The independence of the diode array detector elements was examined in this section. It is assumed that the signal reading of one of the detector elements has no correlation with the signal reading of any other detector elements nearby. The beam from a He-Ne laser was measured to validate the assumption. The laser was aligned so that the laser beam pointed to the detector aperture directly. Two polarizers were used to attenuate the intensity of the laser. The angle between their polarization directions was about 90°, to block off most of the energy.

First, the background signal of the detector was measured. Second, two measurements of the laser source were made, with different transmitted intensities by slightly altering the relative angle of the two polarizers.

After reflection from the grating, the laser beam should be confined within a very small angle, because of the narrow laser spectrum band. Therefore, only several detector elements (near 633nm wavelength) receive the signal. Except for these elements, all

other elements should have a signal level close to that of the background signal level.

3.4.2 Measurement results

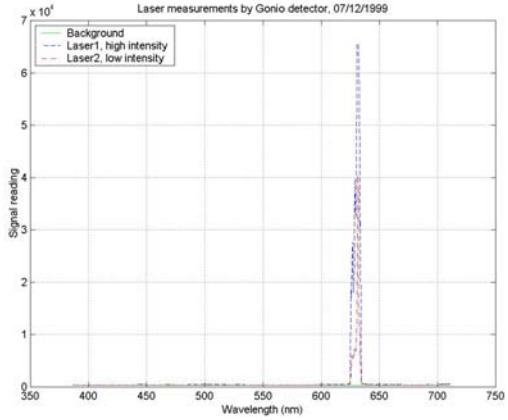

Figure 3.4.1: Signal reading of He-Ne laser irradiation. Signal attenuated by two polarizers crossed at nearly 90°.

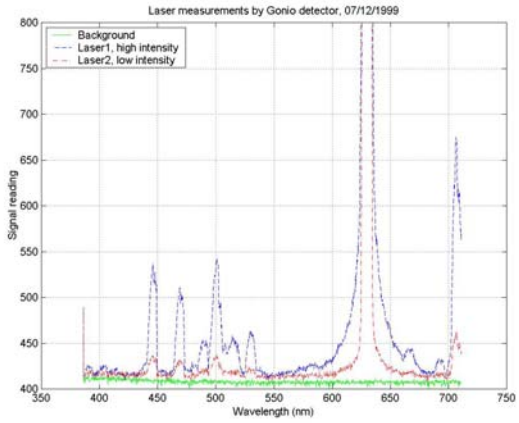

Figure 3.4.2: Signal reading of He-Ne laser irradiation (with expanded vertical axis)

3.4.3 Comments

Figure 3.4.1 and Figure 3.4.2 show that those detector elements near 633nm that received the laser beams had a reading of more than 60000 counts. The signal readings of the other detector elements were only several hundred counts. For our purposes, we conclude that the elements are essentially independent. We attribute the mysterious spikes near 400nm, 500nm, and 700nm to secondary reflections within the interior of the spectroradiometer case, which illuminate the grating at off-angles.

3.5 Measurements of detector footprint: projection of detector slit onto sample surface; spatial variation of detector sensitivity across sample surface (06/02/1999)

3.5.1 Background

It is very important to know the projection of the detector slit onto the sample surface (known as the detector footprint). The projection is the sample area that the detector actually sees. The width of the detector slit was set at 0.28mm. The height of the slit is about 10mm.

The size of the projection area can be used to determine the maximum usable grazing angle of viewing for the Gonioreflectometer. In general, the area of the detector footprint for normal viewing is about 2mm wide by 2mm high, and for viewing up to about a 70° reflection angle is about 6mm wide and 2mm high. The area is relatively small, compared with the size of the sample (127mm wide by 127mm high). However, BRDF measurements generally require view angles beyond 70°. The projection of the detector slit onto the sample at high grazing angles could be correspondingly much larger. The size of the uniform light spot produced by the light source further limits the allowable maximum grazing angle.

3.5.2 Procedure

The setup of the experiment is shown as Figure 3.5.1. A He-Ne laser and an adjustable mirror were installed on the optical breadboard. The adjustable mirror re-directed the laser beam to the center of the sample plane. Two crossed polarizers are used to attenuate

the laser beam. The diameter of the light spot on the sample plane is less than 1mm. A piece of white diffuse paper with a 20×20mm grid pattern at the center (shown in Figure 3.5.2) was mounted on the sample mount. The grid interval was 1mm.

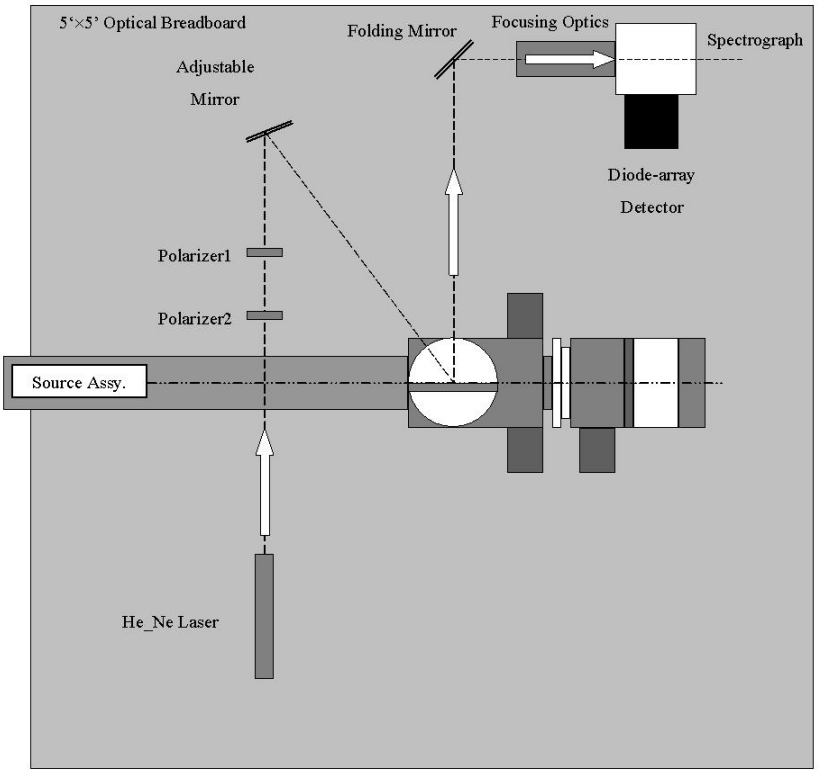

Figure 3.5.1: The setup of the experiment as viewed from above

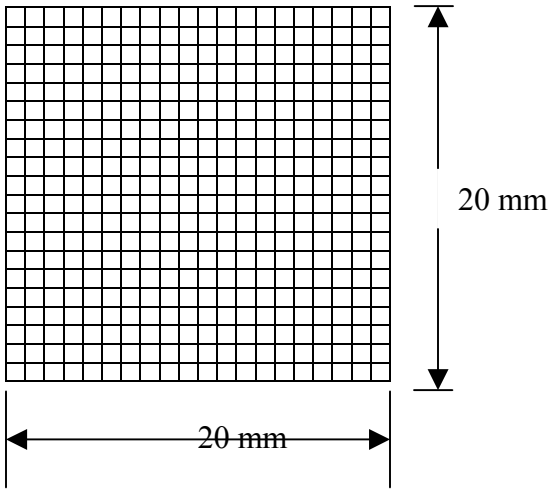

Figure 3.5.2: Grid pattern for the experiment

At the beginning, the laser beam was aligned to the center of the grid. Then the adjustable mirror was adjusted manually to move the light spot horizontally (or vertically) a small distance. Then the reflected signal was measured. The procedure was repeated about 10 times, until the detector no longer received the reflected signal. The grid on the sample plane causes the intensity of the reflected beam to vary, as the laser hits on a black grid or the blank white spaces. By recording the reflected signals, we determine the approximate size of the detector footprint. The number of peaks and valleys that are observed as the mirror is rotated yields the size of the footprint in the horizontal (or vertical) direction. The number has units of millimeters.

3.5.3 Measurement results

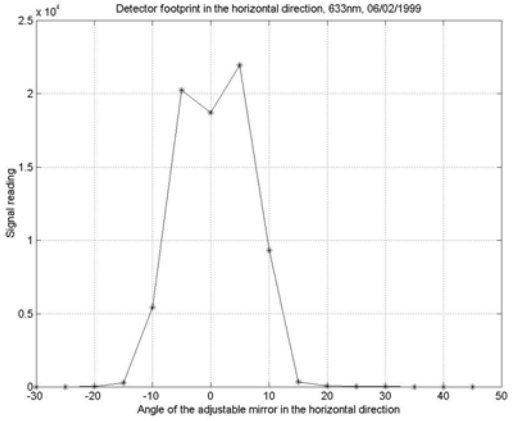

Figure 3.5.3: Detector footprint in horizontal direction; 633nm

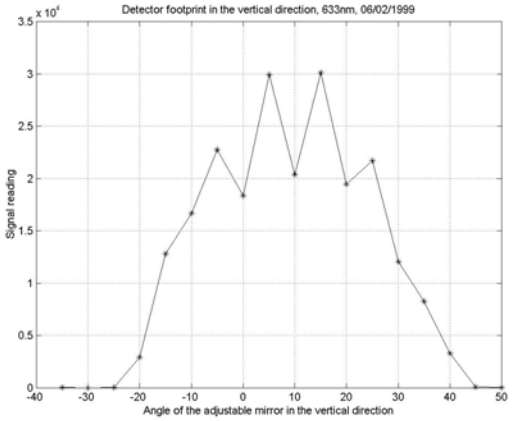

Figure 3.5.4: Detector footprint in vertical direction; 633nm

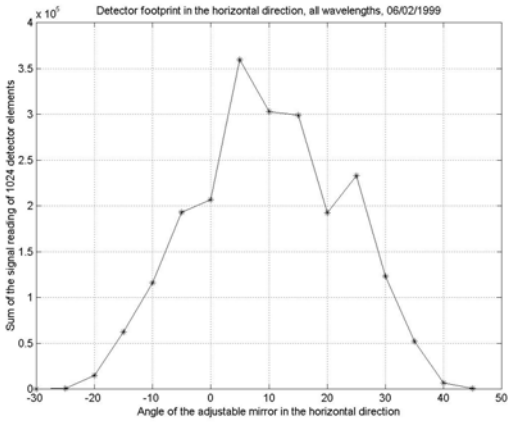

Figure 3.5.5: Detector footprint in horizontal direction; average of the readings of 1024 detector elements.

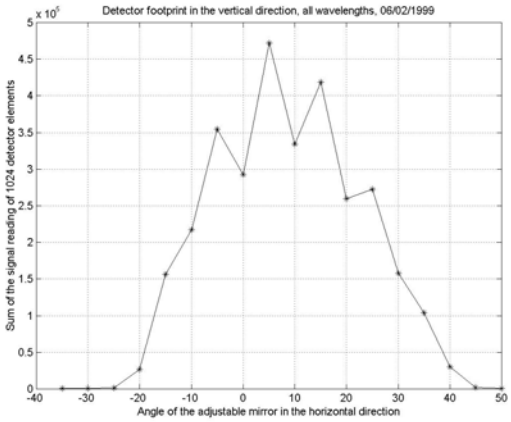

Figure 3.5.6: Detector footprint in vertical direction, average of the readings of 1024 detector elements.

3.5.4 Comments

We observe some differences between the vertical and horizontal scans. The size of the laser light spot is smaller than the detector slit. During the scans, the laser-illuminated light spot moves across the detector slit horizontally or along the detector slit vertically. In a vertical scan, the light spot is always fully inside the slit. We then expect that only one or two detector elements receive the signal. Figure 3.5.4 and Figure 3.5.6 support this idea. The detector-aggregated signal reading of all the elements is almost the same as the signal reading at 633nm wavelength. In a horizontal scan, the light spot moves

across the slit. Several detector elements receive the signal. Figure 3.5.3 and Figure 3.5.5 show that the signal reading at 633nm wavelength is not the same as the detector-aggregated signal reading. Thus, we believe the signal from one detector element (shown in Figure 3.5.3) is not adequate to estimate the detector footprint in the horizontal direction. Figure 3.5.5 and Figure 3.5.6 suggest that the detector footprint, or projection of the detector slit onto the sample, is about 4mm×4 mm when viewing a sample in a direction normal to the surface of the sample.

The detector aperture stop was about 20mm during the measurement. The detector aperture refers to the diameter of the iris located between the polarizer and the achromatic doublet of the detector assembly (shown in Figure 4.3.1).

3.6 Examination of vhbias curve, the correction curve for polarization bias of the Gonio detector (07/27/1999)

3.6.1 Background

The Gonio detector has a polarization bias. The bias depends on wavelength (i.e., detector location). A correction curve was measured and is used to compensate BRDF measurements for the bias. To obtain the correction curve, an integrating sphere was used as a light source to provide unpolarized light. A polarizer was installed before the detector to produce linearly polarized light. The signals with s and p polarization were measured. A difference between these two curves was observed. The ratio of the two curves is used to correct for the bias, which we call the 'vhbias' curve.

It was suspected that the BRDF measurement of Spectralon at 0/45 might be affected by the accuracy of the correction curve. The correction curve was measured again and the new measurement result was used to process the BRDF measurements, to study its influence.

3.6.2 Procedure

a. Carefully align the integrating sphere, to make it point to the detector folding mirror directly;
b. Launch the 'Gonio' program, wait for a while to let the system stable;
c. Measure the background signal, at 10 units exposure time;
d. Set the polarizer at s polarization direction, measure the polarized light signal, at 10 units exposure time;

e. Set the polarizer at p polarization direction, measure the polarized light signal, at 10 units exposure time;

f. Measure the background signal, at 25 units exposure time;

g. Set the polarizer at s polarization direction, measure the polarized light signal, at 25 units exposure time;

h. Set the polarizer at p polarization direction, measure the polarized light signal, at 25 units exposure time.

3.6.3 Measurement results

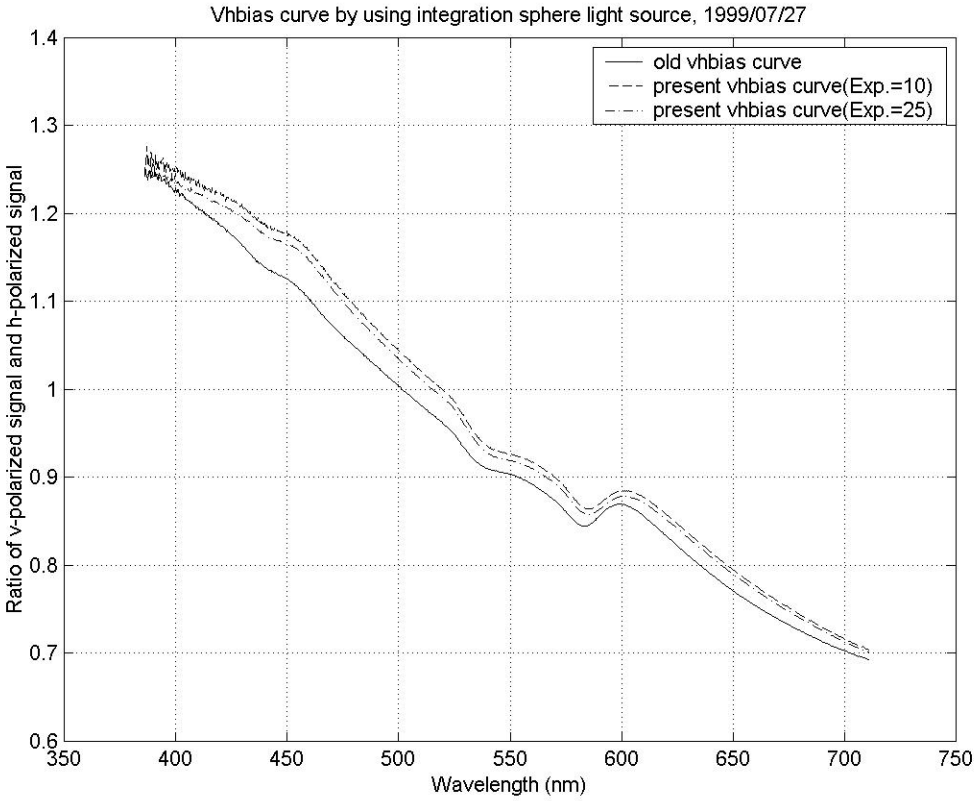

Figure 3.6.1: Comparison of the vhbias curves

3.6.4 Comments

We note that the old correction curve (measured by Foo) is almost the same as the present correction curves. The average of the present correction curves was used to process data for the BRDF measurement of Spectralon at 0/45. The BRDF values were the same with the old and present correction curves. Thus, we conclude that the BRDF measurement is not sensitive to the polarization correction curve.

Thus, the old correction curve is still valid. It is recommended to check it once a year. The properties of the detector and the polarizer might change over long time periods.

3.7 Influence of detector slit on BRDF measurements

To study the effect of the detector slit on the performance of the detector, the BRDF of the Spectralon sample was measured. The size of the detector slit was varied (0.6mm, 0.28mm and 0.05mm). For measurement, we use the recommended relative measurement method, which is described more fully in Chapter 7.

The measured BRDF was integrated numerically over the reflection hemisphere to get the directional-hemispherical reflectance. Subsequently, the spectrum of the reflectance was "corrected" with the recommended relative method. The corrected directional-hemispherical reflectances for the three different slit sizes are shown in Figure 3.7.1, with the OL-750 measurements as reference.

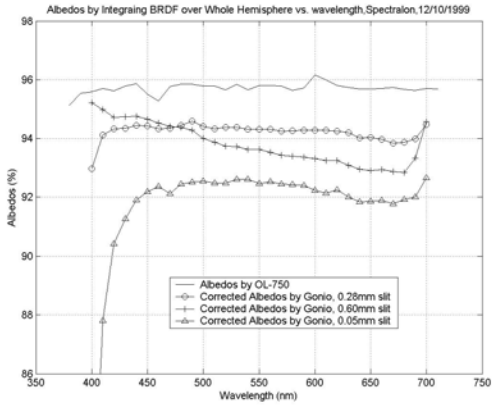

Figure 3.7.1 Comparison of directional-hemispherical reflectance of Spectralon, obtained with the OL-750 reflectometer and the Gonioreflectometer (θ_i=10 and with three detector slits).

The albedos measured by the OL-750 reflectometer are believed to be accurate, with less than a 0.5% error over the entire visible wavelength range. For the corrected reflectances, Figure 3.7.1 shows that the 0.6mm slit leads to some spectral bias; the 0.28mm slit produces the best result, which have a correct spectral variation but 2% error in magnitude; the 0.05mm slit produced the correct spectrum but has a larger error in

magnitude. We assume that the radiance and the spectrum along the detector slit are uniform. In that case, the size of the detector slit should not affect the BRDF measurements. However, the BRDF measurements of Spectralon with different detector slits showed that the assumption might not be true.

To explain the phenomenon described above, for the Spectralon sample, we tried to verify that spectral reflectance measurements for different reflection directions into the reflection hemisphere were the same. For each of three detector slits, we took spectral measurements for 273 different reflection directions (actually half of the reflection hemisphere). Among these, we chose two and compare them in Figure 3.7.2 to Figure 3.7.4, for each slit case. One measurement position is close to the normal direction (θ_i=0°;θ_r=10°) and the other is close to the grazing angle (θ_i=0°;θ_r=80°).

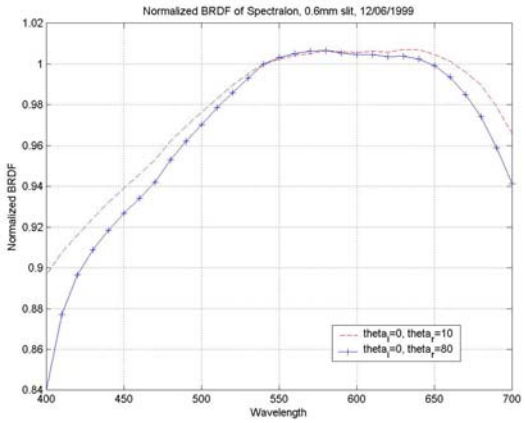

Figure 3.7.2 Comparison of the normalized spectral distribution of 2 exposures, 0.6mm slit

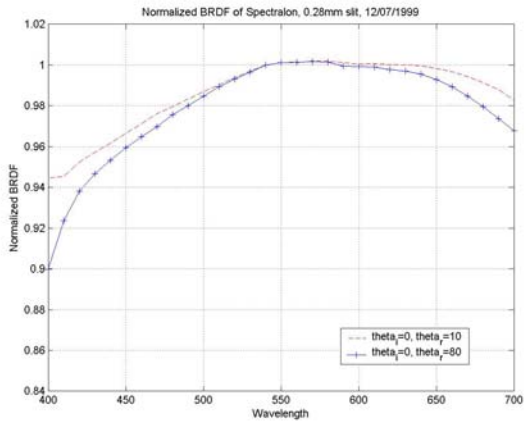

Figure 3.7.3 Comparison of the normalized spectral distribution of 2 exposures, 0.28mm slit

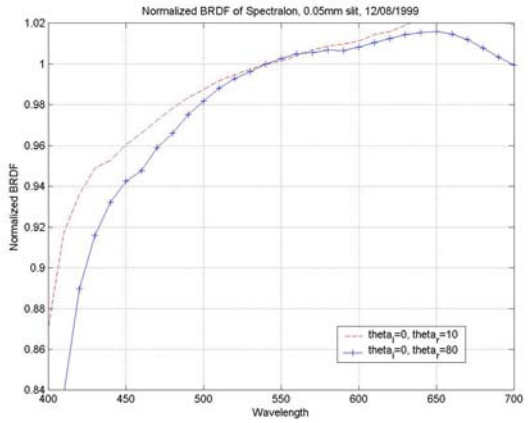

Figure 3.7.4 Comparison of the normalized spectral distribution of 2 exposures, 0.05mm slit

Figure 3.7.2 to Figure 3.7.4 show that the spectral reflectance measurements at 0/10 and 0/80 are different. This is unexpected because the Spectralon sample should have a nearly constant (i.e., neutral) spectral reflectance, for various orientations into the reflection hemisphere. Moreover, the three slits produce different spectral patterns. Thus, we have two problems to explain:

(a) Why do the spectral measurements differ at different reflection angles?

(b) How does the slit size affect these measurements?

For the problem (a), a tentative explanation is given as the following:

$\theta_i = 0°$ and $\theta_r = 10°$.

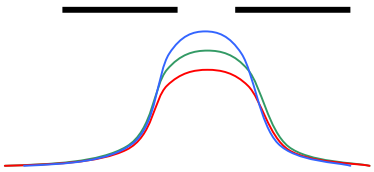

$\theta_i = 0°$ and $\theta_r = 80°$.

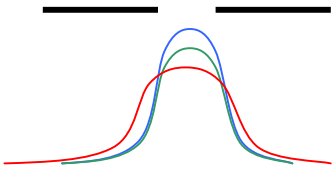

Figure 3.7.5 Distribution of radiance incident onto the detector slit, at different wavelengths

The color curves in Figure 3.7.5 represent the distribution of the radiance incident onto the detector slit, at three different wavelengths. When the detector approaches a grazing angle (θ_i=0°, θ_r=80°), the size of the illuminated spot on the sample surface looks narrower. Its projection on the slit plane might get narrower too. If the radiance at different wavelengths has different foci, as shown in Figure 3.7.5, it might lead to a spectral bias.

If the spectrum of the reflected radiance over the detector slit is not uniform, the problem (b) could be explained too. But there are other possibilities. The peaks of the different wavelengths might not overlap. To verify the tentative explanation, we conducted the following experiments.

First, we measured the spectrum of the light source, with three different slits. The normalized direct measurements of light sources are shown in Figure 3.7.6.

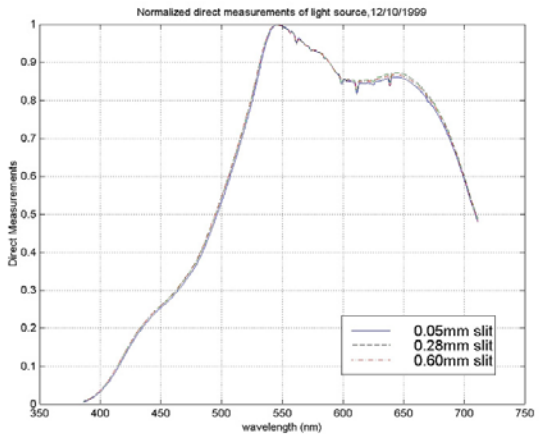

Figure 3.7.6 Normalized direct measurements of light source, by different detector slits

Figure 3.7.7 shows the curves of the measurements with 0.05mm and 0.28mm slits, all normalized by the curve for the 0.6mm slit. The purpose is to show the relative positions of the three sets of measurements.

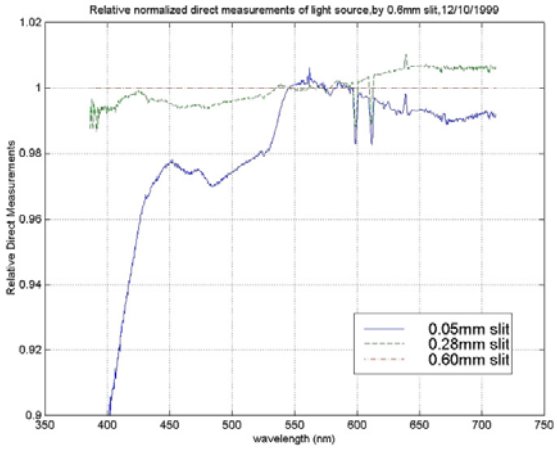

Figure 3.7.7 Relative normalized direct measurements of light source, by different detector slits

These measurements show that the direct measurements of the light source radiance depend on the size of the slit. The magnitude error over the spectrum might be over 10%. The only explanation is that the distributions of the incident radiance across the detector slit are different at different wavelengths.

Secondly, we chose ($\theta_i = 0°$, $\theta_r = 10°$) and ($\theta_i = 0°$, $\theta_r = 80°$) to measure the reflection of Spectralon, by three slits. The BRDF measurements are shown in Figure 3.7.8 and Figure 3.7.9.

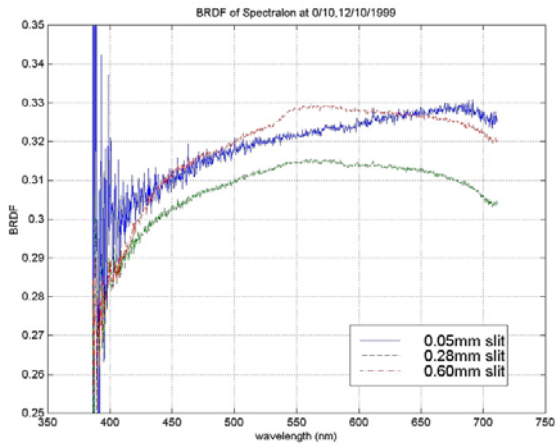

Figure 3.7.8 BRDF of Spectralon at 0/10, by three detector slits

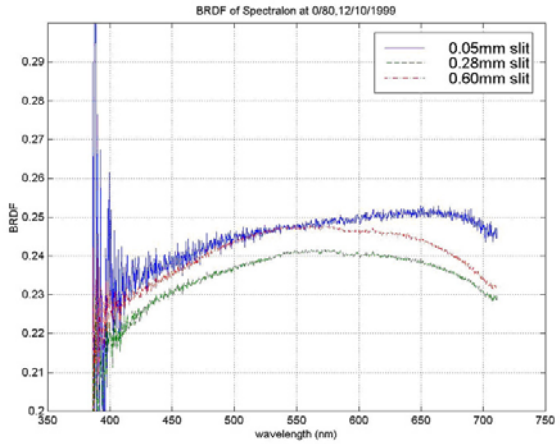

Figure 3.7.9 BRDF of Spectralon at 0/80, by three detector slits

Comparing Figure 3.7.8 and Figure 3.7.9, we can see that the magnitudes of these two measurements differ. In the measurements with 0.6mm slit, the spectra at different reflection angles are fairly different. But in the case of 0.05mm slit and 0.28mm slit, the spectrum shows no considerable change for the two reflection angles. The result supports our explanation: when the slit is small enough, the angular configuration does not have a strong influence on the spectrum measurements. However, too small a slit reduces the

intensity of the incident light, with strong noise, as shown in Figure 3.7.9. Therefore, the 0.28 slit is chosen as the recommended slit for the detector. For the BRDF measurements in Section 7.6, the detector slit was set at 0.28mm.

Chapter 4

Validation of the Gonioreflectometer: The Light Source

In this chapter, we examine the Gonio light source. By replacing the Gonio light source with an integrating sphere light source, we found that the Gonio light source is the primary source of the spectral bias in the BRDF measurements of the Spectralon sample (Section 4.2).

The influence of the light source and detector apertures is studied and the instrument signature is obtained (Section 4.3). These two apertures were set empirically so that the solid angle of the light source would match that of the detector, to achieve maximum angular resolution of the reflected light fields. However, well-matched apertures make the measurements more sensitive to misalignments of the Gonio light source, the Gonio detector, and the angular positioning of the motors.

We also examine the chromatic aberrations of the light source (Section 4.4). The chromatic aberrations refer to a spectrally non-uniform focusing of the light source, so that the focal point and its shape depend on wavelength. Only slight chromatic aberrations were observed when the solid angles of the light source and the detector are matched.

The foregoing observations provide strong guidance in the selection and implementation of a BRDF measurement method. In particular, to eliminate the spectral bias of the light source, a relative measurement method is selected. The method is described in Chapter 7.

4.1 BRDF of Spectralon at 0/45 using the Gonio light source (07/01/1999)

4.1.1 Background

In Section 2.3, we repeated Foo's measurement of the BRDF of the Spectralon sample over the visible spectrum at normal incidence and a 45° reflection angle (0/45). The Spectralon sample should be very Lambertian and have a flat reflected spectrum (within 0.5%) over the visible wavelength region. However, our spectral measurements showed a severe bias. To illustrate the problem, the following additional experiments were carried out.

The 0/45 BRDF of the Spectralon sample was again measured by the Gonioreflectometer. The relative measurement method recommended in Chapter 7 was not used so a spectral bias still exists in the BRDF measurements. The directional-hemispherical reflectance of the sample was measured by using the OL-750 hemispherical-directional reflectometer. The latter measurements should be accurate to ±0.5% for the Spectralon sample.

4.1.2 Measurement results

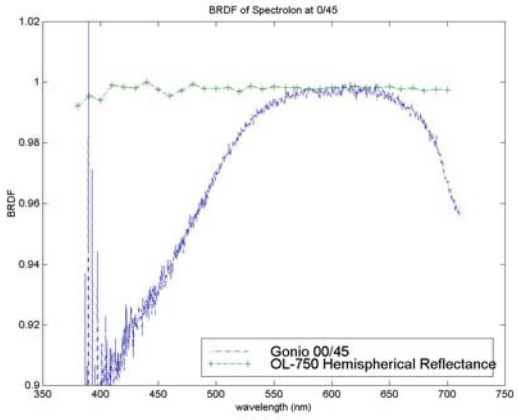

Figure 4.1.1: Spectrum comparison of the normalized BRDF measurement by Gonio and the normalized directional-hemispherical reflectance by the OL-750 reflectometer

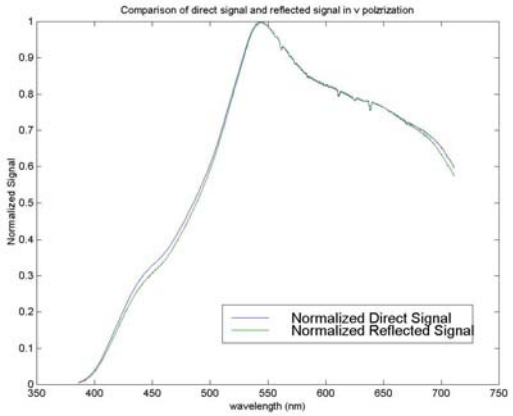

Figure 4.1.2. The direct light-source irradiance and the reflected radiance from Spectralon, both in s polarization and both curves normalized by the curve maxima

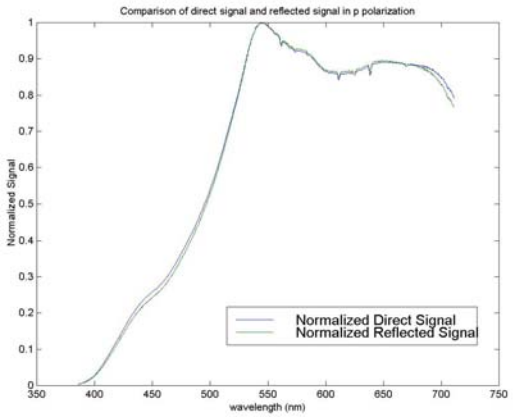

Figure 4.1.3. The direct light-source irradiance and the reflected radiance from Spectralon, both in p polarization and both curves normalized by the curve maxima

4.1.3 Comments

The directional-hemispherical reflectance measured by the OL-750 instrument shows a level reflectance spectrum in Figure 4.1.1, which is consistent with the known properties of Spectralon. However, we have a spectral bias in the (0/45) BRDF measurement by the Gonioreflectometer. Both curves in Figure 4.1.1 were normalized by their respective maxima. Although they are two different physical quantities, they should have very similar spectral distributions. Figure 4.1.1 reveals up to a 10% spectral bias in the Gonio BRDF measurement, which is far more than the 0.5% magnitude error of the OL-750

reflectometer.

Normalized spectral distributions of the light source direct irradiance and the reflected radiance from the Spectralon are shown in Figure 4.1.2 and Figure 4.1.3, respectively, for the s and p components of polarization. (s and p mean perpendicular and parallel, respectively, to the place of incidence.) In each figure, the irradiance and reflected radiance are very close together in magnitude and shape. However, the slight difference between the curves leads to a large percentage difference at short and long wavelengths. The foregoing differences are the source of the large spectral bias in Figure 4.1.1.

Our task is to study why the light source irradiance has a different spectral distribution from the reflected radiance. Extensive work has been done to solve the problem. Most of the experiments mentioned in this report are related to the issue (and were generally carried out before the experiments reported in this section).

4.2 BRDF of Spectralon at 0/45 using an integrating sphere light source (08/09/1999)

4.2.1 Background

To study the spectral bias of the Gonio light source, an integrating sphere light source was used to conduct the BRDF measurements of Spectralon at 0/45, using the Gonioreflectometer. The integrating sphere has a spatially uniform and stable light energy output. The integrating sphere replaced the Gonio light source. By comparing measurements made using the Gonio and integrating sphere light sources, we can evaluate the source of error in the light source irradiance measurements.

4.2.2 Procedure

a. Align the integrating sphere to the Gonio detector;

b. Measure the background signal with exposure time 1;

c. Measure the direct signal at p polarization, with exposure time 1;

d. Measure the direct signal at s polarization, with exposure time 1;

e. Move the integrating sphere to 45°, without unplugging the power, align it to make it point to the sample;

f. Measure the reflected signal at p polarization, with exposure time 500;

g. Measure the reflected signal at s polarization, with exposure time 500;

h. Measure the background signal with exposure time 500.

i. Measure the reflected signal at p polarization, with exposure time 2000;

j. Measure the reflected signal at s polarization, with exposure time 2000;

k. Measure the background signal with exposure time 2000.

4.2.3 Measurement results

A. Validation of integrating sphere light source

The integrating sphere light source was carefully aligned before we used it for BRDF measurements. We examined stray light, the intensity error related to angular alignment, and the effect of the distance between the integrating sphere and the sample.

Stray light. The integrating sphere light source is a diffuse illumination source. To reduce stray light, a hollow, tubular extension was installed in front of the output port of the integrating sphere to act as a light source aperture. The hollow tube was 100mm in inner diameter and 170mm long. However, some stray light escaped from the ends of the extension. To examine the stray light, the end of the extension was blocked off. The Spectralon sample was mounted on the sample mount. The reflected light from the Spectralon was measured. The signal readings were compared with the background signal. No large difference was observed. Thus, we conclude that stray light originating from the apertured light source is negligible.

Angular intensity error. Due to the simple positioning mechanism of the integrating sphere light source, we were unable to align it to the Gonio detector as well as we could align the Gonio light source to the Gonio detector. We wanted to verify that a small angular error of alignment did not lead to severe irradiance errors.

At first, the integrating sphere was carefully aligned to the Gonio detector. The direct spectral irradiance was measured with the Gonio detector. The integrating sphere was then moved sideway in steps of 13mm (or 0.5-inch), in a direction perpendicular to its

optical axis. The direct irradiance was measured after each move. The procedure was repeated for the other lateral direction. The results show that the spectral distribution (magnitude and shape) was unchanged for ±13mm of lateral motion, and changed by 2% or less for ±26mm of lateral motion. Thus, the direct irradiance measurements of the integrating sphere light source are not sensitive to lateral position and angle.

Distance. The light source arm of the Gonioreflectometer guarantees that the distance between the light source and the sample is constant during a measurement. It is hard to meet this requirement when using the integrating sphere light source. Therefore, two direct irradiance measurements of the integrating sphere were conducted. The distance between the integrating sphere and the Gonio detector was doubled ("Distance2") compared to the original setup ("Distance1," about 1.2m). The two irradiance measurements have virtually the same magnitude and spectrum, as shown in Figure 4.2.1.

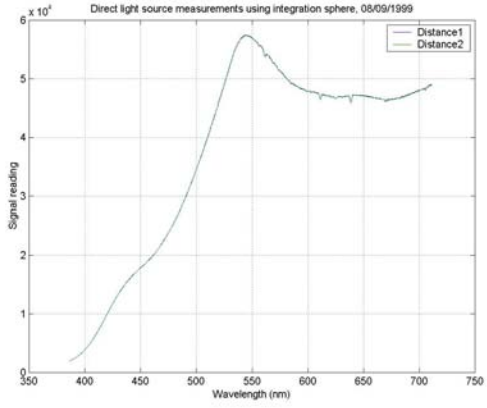

Figure 4.2.1: Spectrum comparison of the direct irradiance measurements of the integrating sphere with different distances

The integrating sphere is a diffuse light source. The emergent radiance should not vary with angle from the optical axis, or with distance from the light source. These characteristics were verified by the previous two tests.

B. BRDF Measurements

Using the integrating sphere light source, we measured the BRDF of Spectralon at 0/45. The result is compared to the 0/45 BRDF obtained by the Gonio light source in Figure 4.2.2.

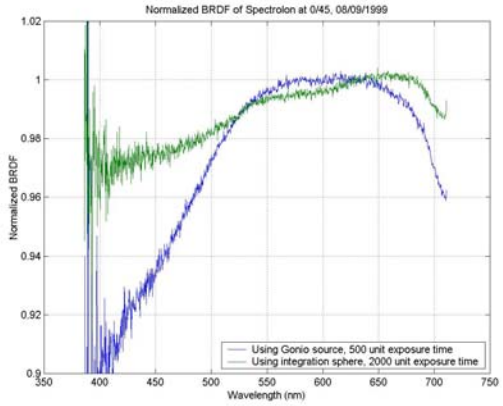

Figure 4.2.2: Comparison of normalized BRDF of Spectralon at 0/45 over the visible wavelengths, by Gonio light source and by integrating sphere

The output radiance of the integrating sphere is much lower than that of the Gonio light source. The lower signal level produces strong noise in the BRDF measurements, especially at short wavelengths. To reduce the noise, we repeated the measurements with longer exposure time, also using the integrating sphere light source. The results are presented and compared in Figure 4.2.3.

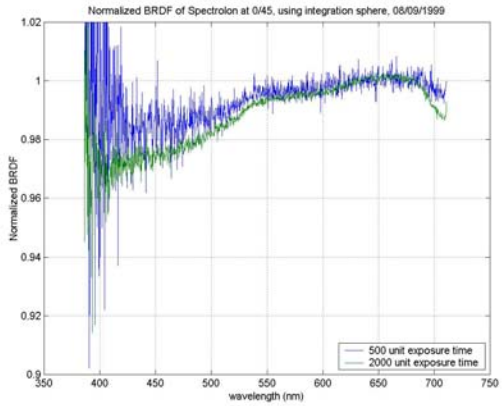

Figure 4.2.3: Comparison of normalized BRDF of Spectralon at 0/45 over the visible wavelengths, using the integration sphere, for two different exposure times

4.2.4 Comments

The integrating sphere was used to measure the 0/45 BRDF of the Spectralon sample. Figure 4.2.2 shows that the spectral bias of the BRDF measurements was reduced from about 10% with the Gonio light source to about 2% with the integrating sphere light source, over the wavelength range of 450~700nm. We thus conclude that the direct irradiance measurement of the light source is the primary source of the spectral bias in the BRDF measurements.

By repeating the measurements at longer exposure times (Figure 4.2.3) for the integrating sphere light source, we could further reduce the spectral bias, to the level of about 1%. It is possible that the non-linear response of the detector to exposure time contributes to the balance of the error.

4.2.1 Matlab Script

```
clear
% By integrating sphere
% Reads the raw data files with measurements and exposure times of the
% background, the direct source, and the measurements.
[exposure_b,bkg28]    = readfile(['bkg28.dat']);
[exposure_b,bkg2k]    = readfile(['bkg2k.dat']);
[exposure_u,direct_v]      = readfile(['directv.dat']);
[exposure_n,direct_h]      = readfile(['directh.dat']);

[exposure_v,measurement_v2] = readfile(['meas2_v.dat']);
[exposure_h,measurement_h2] = readfile(['meas2_h.dat']);

%load vhbias[1024]
load vhbias.mat

%Solid Angle
SolidAngle = 3.837e-004

%Calculate the bidirectional reflectance
for i=1:1024,
   V0(i)= 0.5*((direct_v(i)-bkg28(i))/vhbias(i)+(direct_h(i)-
bkg28(i)))/28;
   Vn(i)= 0.5*((measurement_v2(i)-
```

```
bkg2k(i))/(vhbias(i)*2000)+(measurement_h2(i)-bkg2k(i))/2000);
   fr2(i)=Vn(i)/(V0(i)*SolidAngle);
end;

%By Gonio source
[exposure_b,bkg001]    = readfile(['B1.dat']);
[exposure_b,bkg500]    = readfile(['B500.dat']);

[exposure_u,direct_v]      = readfile(['directv1.dat']);
[exposure_n,direct_h]      = readfile(['directh1.dat']);

[exposure_v,measurement_v] = readfile(['meas_v.dat']);
[exposure_h,measurement_h] = readfile(['meas_h.dat']);

for i=1:1024,
   V0(i)= 0.5*((direct_v(i)-bkg001(i))/vhbias(i)+(direct_h(i)-
bkg001(i)));
   Vn(i)= 0.5*((measurement_v(i)-
bkg500(i))/(vhbias(i)*exposure_v)+(measurement_h(i)-
bkg500(i))/exposure_h);
   fr1(i)=Vn(i)/(V0(i)*SolidAngle);
end;

%plot
x=[386:(325/1023):711];
plot(x,fr1/mean(fr1(600:800)),x,fr2/mean(fr2(700:900)));
legend('By Gonio Source, Exp.=500','By Integrating sphere,Exp.=2000');
title 'Normalized BRDF of Spectrolon at 0/45';
xlabel 'wavelength (nm)';
ylabel 'Normalized BRDF';
axis([350 750 0.9 1.02]);
```

4.3 Influence of light source and detector apertures on instrument signature and BRDF measurements of Spectralon at 0/45 (04/02/1999)

4.3.1 Background

The detector aperture (herein referred to as Aperture 1) refers to the inner diameter of the iris that is located between the polarizer and the achromatic doublet of the detector assembly (shown in Figure 4.3.1). The light source aperture (herein referred to as Aperture 2) refers to the inner diameter of the iris located between the Nikkor lens and the aspheric lens of the light source (shown in Figure 4.3.2). (Note: the Nikkor lens of the light source also has an iris, which is kept at its full aperture)

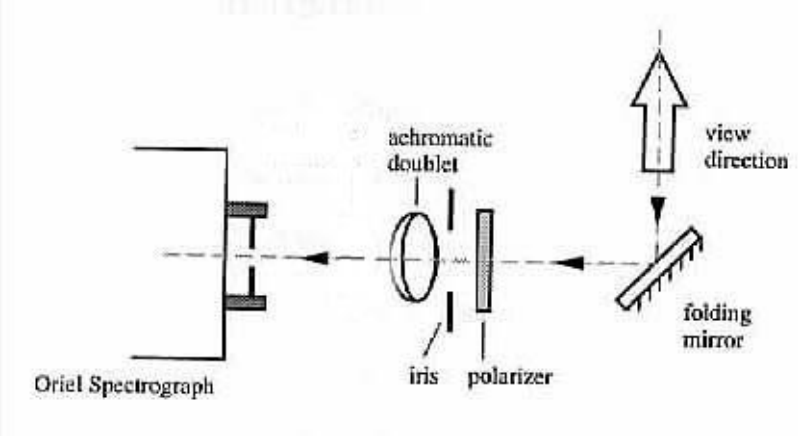

Figure 4.3.1: Schematic of the detector's focusing optics. The inner diameter of the iris is called Aperture 1. [Figure 6.1 of Foo's thesis]

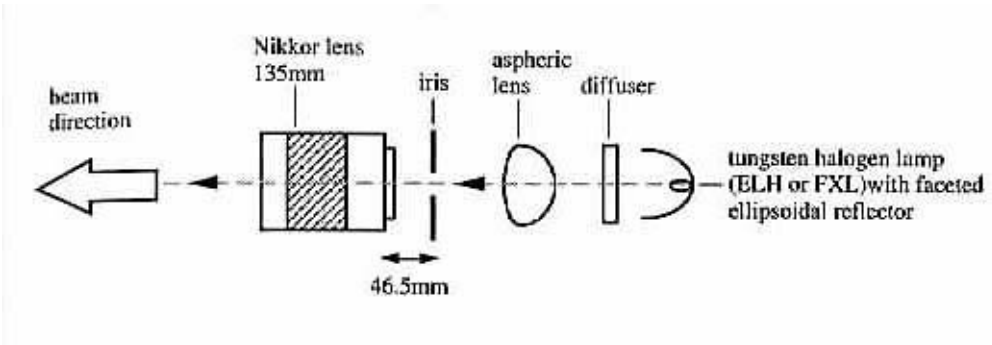

Figure 4.3.2: Schematic of the light source assembly. The inner diameter of the iris is called Aperture 2. [Figure 5.1 of Foo's thesis]

Foo realized that the angular resolution of the Gonioreflectometer is related to the light source and detector apertures. He empirically determined the combination of these apertures that gave the best angular resolution.

To determine the influence of the light source and detector apertures, two series of experiments were carried out for the present report. The first series of experiments measured the BRDF of a Spectralon sample at 0/45 (illumination/reflection) and the instrument signature, with constant Aperture 2 (2.54mm diameter) and varying Aperture 1. The diameter of Aperture 1 was set at 10mm, 14mm, 20mm, and 28mm, so that the area of Aperture 1 is doubled between each step. The second series of experiments measured the BRDF of Spectralon and the instrument signature, with constant Aperture 1 (20mm diameter) and varying Aperture 2 (2.54mm, 3.56mm, 5.08mm, and 7.11mm diameter).

A simulation program was written to calculate the instrument signature by using a simple two-overlapping-disks theory. The theory presumes that the instrument signature may be estimated by the overlap area between two disks, of the same or different diameters. One of the disks moves along a line connecting the centers of the two disks, and transects the second disk. The moving disk plays the role of the light source beam, and the fixed disk plays the role of the detector collection beam. The program provides the "aperture convolution." This model explains the experimental measurements very well. The incident and collection solid angles are almost the same when Aperture 1 is 20mm and Aperture 2 is 2.54mm. Other pairs of apertures would also match the solid angles.

4.3.2 Procedure

The instrument signature and the BRDF measurement of Spectralon at 0/45 are obtained using the procedures in Section 2.1 *Measurements of the instrument signature: scanning of the incident beam in the absence of a test sample, θ_3=178 to180° (03/08/1999)* and Section 2.3 *BRDF measurements of Spectralon (03/08/1999)*.

4.3.3 Results

The effect of varying the detector aperture (Aperture 1) while holding the source aperture (Aperture 2) fixed at 2.54mm is shown in Figure 4.3.3 to Figure 4.3.10. The converse effect of holding the detector aperture (Aperture1) fixed at 20mm while varying the source aperture (Aperture 2) is shown in Figure 4.3.11 to Figure 4.3.18. The simulated aperture convolution is shown in the upper graphs, together with the measurements. The lower graphs show the measured BRDFs, which are normalized and graphed in Figure 4.3.19 and Figure 4.3.20 at the end.

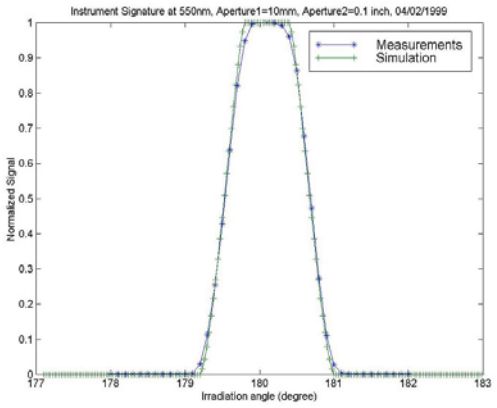

Figure 4.3.3: Instrument signature: Aperture 1=10mm; Aperture 2=2.54mm.

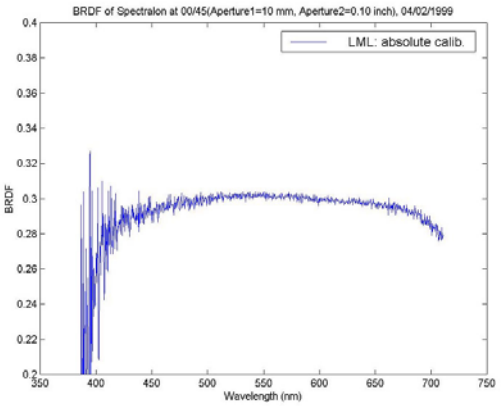

Figure 4.3.4: BRDF of Spectralon at 0/45: Aperture 1=10mm; Aperture 2=2.54mm.

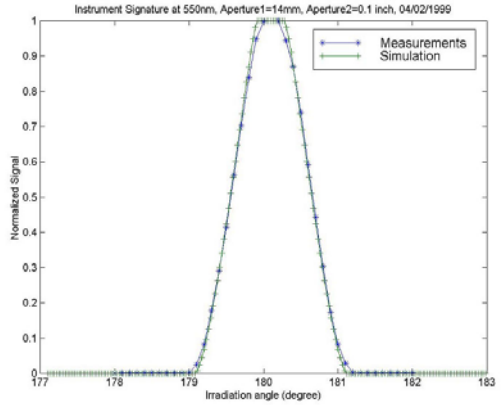

Figure 4.3.5: Instrument signature: Aperture 1=14mm; Aperture 2=2.54mm.

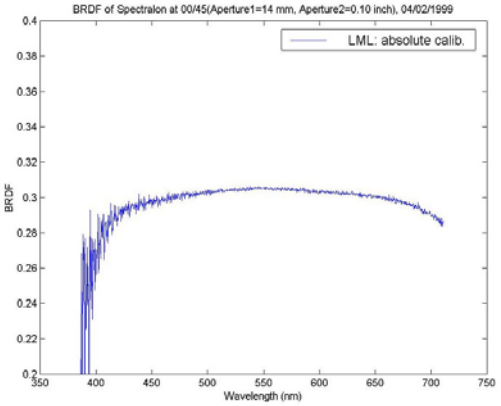

Figure 4.3.6: BRDF of Spectralon at 0/45: Aperture 1=14mm; Aperture 2=2.54mm.

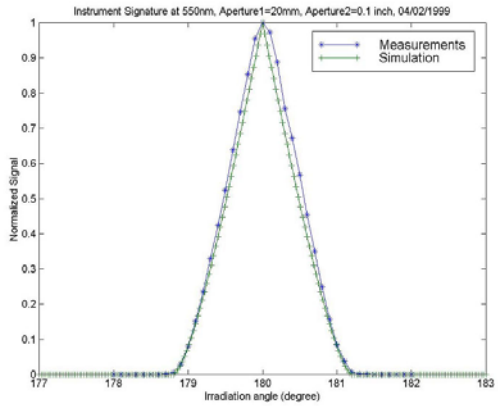

Figure 4.3.7: Instrument signature: Aperture 1=20mm; Aperture 2=2.54mm.

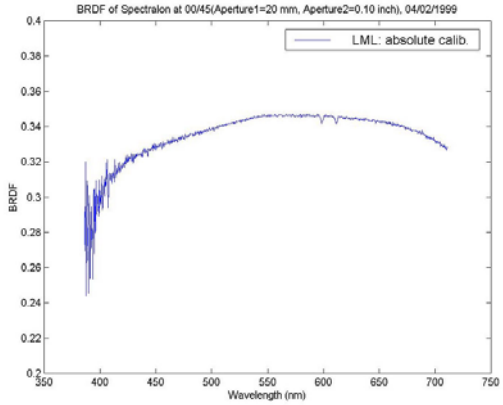

Figure 4.3.8: BRDF of Spectralon at 0/45: Aperture 1=20mm; Aperture 2=2.54mm.

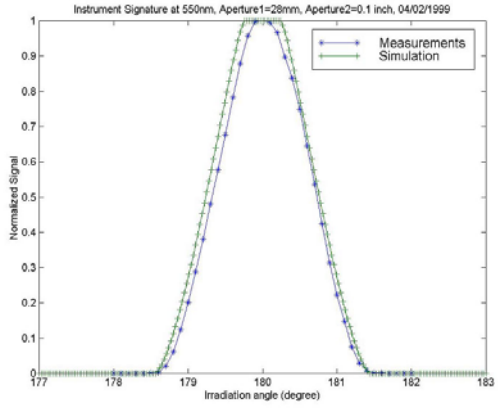

Figure 4.3.9: Instrument signature: Aperture 1=28mm; Aperture 2=2.54mm.

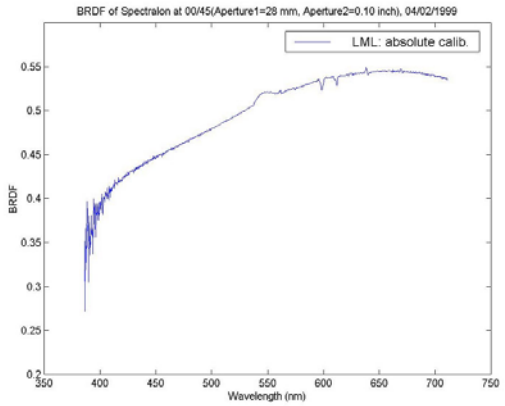

Figure 4.3.10: BRDF of Spectralon at 0/45: Aperture 1=28mm; Aperture 2=2.54mm.

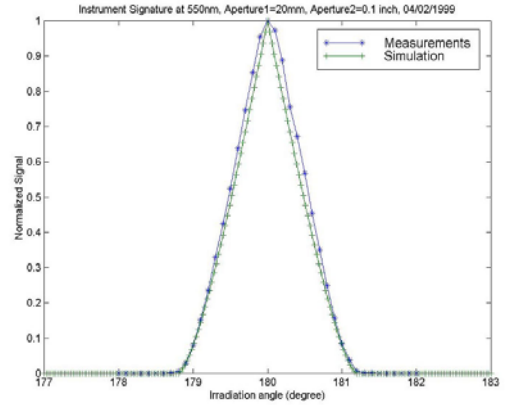

Figure 4.3.11: Instrument signature: Aperture 1=20mm; Aperture 2=2.54mm.

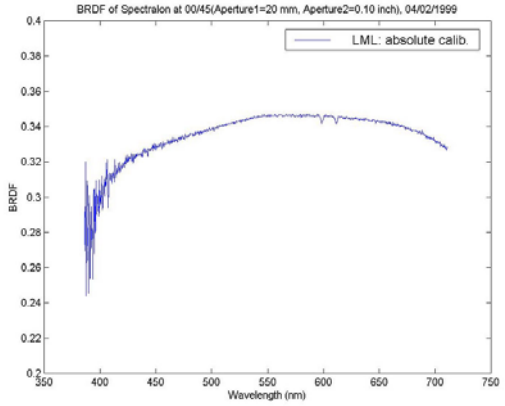

Figure 4.3.12: BRDF of Spectralon at 0/45: Aperture 1=20mm; Aperture 2=2.54mm.

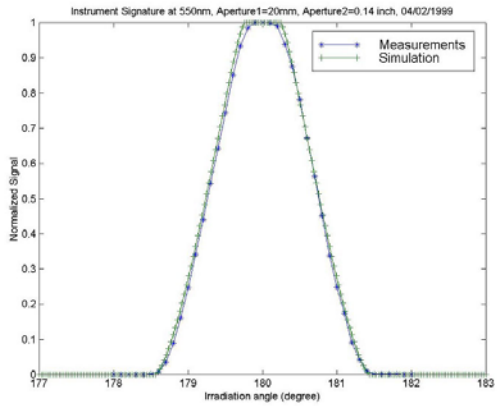

Figure 4.3.13: Instrument signature: Aperture 1=20mm; Aperture 2=3.56mm.

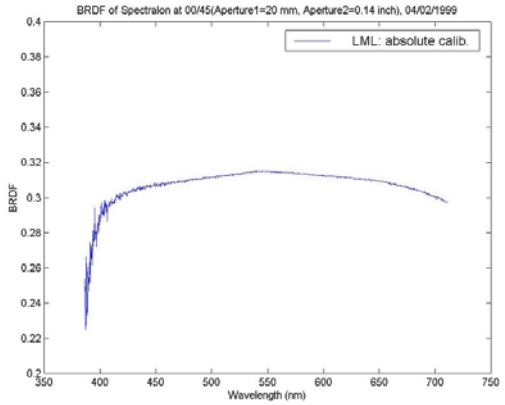

Figure 4.3.14: BRDF of Spectralon at 0/45: Aperture 1=20mm; Aperture 2=3.56mm.

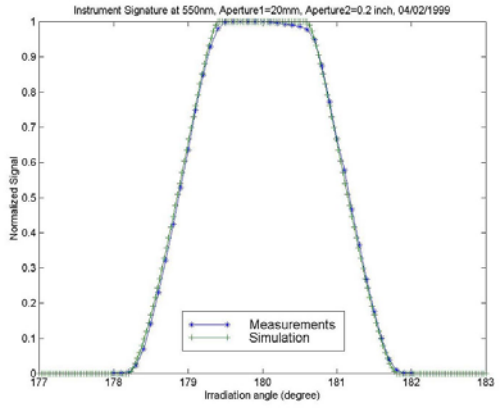

Figure 4.3.15: Instrument signature: Aperture 1=20mm; Aperture 2=5.08mm.

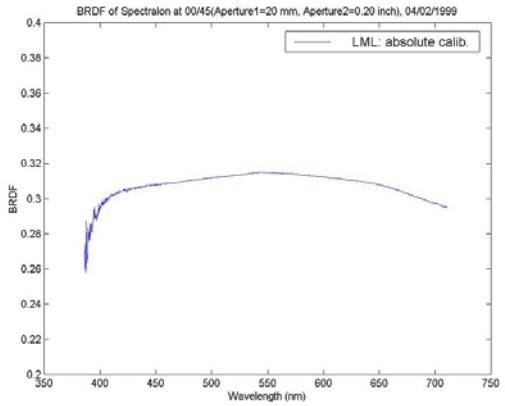

Figure 4.3.16: BRDF of Spectralon at 0/45: Aperture 1=20mm; Aperture 2=5.08mm.

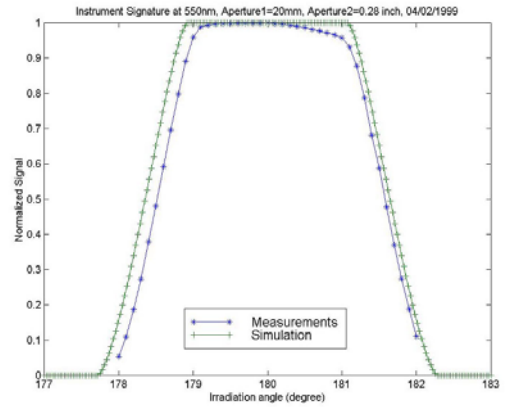

Figure 4.3.17: Instrument signature: Aperture 1=20mm; Aperture 2=7.11mm.

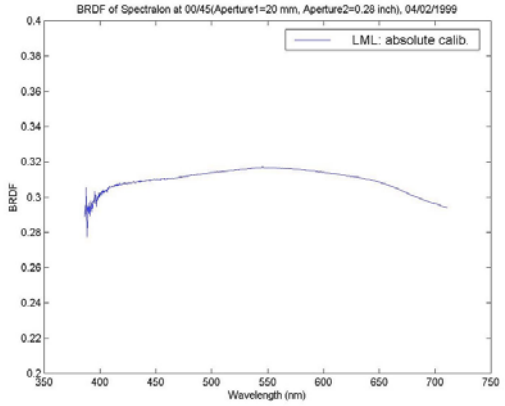

Figure 4.3.18: BRDF of Spectralon at 0/45: Aperture 1=20mm; Aperture 2=7.11mm.

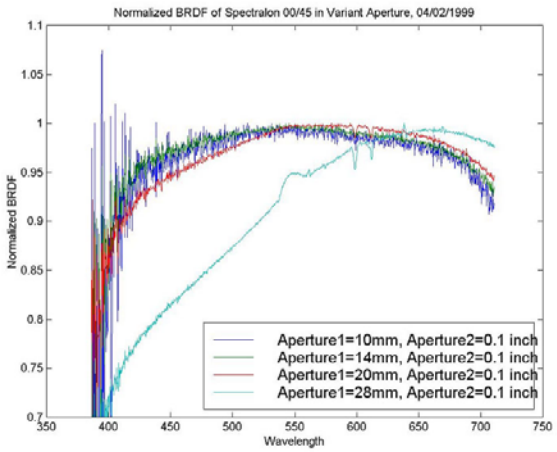

Figure 4.3.19: Comparison of normalized BRDFs at various detector apertures (Aperture1)

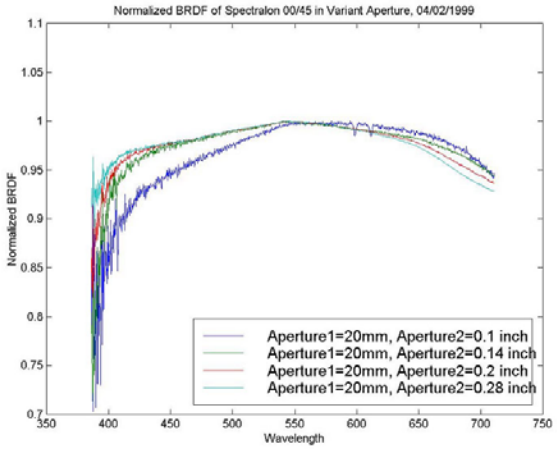

Figure 4.3.20: Comparison of normalized BRDFs at various light source apertures (Aperture2)

4.3.4 Comments

Figure 4.3.3 through Figure 4.3.18 reveal that the light source and detector apertures both have a strong influence, as expected, on the instrument signature and surprisingly, on the BRDF measurements.

With constant Aperture 2 and varying Aperture 1: When Aperture 1 is 10mm, the detector aperture is so small that the received signals in the BRDF measurements are close to the noise signals. Thus, we observe strong noise, while the mean value of the

BRDF is nearly correct (i.e. uniform). When Aperture 1 is more than 20mm, significant error is introduced by chromatic aberrations of the detector lens and over-exposure of the detector elements. The small bump shown in Figure 4.3.10 in the BRDF measurements with Aperture 1 at 28mm is due to the saturated sensor. Thus, the preferred detector aperture should be between 10 and 20 mm, and should be as large as possible to receive a higher signal. The BRDF measurements with constant Aperture 2 and variant Aperture 1 were normalized and are shown in Figure 4.3.19. With large Aperture 1, a strong spectral bias (about 25% variation) appears. Again, the best results correspond to a low noise in the signal and a nearly uniform BRDF: that is, Aperture 1 between 14mm and 20mm.

With constant Aperture 1 and varying Aperture 2: The spectral bias is about 10%. A large light source aperture (Aperture 2) can make the solid angle of the light source larger than that of the detector. In Figure 4.3.11 and Figure 4.3.12, the two solid angles are almost matched. In subsequent figures, the source solid angle is larger than the detector solid angle. Since part of the illuminated area on the sample is not viewed by the detector, the reflected radiance is not measured accurately or correctly. Also, the diameter of the light source beam, when directed at the detector, is larger than the diameter of the polarizer in front of the detector. Therefore, the direct measurement of the light source irradiance is not reliable. Although a large light source aperture has some errors, it has some advantages also. The signal noise levels are reduced, and the measurements of the reflected radiance are less sensitive to angular positioning errors, due to the solid angle of the light source.

Foo empirically set the light source and detector apertures so that the solid angle of the detector is slightly larger than that of the light source. His instrument signature (Figure 2.1.2) is close to that of Figure 4.3.15. Therefore his BRDF measurements of Spectralon (Figure 2.3.3) are very different from the present measurements (Figure 2.3.4), due primarily to the change of the detector aperture relative to that of the light source.

4.4 Chromatic aberrations of Gonio light source (08/12/1999)

4.4.1 Background

The chromatic aberrations of the light source refer to a spectrally non-uniform focusing, so that light source irradiance of different wavelengths is focused differently. The cause is chromatic aberration in the light source optics.

The previous Section described experiments to study the instrument signature and the BRDF of a Spectralon sample at 0/45, as function of light source and detector apertures. The light source and detector apertures both have a strong influence on the spectrum of the BRDF measurements. The chromatic aberrations of the light source could be one of the factors related to the BRDF spectral bias.

To examine whether the light source aperture leads to a spectral bias during the direct measurements of the light source irradiance, one of the experiments from Section 4.3 was repeated. The BRDF of Spectralon at 0/45 was re-measured, with the light source aperture (Aperture 2) at 2.54mm, 3.56mm, and 5.08mm. The detector aperture (Aperture 1) was held constant at 20mm. The spectrum of the direct light-source measurements (Figure 4.4.2 to Figure 4.4.5) and the reflected signal measurements (Figure 4.4.1) are compared.

To examine the directional distribution of the spectral bias of the light source, two-dimensional angular scans of the incident beam were carried out, for various light source apertures. A first-surface aluminum mirror was mounted on the sample mount to reflect

the light beam from the light source to the detector. During the measurements, the mirror rotated in 2D. Motor-1 rotated from 44.5° to 45.5°. Motor-2 rotated from –0.5° to 0.5°. The 2D contour graphs of the light source signal reveal that light of different wavelengths has different foci.

In addition, BRDF measurements on the Bristol gray paint sample #4 were carried out. Two light source apertures were used, 2.54mm and 3.56mm. The directional-hemispherical reflectance was calculated from the BRDF measurements. (Before each measurement, the instrument was re-calibrated to obtain a new instrument parameter.) The calculated directional-hemispherical reflectances of the Bristol gray paint sample are compared for the two light source apertures and are compared with hemispherical-directional reflectances obtained by using the OL-750 instrument (Figure 4.4.15).

4.4.2 Measurement results

A. BRDF measurement of the Spectralon sample

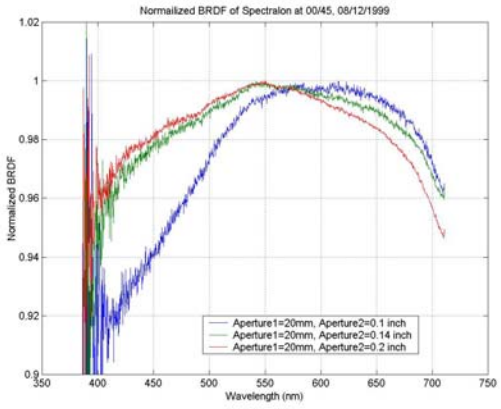

Figure 4.4.1: Comparison of normalized BRDF of Spectralon at 0/45, with various light source apertures (Aperture 2)

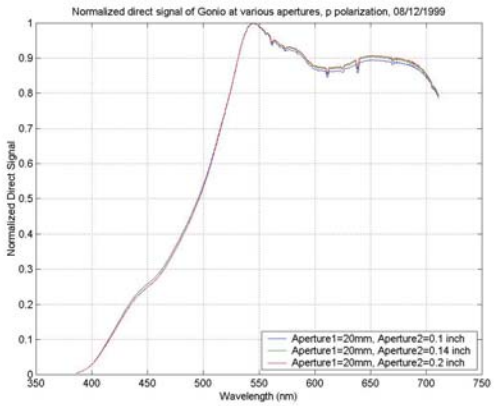

Figure 4.4.2: Normalized direct signal from the light source; with various light source apertures; p polarization (Aperture 2)

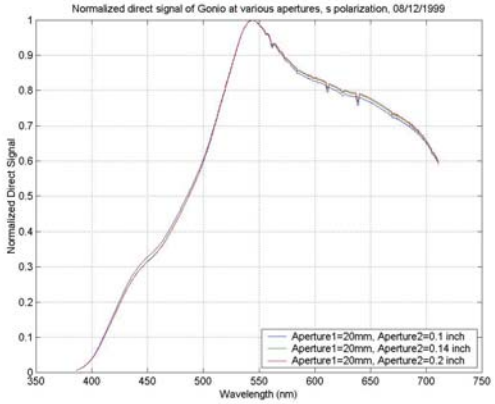

Figure 4.4.3: Normalized direct signal from the light source; with various light source apertures; s polarization (Aperture 2)

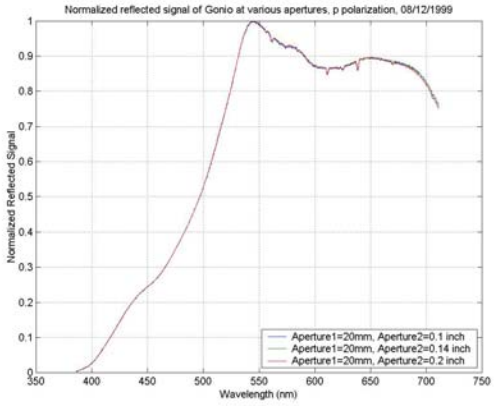

Figure 4.4.4: Normalized reflected signal from the Spectralon sample; with various light source apertures (Aperture 2); p polarization

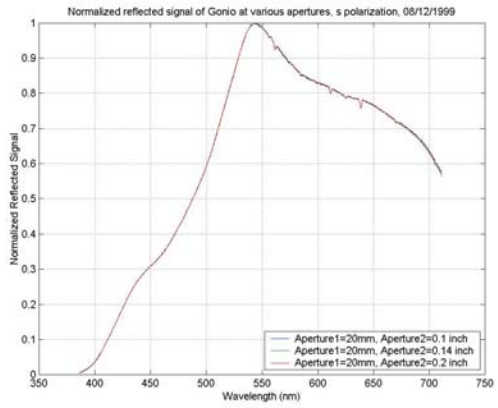

Figure 4.4.5: Normalized reflected signal from the Spectralon sample; with various light source apertures (Aperture 2); s polarization

B. 2-D scans of the incident light source irradiance, obtained by reflection from an Aluminum mirror. Aperture 1 is fixed at 20mm

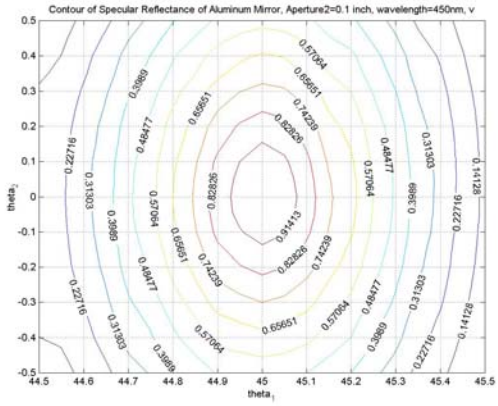

Figure 4.4.6: Contour of normalized reflectance; Aperture 2=2.54mm, λ=450m, s polarization

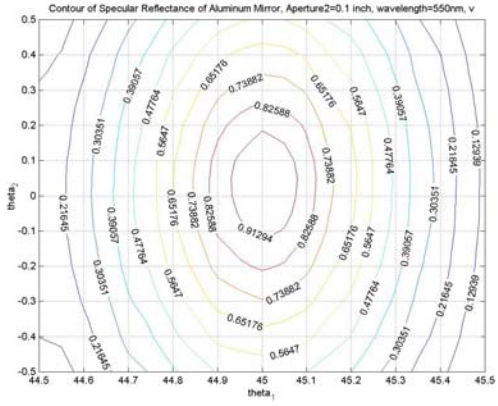

Figure 4.4.7: Contour of normalized reflectance; Aperture 2=2.54mm, λ=550m, s polarization

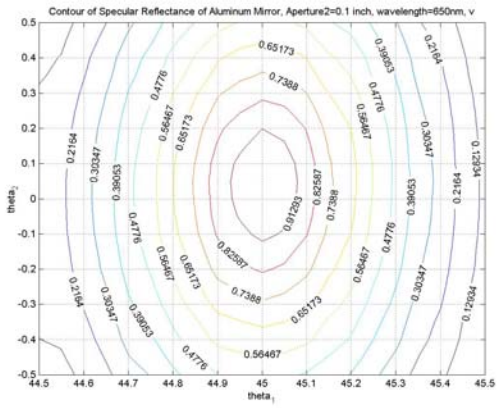

Figure 4.4.8: Contour of normalized reflectance; Aperture 2=2.54mm, λ=650m, s polarization

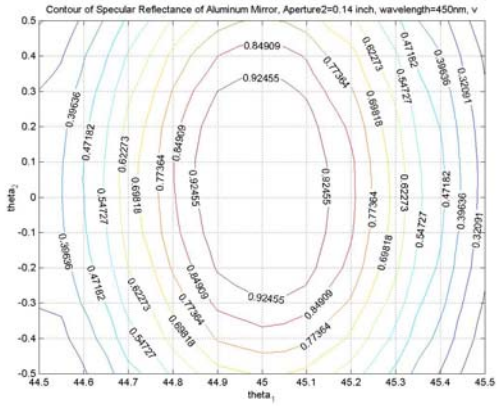

Figure 4.4.9: Contour of normalized reflectance; Aperture 2=3.56mm, λ=450m, s polarization

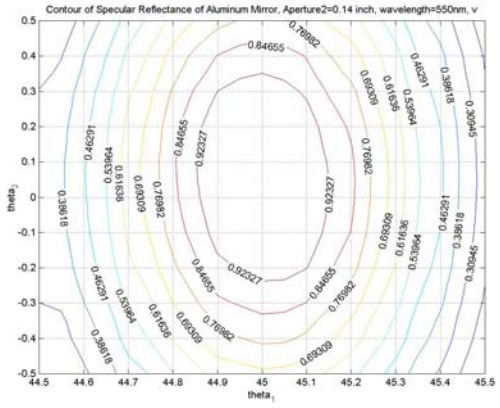

Figure 4.4.10: Contour of normalized reflectance; Aperture 2=3.56mm, λ=550m, s polarization

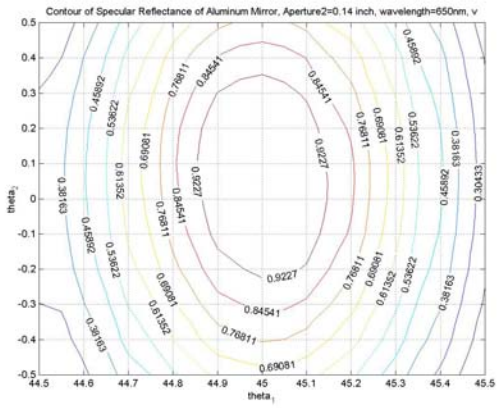

Figure 4.4.11: Contour of normalized reflectance; Aperture 2=3.56mm, λ=650m, s polarization

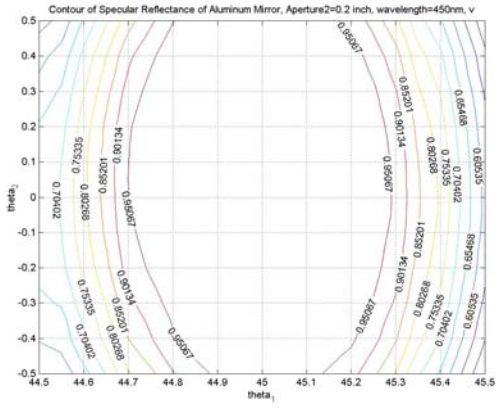

Figure 4.4.12: Contour of normalized reflectance; Aperture 2=5.08mm, λ=450m, s polarization

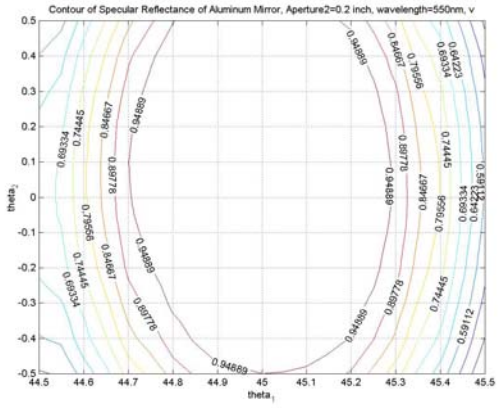

Figure 4.4.13: Contour of normalized reflectance; Aperture 2=5.08mm, λ=550m, s polarization

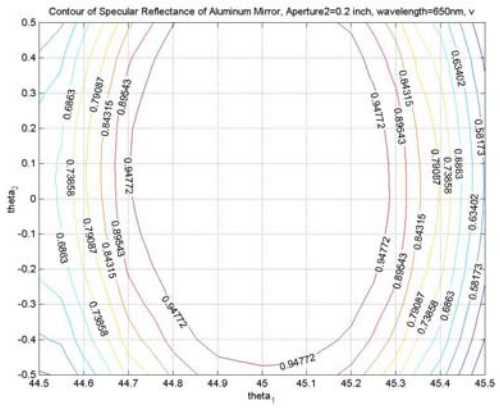

Figure 4.4.14: Contour of normalized reflectance; Aperture 2=5.08mm, λ=650m, s polarization

C. Directional hemispherical BRDF measurement of Bristol#4 sample

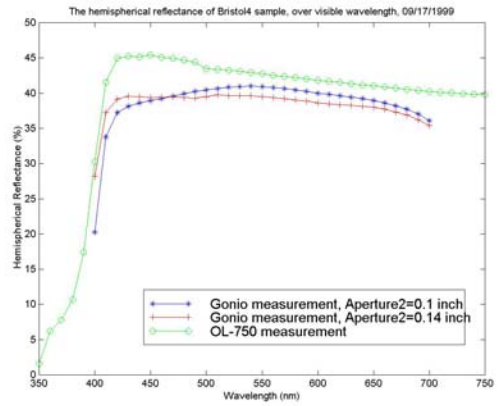

Figure 4.4.15: Comparison of the directional-hemispherical reflectance of a Bristol paint sample, as obtained by Gonio BRDF measurements for two different light source apertures and by OL-750 measurements

4.4.3 Comments

The normalized BRDF of the Spectralon sample at 0/45, with a constant detector aperture and different light source apertures, is presented in Figure 4.4.1. The results are similar to that shown previously in Figure 4.3.20. The light source aperture has a strong influence on the spectrum of the BRDF measurements. The larger apertures generally lead to better spectral measurements.

The spectral bias of the BRDF measurements might come from either the spectral measurement of the light source or the spectral measurement of the reflected light, as these measurements are ratioed. The light source direct irradiance measurements, with constant detector aperture and different light source aperture, are normalized and shown in Figure 4.4.2 (*s* polarization) and Figure 4.4.3 (*p* polarization). A visible spectral bias is observed: different light source apertures produce slightly different spectral distributions. Similarly, the reflected-signal measurements are also normalized, and shown in Figure 4.4.4 (*s* polarization) and Figure 4.4.5 (*p* polarization). No significant differences in the spectral measurements are observed. There is strong subsurface scattering in the Spectralon. Any spatial variations in the incident beam, which are due to a spectral bias in the source optics, and thus are functions of the light source aperture, are spatially homogenized by the sub-surface scattering. As a result, the reflected signal represents the spatially-averaged reflectance, and is not sensitive to the light source aperture. Thus the spectral bias is associated with the measurement of the incident light beam.

A 2-D scan of the incident light beam was carried out. The purpose was to obtain the spatial distribution of the incoming beam as a function of wavelength. Such spatial distributions are shown in Figure 4.4.6 to Figure 4.4.14 for three different source apertures at three wavelengths, 450nm, 550nm, and 650nm. The contours are normalized. Each page corresponds to a different light source aperture, Aperture2. The top-to-bottom graphs show the effect of wavelength. As the wavelength increases, the contours and the center of the contours move upward. The larger apertures produce a larger uniform region in the center.

Thus, larger light source apertures could reduce the spectral bias observed for Spectralon. To test this, we calculated the hemispherical-directional reflectance of Bristol paint sample #4 by integrating BRDF measurements on the sample. This was done for two light source apertures. The hemispherical reflectance was directly measured by the Optronics OL-750 reflectometer. The results are compared in Figure 4.4.15. With the large source aperture, there is less spectral bias. The wavelength-averaged hemispherical reflectance is about the same for the two light source apertures.

Chapter 5

Validation of the Gonioreflectometer: Miscellaneous Topics

In addition to the Gonio light source and the Gonio detector, there are other possible sources of measurement error. The sources include stray light (Section 5.1), polarizer properties (Section 5.2), and non-uniform sample illumination and viewing effects that could be assessed by a check on BRDF reciprocity (Section 5.3). Our experiments below prove that these sources have no significant influence on BRDF measurements.

5.1 Stray light examination and discussion of intrinsic element-dependent detector noise (07/25/1999)

5.1.1 Background

A black curtain surrounds the Gonioreflectometer, to block off the stray light from outside. However, all the surfaces inside the curtain can reflect any stray light that leaks from the housing of the light source. The stray light could eventually reach the sample surface and be reflected to the detector.

To make sure that the magnitude of the stray light is negligible comparing to that of the incident light from the light source, an experiment was carried out. The lens of the light source was blocked off and a Spectralon sample was mounted on the sample mount. Thus, all the light energy collected by the detector was stray light, which was the integration of light reflected from all the surfaces inside the curtain. The signal readings

were taken with and without a light shutter placed in front of the detector housing. The difference between the two signal readings is the signal corresponding to the stray light.

5.1.2 Procedure

a. Launch 'Gonio' program and wait for half an hour
b. Measure the background signal, obtain the data file 'bkg920A.dat';
c. Put the Spectralon sample on the sample mount;
d. Remove the light shutter from the detector, measure the reflected signal from the Spectralon sample (mainly due to the stray light from outside the curtain), obtain the data file 'Bkg_off.dat', Exposure time is 500;
e. Turn on the light source of the Gonioreflectometer to 50 Volts, turn the light source arm to 45°, block of the light source, and measure the reflected signal, obtain the data file 'Bkg45_50.dat', Exposure time is 500;
f. Change the light source voltage to 80 Volts, measure the reflected signal, obtain the data file 'Bkg45_80.dat', Exposure time is 500;
g. Change the light source voltage to 110 Volts, measure the reflected signal, obtain the data file 'Bkg45_11.dat', Exposure time is 500;
h. Turn the light source arm to 90°, measure the reflected signal, obtain the data file 'Bkg90_11.dat', Exposure time is 500;
i. Turn the light source arm to 180°, measure the reflected signal, obtain the data file 'Bkg18_11.dat', Exposure time is 500;
j. Measure the background signal again, obtain the data file 'bkg925A.dat'.

The procedure measures the stray light, while the light source is at various voltages and is located in various positions.

5.1.3 Measurement results

Figure 5.1.1 shows the detector signal reading with the light shutter placed in front of the detector housing. The lens of the light source was blocked off. The signal reading represents the background noise in the detector.

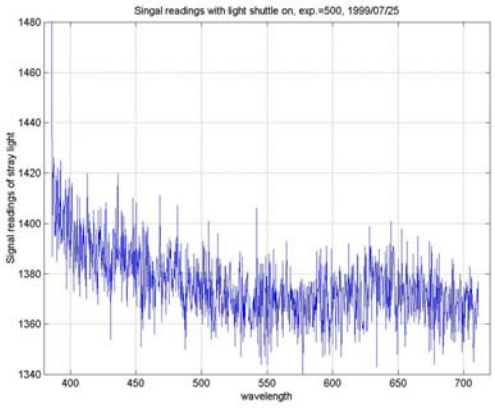

Figure 5.1.1: Detector signal reading with the light source and detector shuttered, at 500 units of exposure time

Subsequently, the detector light shutter was removed and the Spectralon sample was mounted on the sample mount. The lens of the light source was still blocked off. The detector received the reflected stray light from within the curtained test area. Detector signal readings were taken over the visible wavelengths, with various angular configurations of the light source and various light source voltages. All the signal readings vs. wavelength are plotted in Figure 5.1.2. Also included are the data from Figure 5.1.1. Figure 5.1.2 shows how much the readings of stray light deviate from the signal reading with the detector shuttered and blocked off. The trends are more obvious in Figure 5.1.3 to Figure 5.1.5, which use an expanded scale of wavelength.

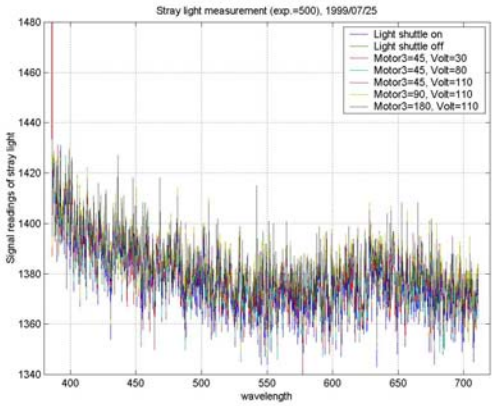

Figure 5.1.2: Comparison of the detector signal readings of the stray light signals under various angular and voltage conditions, at 500 units of exposure time

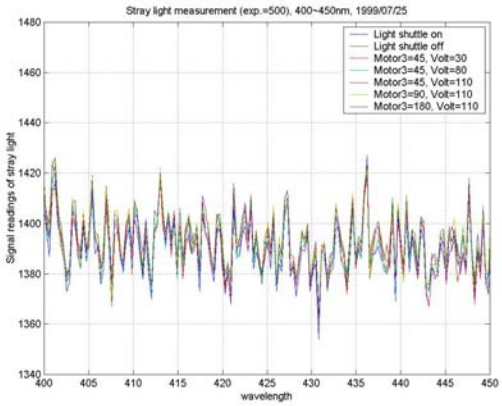

Figure 5.1.3: Comparison of the stray light signals, 400~450nm (same to Figure 5.1.2, but in expanded scale of wavelength)

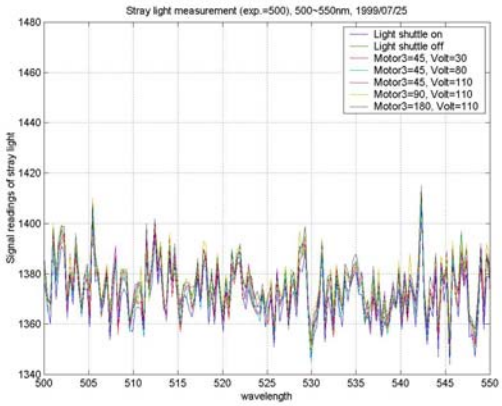

Figure 5.1.4: Comparison of the stray light signals, 500~550nm (same to Figure 5.1.2, but in expanded scale of wavelength)

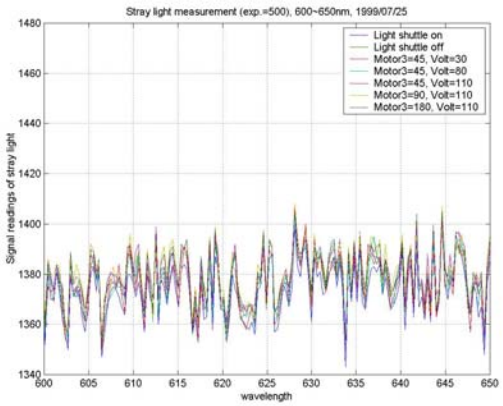

Figure 5.1.5: Comparison of the stray light signals, 600~650nm (same to Figure 5.1.2, but in expanded scale of wavelength)

5.1.4 Comments

First, we plot the background noise signal in the detector at 500 units of exposure time, shown as Figure 5.1.1. Second, we plot all the signal readings, with and without the light shutter, in Figure 5.1.2. By comparing Figure 5.1.1 and Figure 5.1.2, we can see that the signal readings of the detector have no apparent change with or without the light shutter. We conclude that the stray light is negligible, due to the very small solid angle of the detector.

We find that the background signals have stable element-dependent noise, by expanding the wavelength axis. Three wavelength bands (400~450nm, 500~550nm, and 600~650nm) were chosen to compare the signal readings, as shown in Figure 5.1.3, Figure 5.1.4, and Figure 5.1.5, respectively. The deviation of the signal readings of the detector array elements is about 50 counts at 500 units of exposure time. The small deviation is negligible except for the measurements of very low incident energy.

5.2 Influence of a polarizer on BRDF measurements of Spectralon at 0/45 (07/30/1999)

5.2.1 Background

To study the influence of the polarizer on the BRDF measurements, a simple experiment was carried out. The background signal, the light source direct irradiance, and the reflected radiance from the Spectralon sample at 0/45 were measured. These measurements were carried out, with and without a polarizer in front of the detector. The voltage of the light source was reduced to 80 Volts, to prevent the light source from saturating the detector. The two sets of data were processed to obtain the BRDFs of the Spectralon sample. The results were compared to examine the influence of the polarizer on the BRDF measurements.

5.2.2 Measurement results

The BRDFs with and without the polarizer were calculated and are plotted in Figure 5.2.1. The two curves were also normalized by the curve maxima, and are presented in Figure 5.2.2.

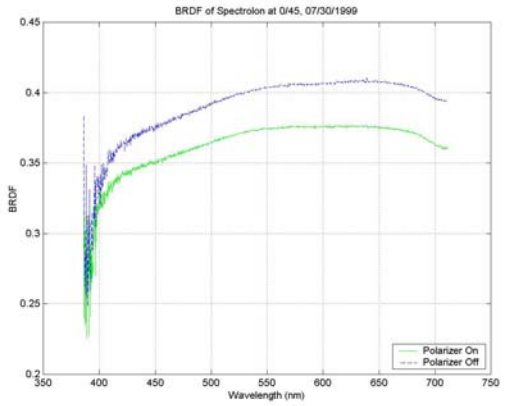

Figure 5.2.1: Comparison of BRDFs of the Spectralon sample at 0/45, with and without the polarizer

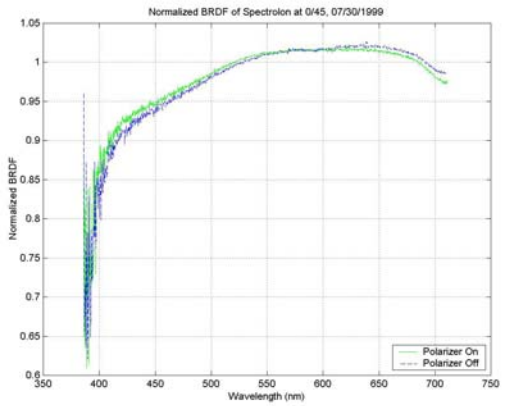

Figure 5.2.2: Comparison of BRDFs of the Spectralon sample at 0/45, with and without the polarizer. The BRDFs are each normalized by the curve maxima

5.2.3 Comments

Figure 5.2.1 shows about 10% magnitude difference between the two measurements, which is due to the attenuation of the polarizer. Figure 5.2.2 shows little difference in the spectral distribution of the BRDFs. The conclusion is that the polarizer is not related to the spectral bias of the BRDF measurement.

5.3 Reciprocity Confirmation (06/18/1999)

5.3.1 Background

Theoretically, the BRDF function satisfies the Helmholtz reciprocity:

$$f_r(\lambda,\theta_r,\phi_r,\theta_i,\phi_i) = f_r(\lambda,\theta_i,\phi_i,\theta_r,\phi_r) \qquad \text{Equation 5.3.1}$$

Therefore, a BRDF measurement system should also satisfy reciprocity. When the positions of the light source and the detector are interchanged, the measured BRDF values should be the same.

In an experiment, however, there can be non-uniform illumination and/or viewing of the sample in the two reciprocal positions. These are geometric effects that can be assessed by a check on reciprocity. To confirm reciprocity, the reflectance of a Spectralon sample was measured in the plane of incidence, where $\phi_i=\phi_r=0°$. Subsequently, we compared the signal readings of two measurements, each satisfying $\theta_{i1} = \theta_{r2}$ and $\theta_{i2} = \theta_{r1}$.

5.3.2 Procedure

a. Launch the 'Gonio' program, turn on the light source, wait for a while to make the system stable;
b. Measure the background noise, save the data into bkg.dat;
c. Turn the Motor 2 to $\theta_2 = 0°$, turn the Motor 3 to $\theta_3 = 120°$;
d. Put the Spectralon on the sample mount;
e. Measure the reflected signal at p polarization, with the scan route file 'Recip.123', which rotate to Motor1 from 30° to 90°;

f. Measure the reflected signal at s polarization, with the scan route file ‘Recip.123’.

5.3.3 Measurement results

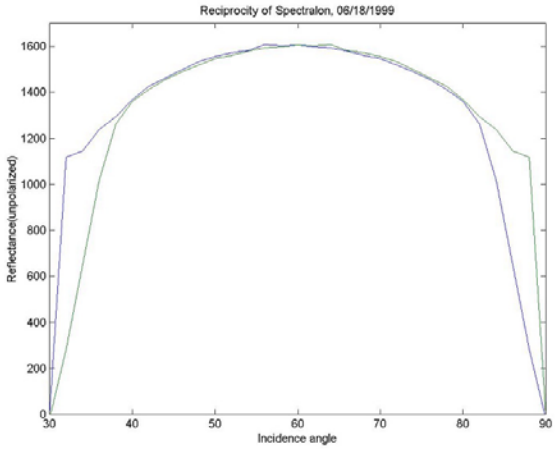

Figure 5.3.1: Reciprocity of the BRDF measurements of the Spectralon sample (the signal reading of the reflected light with various incident angles and its mirror curve)

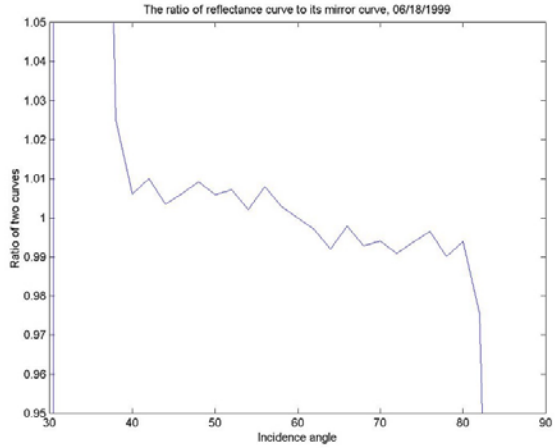

Figure 5.3.2: The ratio of the reflectance curve to its mirror curve

5.3.4 Comments

During the measurements, the angle between the light source and the detector was fixed at 120°. θ_2 was set at 0° in advance (i.e., the measurements were conducted in the incident plane). θ_r (polar angle of reflection) varied from 30° to 90° while θ_i (polar angle

of incidence) varied from 90° to 30°. We can examine reciprocity by comparing the pairs of signal readings with positions satisfying:

$$\theta_{i1} = \theta_{r2} \text{ and } \theta_{i2} = \theta_{r1}$$

Figure 5.3.1 displays the signal reading of the reflected light and its mirror curve. Figure 5.3.2 shows the ratio of the two curves appearing in Figure 5.3.1. From Figure 5.3.1 and Figure 5.3.2, we conclude that the Gonioreflectometer measurements obey reciprocity in the range of θ_i=40°~80°. Within this range, the deviations of the signal readings are less than 2%, with $\theta_i+\theta_r$ fixed at 120°. From the above, we believe that the measurement system is in a fairly good state, with respect to reciprocity. When θ_i or θ_r is near 90°, we are at the angular limits of measurement and reciprocity cannot be satisfied in the experiments.

Reciprocity should be frequently examined. Reciprocity is related to the alignment of the light source and motors, and to the sample-surface uniformity of the illuminating and reflected beams. Whenever the system is readjusted, its reciprocity should be re-confirmed.

Chapter 6

Specular Reflectance Measurements

We present the specular reflectance measurements of a gold mirror (Section 6.1) and two plastic samples (Section 6.2). The positioning angular error of the Gonioreflectometer is discussed and an absolute measurement method is proposed to improve the accuracy of the specular reflectance measurements.

6.1 Specular reflectance of gold mirror over visible wavelengths, and discussion of the angular error of the Gonioreflectometer (06/13/1999)

6.1.1 Background

The positioning angular error of the Gonioreflectometer adds complication to the specular measurements of mirror-like surfaces. From the instrument signature measurements (Section 4.3), we can establish that 0.2° of positioning angular error leads to 10% error in the reflectance measurement. Each motor of the instrument does have a positioning angular error of about 0.3~0.4° (Foo's thesis [1]), which produces a significant error both in light source direct irradiance measurements and in reflected radiance measurements. Therefore, the traditional measurement procedures used for a diffuse sample are not valid for the specular measurements.

For each incident angle, we have to scan the specular direction to find the maximum specular reflected radiance. In this experiment, we scanned the specular direction from a gold mirror for several incident angles, 15°, 30°, 45°, 60°, and 75°. The sampling density

was 0.1°. The specular reflectance can be derived from the maximum reflected radiance and the light source direct irradiance measurements. The theoretical specular reflectance of gold has been pre-calculated. By comparing the theoretical and measured specular reflectance, we can validate the measurements.

Since all the difficulties of specular measurement come from the narrow specular lobe, we tried to get better measurements by changing the instrument signature (i.e., light source aperture in Section 6.1.3D). It was determined that a large aperture for the light source can make the measurements less sensitive to angular error. The aperture of the light source was enlarged from 2.54mm to 5.1mm. Then the new instrument signature curve had a level top from –1° to 1°. The new instrument signature and the corresponding measurement results are presented in 6.1.3D.

6.1.2 Procedure

a. Turn the light source on, wait for a while to let the system stable;
b. Rotate control motors, make θ_1=0°, θ_2=0°, θ_3=180°;
c. Measure the direct signal at s polarization;
d. Measure the direct signal at p polarization;
e. Rotate Motor 3 to 30° (or 60°, 90°, 120°, 150°)
f. Conduct the 2-D scan by rotating the Motor 1 form 14~16° (depends on incident angle) and Motor 2 from –1~1°, 0.1° for one step, record the direct signal, exposure time is 1, at s polarization;
g. Repeat step 6 at p polarization;

h. Measurement the background signal at exposure time 1.

6.1.3 Measurement results

A. Data

Table 6.1.1: Theoretical specular reflectance of gold

Wavelength\θ_i		15°	30°	45°	60°	75°
450 nm	S	0.3998	0.4426	0.5180	0.6314	0.7898
	P	0.3722	0.3317	0.2683	0.2028	0.2446
500 nm	S	0.5257	0.5675	0.6363	0.7315	0.8528
	P	0.4980	0.4598	0.4048	0.3663	0.4516
550 nm	S	0.8540	0.8695	0.8937	0.9247	0.9607
	P	0.8432	0.8266	0.7986	0.7642	0.7693
600 nm	S	0.9162	0.9252	0.9393	0.9572	0.9778
	P	0.9099	0.8999	0.8823	0.8582	0.8538
650 nm	S	0.9418	0.9481	0.9580	0.9704	0.9847
	P	0.9374	0.9304	0.9177	0.8995	0.8933
700 nm	S	0.9640	0.9678	0.9739	0.9816	0.9905
	P	0.9613	0.9569	0.9484	0.9338	0.9184

Table 6.1.2: Measured specular reflectance of the gold mirror by the Gonioreflectometer

Wavelength\θ_i		15°	30°	45°	60°	75°
450 nm	S	0.3779	0.4168	0.5039	0.6205	0.7634
	P	0.3452	0.3137	0.2594	0.2037	0.2515
500 nm	S	0.5043	0.5481	0.6259	0.7245	0.8296
	P	0.4676	0.4325	0.3856	0.3660	0.4530
550 nm	S	0.8250	0.8473	0.8807	0.9134	0.9359
	P	0.7990	0.7863	0.7748	0.7456	0.7450
600 nm	S	0.9168	0.9315	0.9498	0.9673	0.9665
	P	0.8930	0.8899	0.8930	0.8686	0.8411
650 nm	S	0.9478	0.9591	0.9708	0.9817	0.9729
	P	0.9303	0.9311	0.9371	0.9203	0.8872
700 nm	S	0.9584	0.9668	0.9745	0.9821	0.9688
	P	0.9380	0.9399	0.9476	0.9339	0.8968

The measured specular reflectance is the maximum specular reflectance obtained by the 2-D scan. With the scan, the positioning angular error is within 0.05°. The light source aperture (2.5mm) and the detector aperture (28mm) are selected empirically to match the solid angles of illumination and detection, and to achieve the maximum angular resolution of the reflected light fields.

B. Comparison of the theoretical and measured specular reflectance of gold

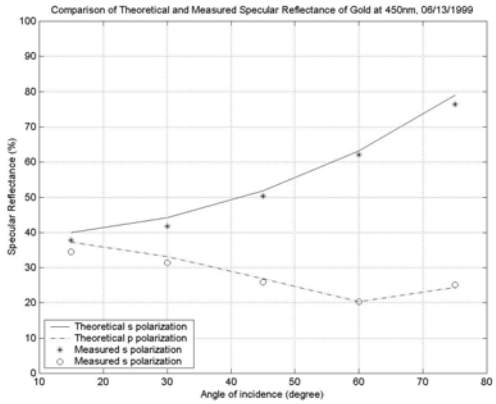

Figure 6.1.1: Comparison of the theoretical and measured specular reflectance of gold at both polarizations; λ=450nm

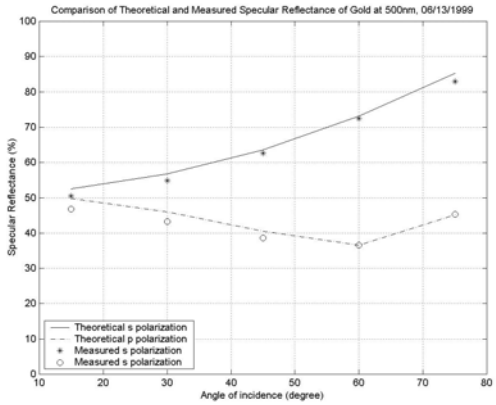

Figure 6.1.2: Comparison of the theoretical and measured specular reflectance of gold at both polarizations; λ=500nm

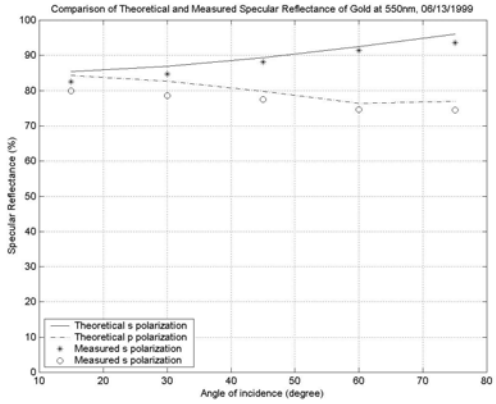

Figure 6.1.3: Comparison of the theoretical and measured specular reflectance of gold at both polarizations; λ=550nm

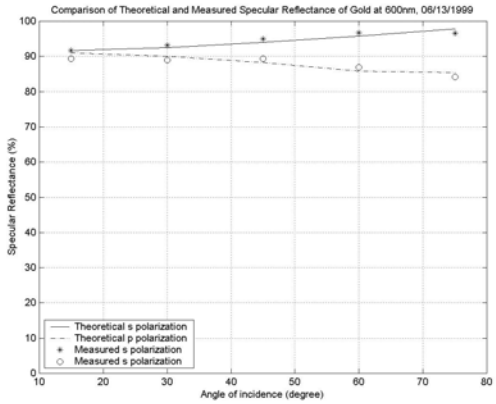

Figure 6.1.4: Comparison of the theoretical and measured specular reflectance of gold at both polarizations; λ=600nm

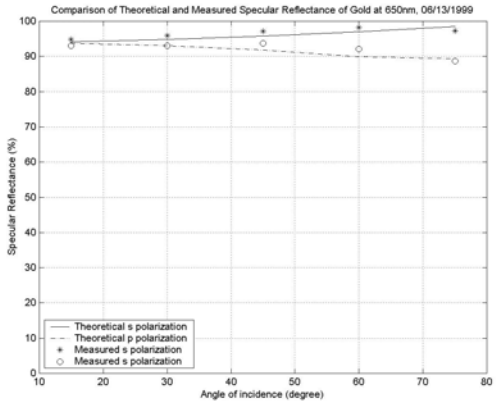

Figure 6.1.5: Comparison of the theoretical and measured specular reflectance of gold at both polarizations; λ=650nm

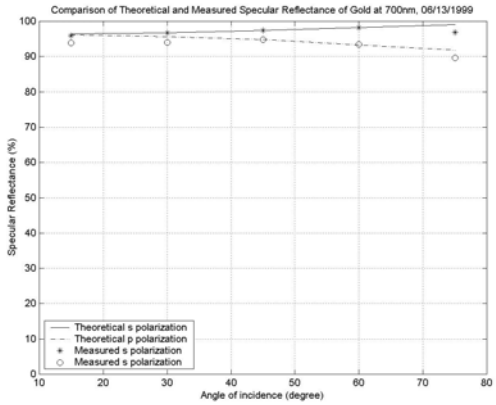

Figure 6.1.6: Comparison of the theoretical and measured specular reflectance of gold at both polarizations; λ=700nm

C. The scan of specular direction

Apparently, the radiance distribution of two-axis scan is a cone. And the top of the cone is the maximum reflected radiance. The following are the actual positions of the maximum reflections obtained by the 2-D scan:

$\theta i = 15°$: (θ_1=14.9°, θ_2=0.1°)

$\theta i = 30°$: (θ_1=29.9°, θ_2=0.1°)

$\theta i = 45°$: (θ_1=44.9°, θ_2=0°)

$\theta i = 60°$: (θ_1=59.9°, θ_2=-0.2°)

$\theta i = 75°$: (θ_1=74.9°, θ_2=-0.4°)

This result can explain why the traditional procedure cannot obtain the correct result.

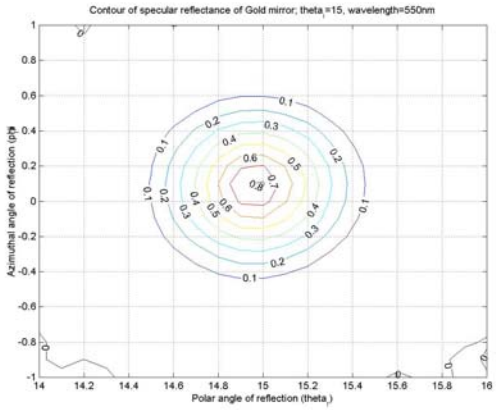

Figure 6.1.7: Contour of specular reflection measurements of gold; θ_I = 15°, λ=550nm

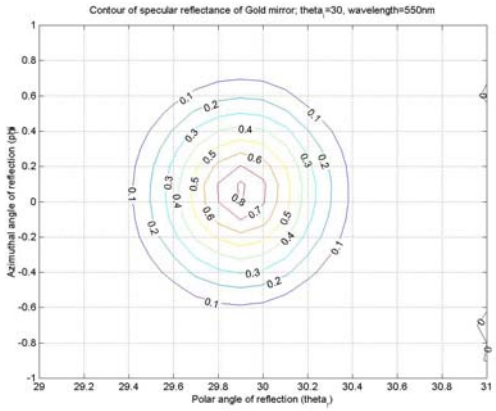

Figure 6.1.8: Contour of specular reflection measurements of gold; θ_I = 30°, λ=550nm

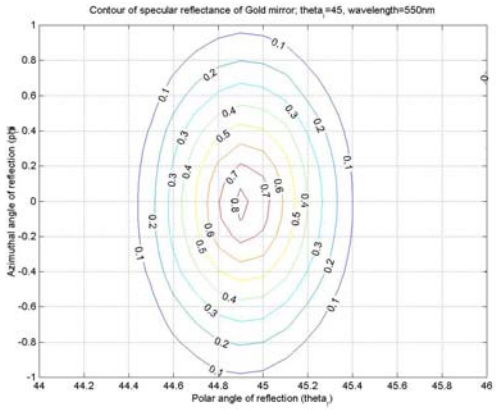

Figure 6.1.9: Contour of specular reflection measurements of gold; $\theta_I = 45°$, λ=550nm

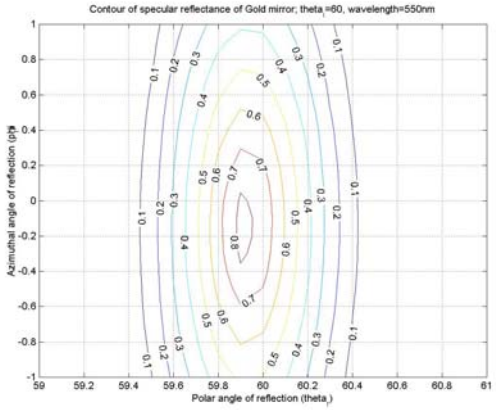

Figure 6.1.10: Contour of specular reflection measurements of gold; $\theta_I = 60°$, λ=550nm

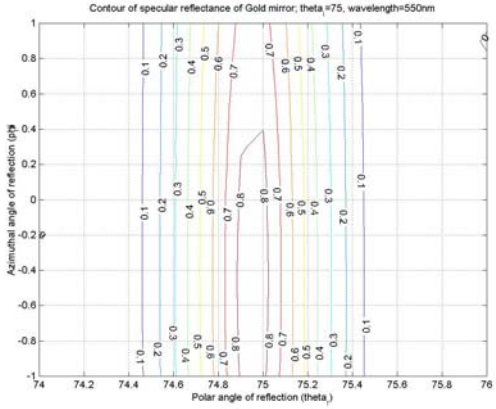

Figure 6.1.11: Contour of specular reflection measurements of gold; $\theta_I = 75°$, λ=550nm

D. The new instrument signature and the measurement result when the light source aperture was increased from 2.54mm to 5.1mm

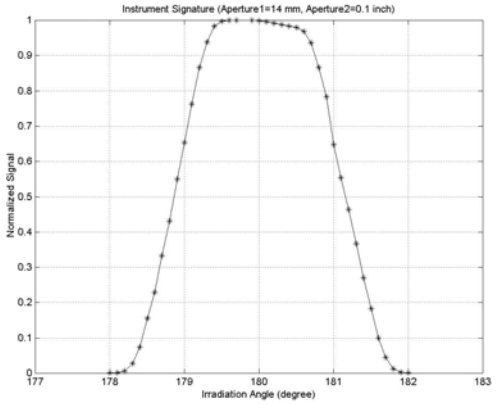

Figure 6.1.12: Instrument signature at Aperture 1=20mm, Aperture 2=5.1mm

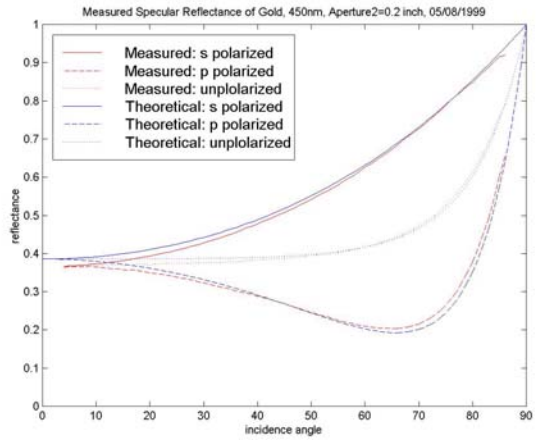

Figure 6.1.13: Comparison of theoretical and measured specular reflectance of gold in the plane of incidence, at new Aperture 2, 450nm

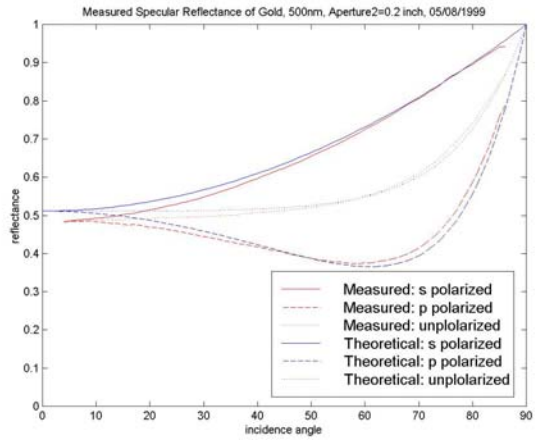

Figure 6.1.14: Comparison of theoretical and measured specular reflectance of gold in the plane of incidence, at new Aperture 2, 500nm

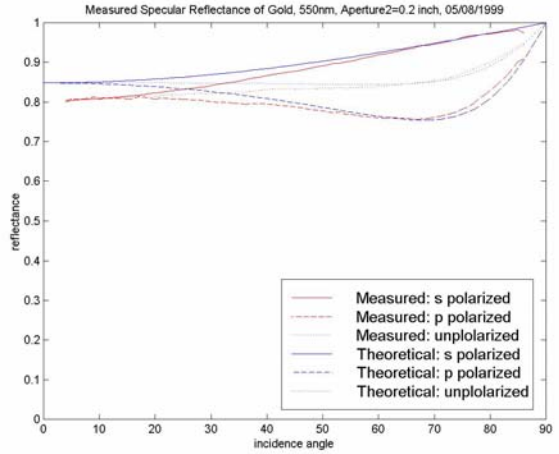

Figure 6.1.15: Comparison of theoretical and measured specular reflectance of gold in the plane of incidence, at new Aperture 2, 550nm

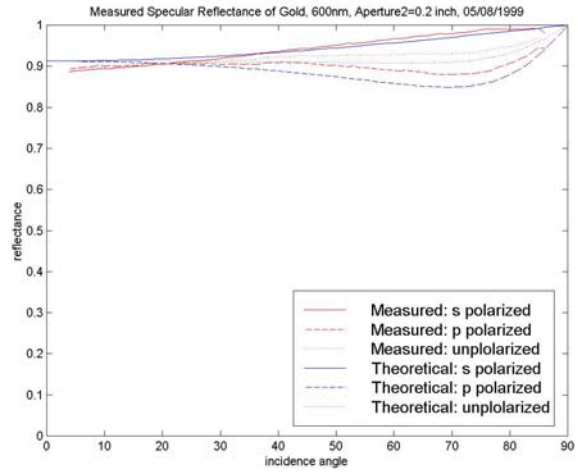

Figure 6.1.16: Comparison of theoretical and measured specular reflectance of gold in the plane of incidence, at new Aperture 2, 600nm

6.1.4 Comments

Table 6.1.1 and Table 6.1.2 show that all the measured specular reflectances are slightly smaller than the theoretical values. The error of reflectance measurement in any case is less than 0.03 (3%). The data are also visualized, as shown in the Figure 6.1.1~Figure 6.1.6.

Figure 6.1.7~Figure 6.1.16 show that the contour of specular reflection measurements of gold at 550nm, and at various angles of incidence. The traditional procedure, which only measures the reflected radiance at the specular direction (determined by the positioning mechanism of the Gonioreflectometer, with some angular errors), is unable to provide satisfactory measurement results. Figure 6.1.7~Figure 6.1.16 show that the traditional procedure of the reflected radiance measurement has more than 10% error. The light source direct irradiance measurement was also not completely accurate, because we are only able to align the light source position in the horizontal direction (by 'gonio' software). The alignment of the light source in the vertical direction depends on our manual alignment skill. And the accuracy of the alignment is difficult to evaluate.

After the light source aperture was enlarged, we obtained better measurements of the specular reflectance of gold. However, an intrinsic error could be observed. It seems that there are two main sources of positioning angular error. The first one is random noise, due to the mechanical vibration and the holes on the table. The second one is the intrinsic error of the system, including the angular positioning error of the axes of the motors. Apparently, the axis of Motor 1 is not perpendicular to the top of the optical table, and the axis of Motor 2 is not exactly parallel to the tabletop. There is an error of approximately 0.1~0.3 degree. The changed instrument signature can only filter out the random noise.

6.1.5 Matlab Script

```
clear
% Reads the raw data files with measurements and exposure times of the
% background, the direct source, and the measurements.
[exposure_b,background]    = readfile(['Bkg.dat']);
[exposure_u,direct_v]      = readfile(['Directv.dat']);
[exposure_n,direct_h]      = readfile(['Directh.dat']);
[exposure_v,measurement_v] = readfile(['measv.dat']);
[exposure_h,measurement_h] = readfile(['meash.dat']);
%*****************************************************
%Calculate of the Specular reflection both
wv=517      %Locate signal data of 550nm
theta_i=30;
x_max=0;
y_max=0;
max=0;
for i=1:21,
   for j=1:21,
      n=(i-1)*21+j;
      tempv = ((measurement_v(wv,n)-
background(wv,1))/exposure_v(n))/(direct_v(wv)-background(wv,1));
      temph = ((measurement_h(wv,n)-
background(wv,1))/exposure_h(n))/(direct_h(wv)-background(wv,1));
      z(i,j)=0.5*(tempv+temph);
      if z(i,j)>max,
         max=z(i,j);
         x_max=j;
         y_max=i;
      end;
   end;
end;

%plot
x=[-1+theta_i/2:0.1:1+theta_i/2];
y=[-1:0.1:1];
surf(x,y,z,z);
title 'Measured Specular Reflectance of gold, theta_i=15,
wavelength=550nm'
xlabel 'theta_1'
ylabel 'theta_2'
zlabel 'reflectance'

figure
[c,h]=contour(x,y,z);
grid on
title 'Contour of Specular Reflectance of gold, theta_i=15,
wavelength=550nm, 06/13/1999'
xlabel 'theta_1'
ylabel 'theta_2'
clabel(c,h);
x_max=theta_i/2+(x_max-11)*0.1
y_max=(y_max-11)*0.1
max
```

6.2 Specular reflectance of black plastic and blue plastic (03/27/1999)

6.2.1 Background

The specular reflectance of a blue plastic sample and a black plastic sample was measured with the Gonioreflectometer. The blue plastic sample is several years old. Its spectral specular reflectance was measured at an incidence angle of 45° (Section 2.2 *Specular reflectance of a blue plastic at an incidence angle of 45°, over visible wavelengths (03/25/1999)*, which was a duplication of Foo's measurements). It appears that this sample is very stable and robust. It is also easy to clean and store. The black plastic sample is new, with an untouched surface. Fortunately, a formula for the theoretical specular reflectance is also available, and is known as the Fresnel reflectance. The refractive index of plastic is approximately 1.48 [7], which is independent of wavelength. The immediate physical consequence is that the specularly reflected light from the sample surface will have the same spectral distribution as the incident light. The specular reflectance will be independent of wavelength. The color of the plastic comes from the sub-surface scattering. The radiance of the sub-surface scattering is negligible compared the radiance in the specular direction.

6.2.2 Measurement results

A. Measured specular reflectance of black plastic

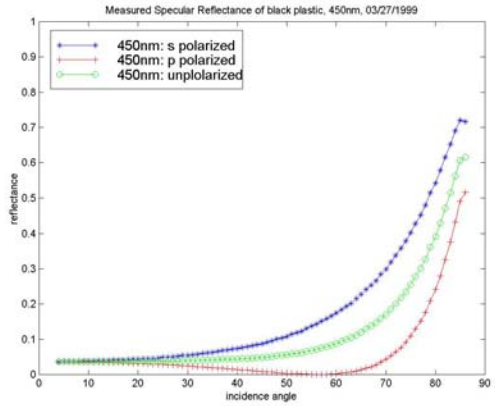

Figure 6.2.1: Measured specular reflectance of black plastic in the plane of incidence; λ=450nm

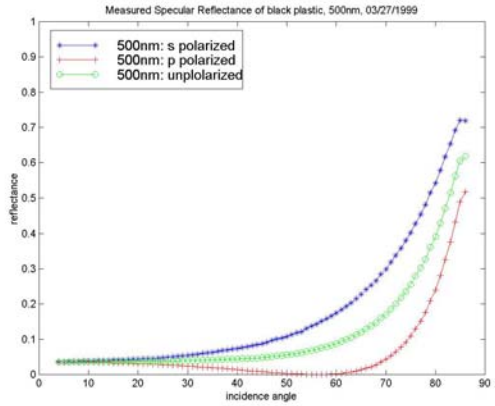

Figure 6.2.2: Measured specular reflectance of black plastic in the plane of incidence; λ=500nm

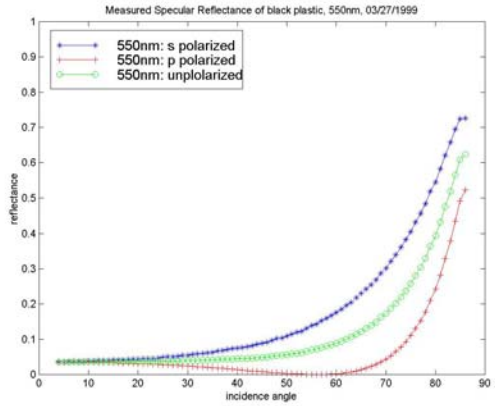

Figure 6.2.3: Measured specular reflectance of black plastic in the plane of incidence; λ=550nm

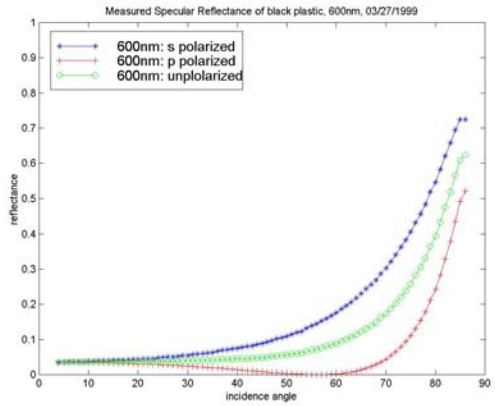

Figure 6.2.4: Measured specular reflectance of black plastic in the plane of incidence; λ=600nm

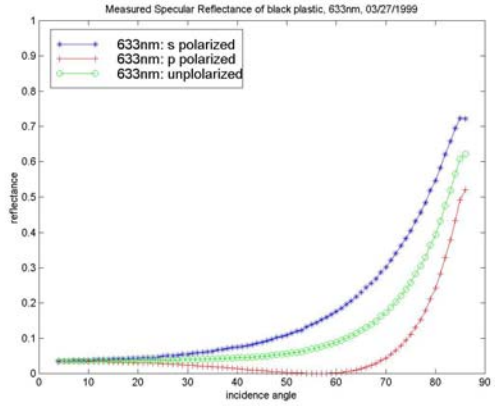

Figure 6.2.5: Measured specular reflectance of black plastic in the plane of incidence; λ=633nm

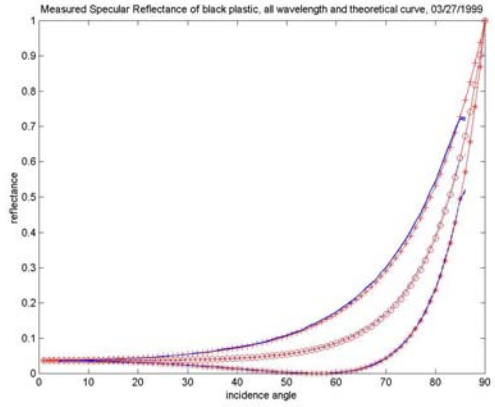

Figure 6.2.6: Measured specular reflectance of black plastic in the plane of incidence. Results for all of the wavelelengths measured are shown, as well as the theoretical curve

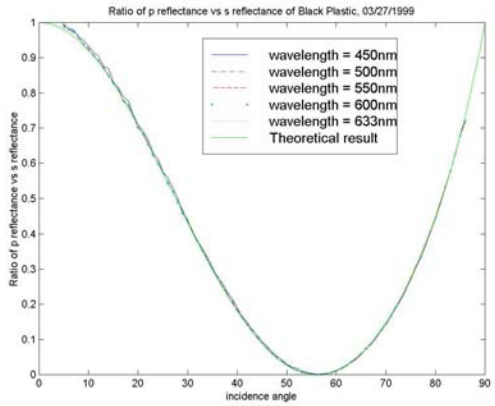

Figure 6.2.7: Ratio of p and s reflectances of black plastic. Results for all wavelengths are shown, as well as the theoretical curve

B. Measured specular reflectance of blue plastic

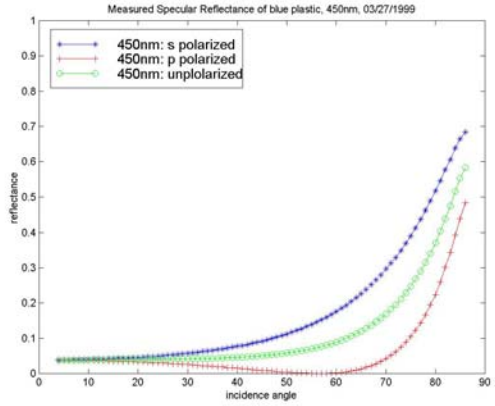

Figure 6.2.8: Measured specular reflectance of blue plastic in the plane of incidence, λ=450nm

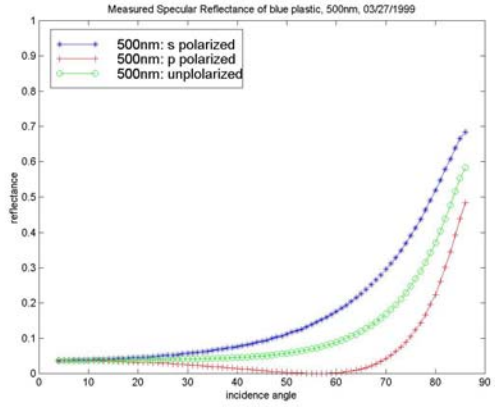

Figure 6.2.9: Measured specular reflectance of blue plastic in the plane of incidence, λ=500nm

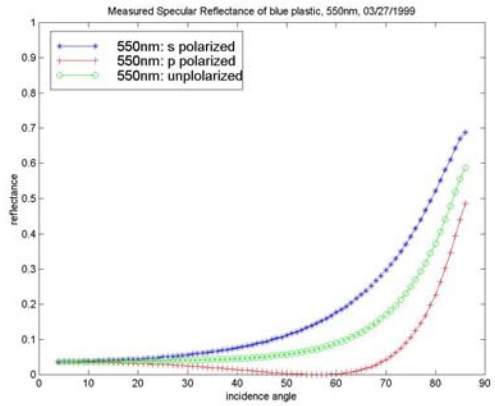

Figure 6.2.10: Measured specular reflectance of blue plastic in the plane of incidence, λ=550nm

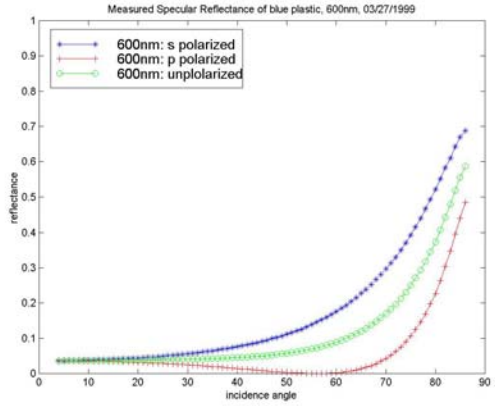

Figure 6.2.11: Measured specular reflectance of blue plastic in the plane of incidence, λ=600nm

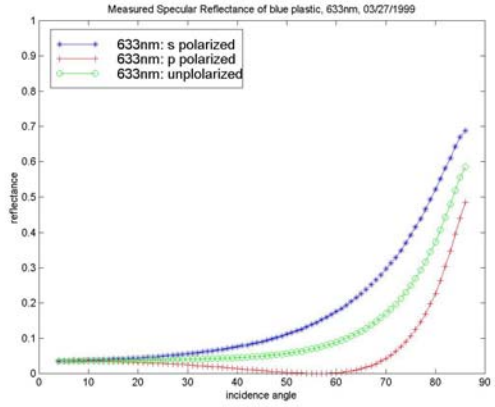

Figure 6.2.12: Measured specular reflectance of blue plastic in the plane of incidence, λ=633nm

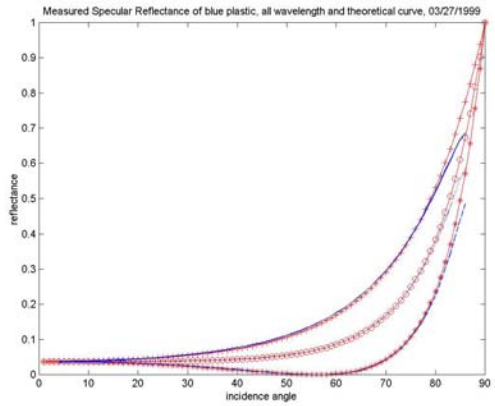

Figure 6.2.13: Measured specular reflectance of blue plastic in the plane of incidence. Results for all of the wavelelengths measured are shown, as well as the theoretical curve

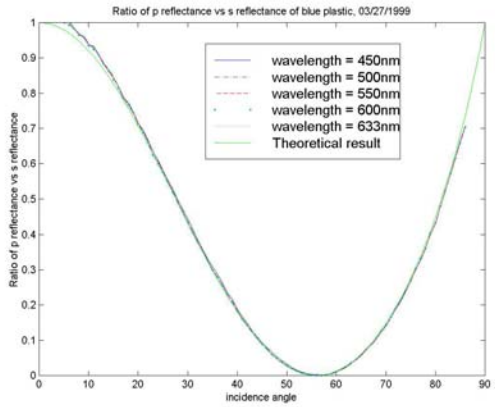

Figure 6.2.14: Ratio of p and s reflectances of blue plastic. Results for all wavelengths are shown, as well as the theoretical curve

6.2.3 Comments

Figure 6.2.1~ Figure 6.2.5 show the measured specular reflectance of black plastic in the plane of incidence, for different wavelengths. In Figure 6.2.6, the measured specular reflectances for all of the wavelengths are graphed, with the theoretical curve. All the curves coincide and the measurements agree with the theory. This confirms that the specular reflectance is independent of wavelength. In Figure 6.2.7, the ratios of the reflectances in the s and p polarization are graphed for the 5 wavelengths, as well as the theoretical curve. The curves agree to each other very well. From Figure 6.2.14, the zero

point provides an independent confirmation of the value for the index of refraction, 1.48, which agrees with the value found in the literature.

Similarly, the measured specular reflectances of the blue plastic, for various wavelengths, are shown in Figure 6.2.8~ Figure 6.2.14. In the last two figures, the theoretical reflectance curves for an index of refraction of 1.48 are also shown. The conclusions mentioned for the black plastic also apply to the measurements for the blue plastic.

Chapter 7:

Recommended Relative Reflectance Method

In this Chapter, we propose a new relative method, which can achieve accurate and efficient BRDF measurements. In Section 7.1, we summarize the tests presented in Chapter 3 to 6 on the instrument components (detector, light source, etc.). These tests provide strong guidance for the selection and implementation of the proposed relative method. In Section 7.2, we briefly review the standard BRDF measurement methods, including some absolute and relative methods. The methodology of calibration is mentioned. In Section 7.3, we describe the new relative reflectance method; the technical steps of measurement are listed in Section 7.4. The BRDF value for Spectralon at 0/10 is the critical calibration constant for the new relative method; the procedure for obtaining this constant is given in Section 7.5. To validate the relative method, the BRDFs of six samples are measured, presented, and discussed in Section 7.6. Applicability of the new relative method is discussed in the conclusion, Section 7.7.

7.1 Summary of previous tests

Each part of the Gonioreflectometer was systematically tested, as described in Chapters 3 to 5. For the detector (Chapter 3), we tested the background signal, the linearity, the spectrum response, the footprint, the polarization effect of the detector, and the influence of the detector slit on BRDF measurements. For the Gonio light source (Chapter 4), we examined the spectral bias by using a second light source, the chromatic aberration of the Gonio light source, the instrument signature, and the influence of light source and

detector apertures on the instrument signature. Other possible sources of measurement error were also examined (Chapter 5), including stray light, intrinsic detector noise, polarizer effects, and a reciprocity confirmation. In addition, as part of the testing, we measured the specular reflectance of a gold mirror and some smooth-surface plastics (Chapter 6). The positioning angular error of the Gonioreflectometer was discussed there and an absolute method was proposed to improve the accuracy of the specular reflectance measurements.

The systematic tests of the Gonioreflectometer enabled us to identify some possible sources of measurement error, including:

- The spectral bias in the light source irradiance measurements (Section 4.2);
- The spectrally non-uniform focusing of the light source (Section 4.4);
- The mismatch of the light source and detector apertures (Section 4.3);
- The error in the background-signal measurement (Section 3.1);
- The non-linearity of the detector response at very low signal levels (less than 20 counts) (Section 3.3);
- The influence of the detector slit on the BRDF measurements (Section 3.7);
- The misalignment of the light source, the detector, and the motors (Section 3.5, Section 5.3, and Section 6.1);
- The position angular error of the light source and the sample holder (Section 6.1).

We can avoid some of these problems with careful operation and improved procedures:

- The spectrally non-uniform focusing of the light source can be reduced by careful alignment of the light source components;
- The light source and detector apertures can be empirically matched to increase the angular resolution;
- The error in the background-signal measurements can be reduced by averaging multiple background-signal measurements and by a longer cooling-down time at startup (more than 30 minutes);
- The non-linearity of the detector response can be avoided with longer exposure times, which increase the signal level;
- An optimal size for the detector slit was determined empirically (0.28mm).

It was proved experimentally that these operations and improved procedures could enhance the performance of the Gonioreflectometer.

However, all the efforts mentioned above failed to eliminate the spectral bias of the BRDF measurements. In Sing-Choong Foo's thesis [1], he introduced two measurement methods, one relative and one absolute. His relative method is different from the new relative method proposed in this chapter. For his two methods, direct measurements of the light source irradiance are required. However, for his two methods, we were still unable to eliminate the spectral bias in the light source irradiance measurements, despite careful operation and improved procedures. Therefore, we need a new procedure and calibration method, preferably one which avoids any direct light source irradiance measurements.

7.2 BRDF measurement methods

Because of the difficulty of measuring a BRDF, the American Society for Testing and Materials (ASTM) carried out a study of BRDF measurement procedures. The result of the study is a recommended standard practice for BRDF measurements [8].

The ASTM standard also describes two standard methods for carrying out BRDF measurements, the relative method and the absolute method.

The relative method for measuring BRDFs uses a reference sample with known bidirectional reflectance (BRDF). The unknown sample and the reference sample are measured under the same conditions. Assuming the BRDF of the reference sample is known, we can obtain the BRDF of the unknown sample relative to that of the reference by ratioing the measured signals from the two samples. This is done for every pair of incidence and reflection angles, and all wavelengths for which measurements are carried out. It is unnecessary to (directly) measure the light source irradiation. The relative method is reliable but expensive in terms of time. For example, the average measurement time needed to measure a sample with our Gonioreflectometer is about 11 hours, for approximately 1500 pairs of incidence/reflection angles and 1024 wavelengths. That means 22 hours are required to measure both the unknown and reference samples. Accurate absolute BRDF measurements of the reference sample, which form the basis for the relative method, are also difficult to obtain.

The absolute method for measuring BRDFs requires that the detector capture the entire source irradiating flux that impinges on the reflecting area of the sample. The light

source is first aimed directly at the detector with no sample present, and a reading of the irradiance is made with the spectroradiometer-detector. Subsequently, the reflected radiance from the sample at each angular configuration is measured. To calculate the BRDF for a given angular configuration, the spectroradiometric reading of the reflected radiance for each angular configuration is divided by the reading of the direct light-source measurement, the incident cosine, and a calibration factor. The calibration factor is an instrument configuration factor.

The absolute method is more efficient in terms of time. However, the detector must accurately respond over many orders of magnitude of signal intensity. For test cases, we observed considerable errors in the resulting spectrum and magnitude. Based on the analysis presented in Section 4.2, direct measurements of the light source irradiance were the primary source of the error for our absolute BRDF measurements.

In conclusion, there are two standard methods for measuring a BRDF: relative and absolute. The relative method requires a reference sample of known, accurate, and stable BRDF. This represents, essentially, a "calibration factor." The absolute method of measurement requires "an instrument configuration factor," which involves known quantities, and an imprecisely known solid angle for the light source. Further, in our instrument, we found chromatic differences between direct light source measurements and reflectance measurements from a neutral (white) sample. This implies that the source beam spatial-structure varies chromatically with distance from the light source. For our instrument, this necessitates a second "calibration factor" for absolute measurements. On

the other hand, the relative measurement method is not sensitive to errors due to the direct measurement of the light source irradiance.

The ASTM recommended standard for BRDF measurements [8] presents both the absolute method and the relative method, as described above. Besides, the ASTM standard gives two variations of the relative method, relative specular reflectance method and relative total reflectance method. The new relative method we are going to propose in the next section is similar to the relative total reflectance method described in the ASTM standard. Discussions of BRDF measurement methods are also available in many reports [2, 10].

7.3 Proposed relative reflectance method

To achieve accurate and efficient BRDF measurements, we recommend a relative reflectance method. First, the sample is mounted on the goniometer (sample mounting stage), and the reflected radiance is measured for each desired angular configuration. Second, we measure the reflected radiance of the Spectralon at one particular angular configuration, with a polar angle of incidence of 0° and a polar angle of reflection of 10° (0/10). The reflected radiance is polarization-averaged by measuring the reflected radiance twice with different polarizations and combining. The absolute BRDF of Spectralon at the angular configuration (0/10) becomes the instrument calibration factor. The 0/10 BRDF of Spectralon is obtained from separate measurements, done previously (described in Section 7.5), of both the angular distribution of the reflected radiance from the Spectralon and the directional hemispherical reflectance.

The spectroradiometric reading of the reflected radiance from the sample for each angular configuration is then divided by the spectroradiometric reading of the reflected radiance from the Spectralon at 0/10. When the ratio is multiplied by the absolute BRDF of Spectralon at 0/10 and a cosine factor, the result is the sample's BRDF:

$$f_r(\lambda,\theta_i,\phi_i,\theta_r,\phi_r) = \frac{\left(V_{r,sample}(\lambda,\theta_i,\phi_i,\theta_r,\phi_r) - V_{bg}\right)}{\left(V_{r,spectralon}(\lambda,0,0,10,0) - V_{bg}\right)\cdot\cos(\theta_i)} \cdot f_{r\ spectralon,absolute}$$

Equation 7.3.1

$V_{r,sample}(\lambda, \theta_i, \phi_i, \theta_r, \phi_r)$ is the spectroradiometric reading of the reflected radiance from the sample for each angular configuration. $V_{r,Spectralon}(\lambda, 0, 0, 10, 0)$ is the spectroradiometric reading of the reflected radiance from the Spectralon at 0/10. V_{bg} is the spectroradiometric reading of the background signal. $f_{r,Spectralon,absolute}$ is the absolute BRDF of Spectralon at 0/10.

The recommended method is a relative method because the final result is not related to the direct measurement of the light source. Instead of evaluating the ratio of the reflected radiance from the sample to the direct radiance from the light source, we evaluate the ratio of the reflected radiance from the sample to the reflected radiance from the Spectralon, both at a particular angular orientation (θ_i=0° and θ_r=10°). The method is faster than a two-scan relative method because we do not measure the reflected radiance from the Spectralon at each angular configuration but assume it to be a known, previously measured function.

However, we still take a direct light-source measurement before and after the sample BRDF measurements. We use this to verify the time stability of the light source. The original control program of the Gonioreflectometer is automated and allows the direct light-source measurements.

7.4 Procedure for the proposed relative reflectance method

The procedure for BRDF measurements is summarized as following:

a. Take the spectroradiometric reading of the background noise signal, save the data into bkg.dat;
b. Put the sample on the goniometer;
c. Set the polarizer in front of the detector to vertical direction, using the route file (*.123 file), take the spectroradiometric reading of the reflected radiance from the sample for each angular configuration, exposure time is 500, save the data into measv.dat;
d. Set the polarizer in front of the detector to horizontal direction, using the route file (*.123 file), take the spectroradiometric reading of the reflected radiance from the sample for each angular configuration, exposure time is 500, save the data into meash.dat;
e. Turn the Motor 3 to $\theta_3 = 10°$;
f. Turn the Motor 1 to $\theta_1 = 10°$;
g. Put the Spectralon on the goniometer;

h. Set the polarizer in front of the detector to vertical direction and take the spectroradiometric reading of the s polarization reflection signal, exposure time is 500, save the data into s0010v.dat;

i. Set the polarizer in front of the detector to horizontal direction and take the spectroradiometric reading of the p polarization reflection signal, exposure time is 500, save the data into s0010h.dat.

7.5 BRDF of Spectralon at 0/10; the determination of the instrument calibration constant

The new relative measurement method requires a separate determination of the absolute BRDF of Spectralon at θ_i=0° and θ_r=10° (0/10).

First, the directional BRDF of the Spectralon sample is measured in the incident plane at normal incidence with the absolute method. Results are presented in Figure 7.5.1 and Figure 7.5.2 at a wavelength of λ=550nm. It is obvious that the surface is not perfectly Lambertian, which would correspond to a constant value of the BRDF with reflection angle. From Figure 7.5.1, we find that the BRDF of the Spectralon sample at 0/10 is about 0.3091. However, a magnitude error exists due to the spectral bias of the direct light-source measurement. The measured BRDF magnitude is lower than the true value. Next, we use the OL-750 reflectometer to correct the magnitude of this value.

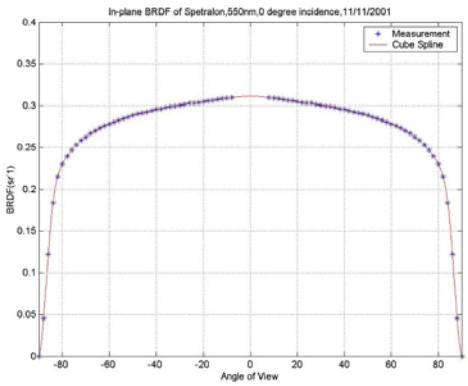

Figure 7.5.1 In-plane BRDF measurement of Spectralon vs. angle of reflection, cartesian coordinates; θ_i=0°, λ=550nm

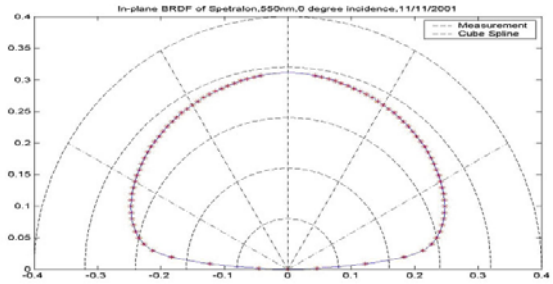

Figure 7.5.2 In-plane BRDF measurement of Spectralon vs. angle of reflection, polar coordinates; θ_i=0°, λ=550nm

Assuming that the Spectralon sample is isotropic (i.e., no azimuthal dependence), we can derive the BRDF over the hemisphere of reflection from the incident-plane measurements, as shown in Figure 7.5.3. The figure portrays a mapped hemisphere, to be described more fully later on, with the BRDF as the vertical axis.

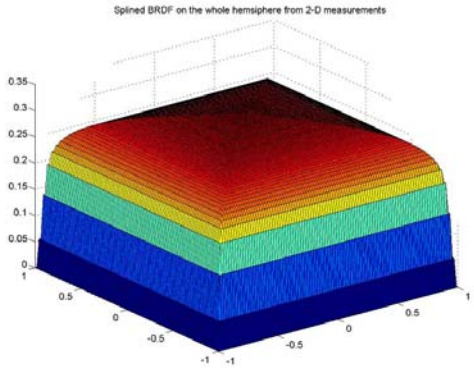

Figure 7.5.3 BRDF of Spectralon over the whole hemisphere, as derived from incidence-plane measurements; λ=550nm

The directional hemispherical reflectance is found by integrating the BRDF numerically over the reflection hemisphere. At the wavelength of 550nm, the calculated directional hemispherical reflectance is 0.8915. By OL-750 measurements, we determine that the directional hemispherical reflectance at 550nm wavelength is 0.95 to an accuracy of ±0.5%. Thus, we can get a magnitude correction factor at this wavelength, which is 0.95/0.8915=1.0656. Applying this magnitude correction factor to the BRDF of Spectralon at 0/10, we can determine that the BRDF value is closer to 0.3091×1.0656=0.3294, which we call the hemispherically-corrected BRDF.

For each wavelength, we use the sample algorithm below to obtain the hemispherically-corrected BRDF of the Spectralon sample at 0/10:

a. Measure the BRDF of the Spectralon sample in the plane of incidence for an incidence angle of 0°, using the absolute BRDF measurement method;
b. Note the BRDF of the Spectralon sample at 0/10, $fr_{Spectralon,0010}(\lambda)$ (with a scaling error);
c. Fit a cubic spline to the BRDF data in the place of incidence, assume isotropy, and thus obtain the BRDF of the Spectralon sample over the whole reflection hemisphere;
d. Obtain the directional hemispherical reflectance of the Spectralon $\rho_{dh}(\lambda)$, by numerical integration over the reflection hemisphere;
e. Obtain the directional hemispherical reflectance of the Spectralon $\rho_{dh750}(\lambda)$ by direct measurements with the OL-750 instrument;
f. Obtain the hemispherically-corrected BRDF of the Spectralon sample at 0/10 from

$$fr_{absolute,Spectralon,0010}(\lambda) = fr_{Spectralon,0010}(\lambda) * \rho_{dh750}(\lambda) / \rho_{dh}(\lambda) \qquad (7.5.1)$$

Finally, the hemispherically-corrected BRDF of the Spectralon sample at 0/10, over the visible wavelength region, is shown in Figure 7.5.4. The result shows that the BRDF is about 0.3295 over the visible wavelength region, with a one-point maximum variation of 0.5%. Believing that the BRDF of the Spectralon sample at 0/10 is nearly spectrum independent, we applied 0.33 for the entire visible wavelength region for simplicity, and denote this as $fr_{absolute,Spectralon,0010}$.

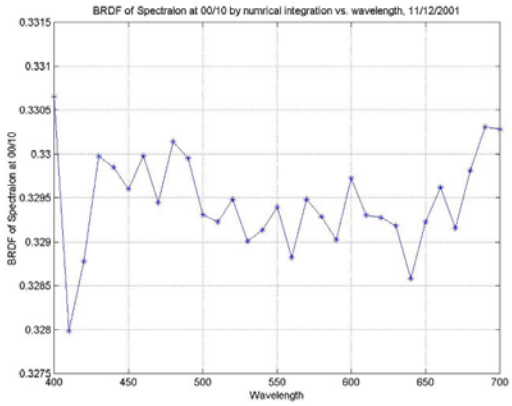

Figure 7.5.4 Hemispherically-corrected BRDF of Spectralon at 0/10 versus wavelength

BRDF measurements from NIST, for four materials (including Spectralon) at 633nm wavelength, are shown in Figure 7.5.5 [11]. For the Spectralon, Figure 7.5.5(a), the BRDF at normal incidence and a 10° reflection angle (0/10) has a magnitude of approximately 0.34, which is close to our hemispherically-corrected BRDF for Spectralon at 0/10. The variation with reflection angle is proportionally similar to our Figure 7.5.1.

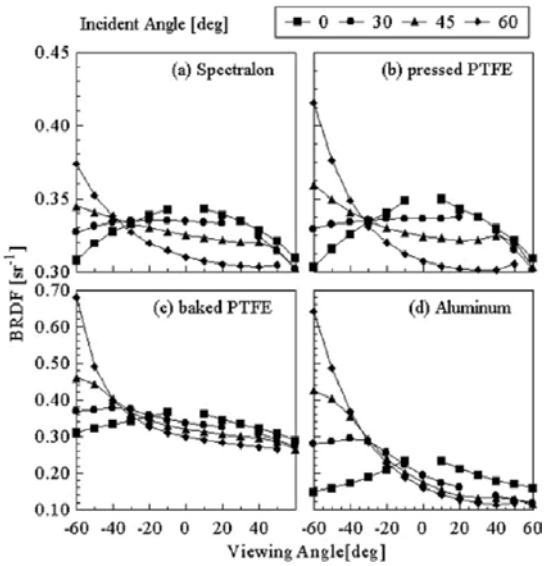

Figure 7.5.5 Comparison of BRDF measurements by NIST; 633nm wavelength [**11**]

7.6 Validation for general surfaces (many are highly diffusive)

To validate the recommended relative method, the BRDFs of six samples were measured.

The samples are listed in Table 7.6.1.

Table 7.6.1: Samples measured to validate the recommended relative method

Sample	Material	Color	Manufacturer	Roughness
Ford metallic paint	Clear with silver flakes	gray	DuPont	
Q-Panel R-46*	A reference steel panel used in the paint and manufacturing industries, slightly rough	silver	Q-Panel Lab	1.3μm
Krylon 7205 True Blue Paint	Latex enamel with Q-Panel substrate	blue	Krylon	
Paint (Bristol#4)	Latex	light gray	Bristol Univ.	
Ground glass	Flat plate glass, surface ground with 240 grid SiC, evaporated aluminum top coating	silver	Cornell PCG	0.63μm
Ground glass	Flat plate glass, surface ground with 120 grid SiC, evaporated aluminum top coating	silver	Cornell PCG	0.92μm

*: More information of Q-Panel is available at http://www.q-panel.com/html/panels.html.

For all samples, the spectral-directional BRDF was measured using the recommended relative measurement method. In addition, the measured BRDF was integrated numerically over the reflection hemisphere to get the directional-hemispherical reflectance; the latter was compared with separate hemispherical reflectance measurements from the OL-750 reflectometer in our laboratory.

7.6.1 Ford metallic paint:

The Ford metallic paint is a gray, somewhat specular, but diffusing sample. The BRDF measurements of Ford metallic paint over the mapped reflection hemisphere are presented in Figure 7.6.1.

The sampling positions were uniformly distributed over the reflection hemisphere. The points are plotted in a uniform parameterization of the hemisphere [8]. Each grid space in the graph represents a region on the hemisphere with the same solid angle. The creases along the diagonals of the square are a result of the parameterization and are not related to the plotted function. The vertical axis is the BRDF; the left and right orthogonal axes map the spherical coordinates above a surface. The plane of incidence corresponds to 0 on the left axis. Later figures use the same mapping representation.

The directional-hemispherical reflectance measurements, obtained from the Gonioreflectometer and the OL-750 reflectometer, are shown in Figure 7.6.2. The Gonioreflectometer values were obtained by numerically integrating the measured

directional BRDFs. The numerically-integrated Gonio values are shown before and after applying the hemispherical correction factor for the spectral bias of the light source.

The hemispherically-corrected, directional-hemispherical reflectance obtained from the Gonioreflectometer data is close to that measured by the OL-750 instrument with a light trap. The light trap absorbs the specular reflection from the sample. The error is within 1%. The measurements imply that the Gonioreflectometer did not accurately measure and capture the specular, mirror-like reflection from the surface. This is a reasonable conjecture because the sample is very glossy. The specular reflection is within such a narrow solid angle that the Gonioreflectometer is unable to put the detector at the exact position to receive the specular reflection, due to the angular positioning error of the mechanism. The maximum BRDF in Figure 7.6.1 is less than 0.8, which is inconsistent with the glossy surface.

As the Gonioreflectometer missed the specular reflection, the reflection around the specular direction was scanned in finer detail to find the maximum BRDF and the lateral shape of the specular lobe. The contour of the specular reflection peak is shown as Figure 7.6.3. The specular reflection is off-center due to the angular errors of the positioning mechanism, and the peak is narrow compared to the sampling frequency on the larger hemispherical grid. The maximum of the BRDF at the specular direction is about 90, which is consistent with a glossy surface. The value of 90, when multiplied by the half-solid angle of the specular lobe ($\pi \times \sin^2(1.4)/2=0.00094$), yields a value of 0.085

(8.5 albedo units). This is approximately the difference between the two upper curves in Figure 7.6.2, thus confirming that the specular peak was missed.

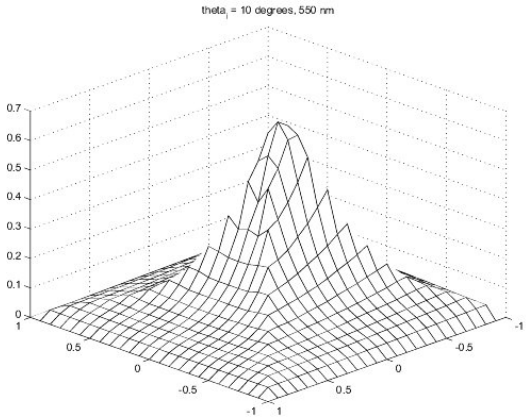

Figure 7.6.1 BRDF of Ford metallic paint over the mapped reflection hemisphere for θ_i=10 and λ=550nm

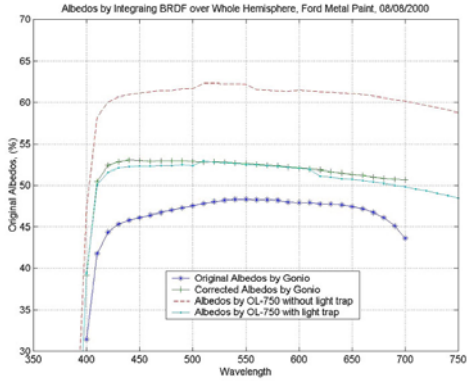

Figure 7.6.2 Comparison of directional-hemispherical reflectance of Ford metallic paint, as measured by two instruments; θi=10 and 0.28mm slit

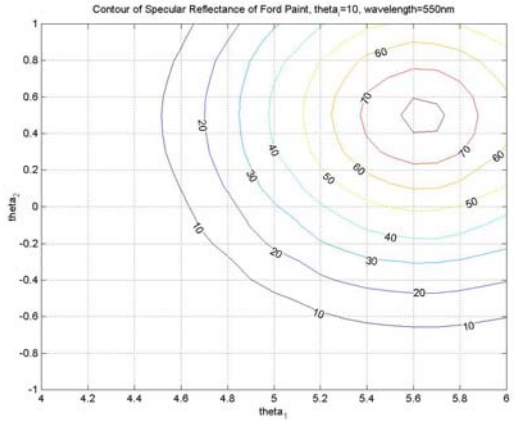

Figure 7.6.3 Contour of the specular reflection of Ford metallic paint; θ_i=10 and λ=550nm

7.6.2 Q-panel (steel):

Similarly, for the Q-Panel sample, we measured the BRDF over the hemisphere and the specular (mirror) reflectance. The directional-hemispherical reflectance was obtained by numerical integration of the BRDF. For this sample we used sufficient spatial sampling of the BRDF to catch the specular lobe and include it in the hemispherical integration. The Q-panel is a piece of "uniformly roughened steel panel," which is half-specular-half-diffuse.

Figure 7.6.4 shows the BRDF over the mapped reflection hemisphere. The Q-panel appears more diffuse to the human eye than the Ford metallic paint. However, the maximum value of the measured BRDF in Figure 7.6.4 is higher than the corresponding maximum for the Ford metallic paint in Figure 7.6.1. The true maxima are not shown in these figures.

Figure 7.6.6 shows a contour of the specular reflection peak for the Q-panel. The specular peak of the Q-panel is much broader than for the metallic paint in Figure 7.6.3. Further, the maximum BRDF is about 6, as compared to about 90 for the metallic paint. The lower, broader peak is consistent with the more diffuse visual appearance of the Q-Panel.

The directional-hemispherical reflectance in Figure 7.6.5 obtained from the Gonio is between those obtained with the OL-750 reflectometer, with and without the light trap. The measurements imply that the Gonio was able to "catch the peak," because the peak is broader. However, it is unable to determine the exact position of the maximum specular

reflection. The maximum of the BRDF at the specular direction (about 6), when multiplied by the half-solid angle of the specular lobe ($\pi \times \sin^2(2.7)/2=0.0035$), yields a value of 0.021 (2.1 albedo units). If we add this value to the upper Gonio curve in Figure 7.6.5, the curve shifts upward 2.1 albedo units, yielding a close match to the upper OL-750 measurements (without a light trap).

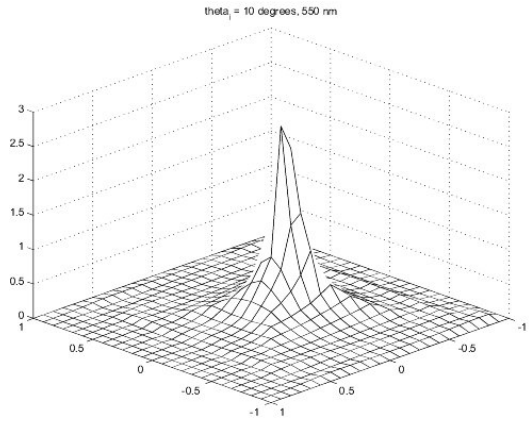

Figure 7.6.4 BRDF of Q-panel over the mapped reflection hemisphere for θ_i=10 and λ=550nm

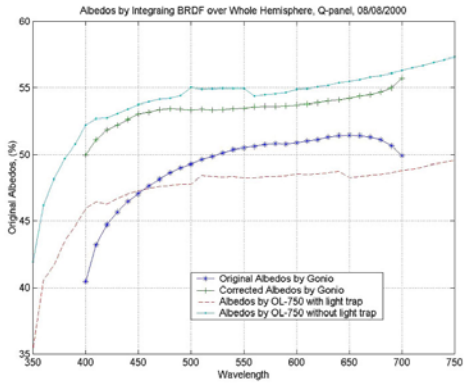

Figure 7.6.5 Comparison of directional-hemispherical reflectance of Q panel, as measured by two instruments; θ_i=10 and 0.28mm

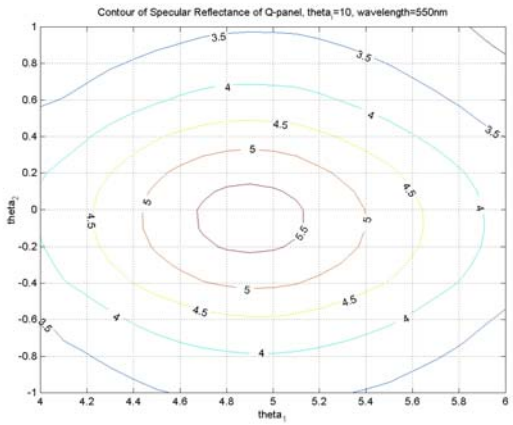

Figure 7.6.6 Contour of the specular reflection of Q-panel; θ_i=10 and λ=550nm

7.6.3 Krylon blue paint:

The sample is a Q-panel painted with Krylon blue paint. The paint is dark blue and diffusive. The hemispherically-mapped BRDF appears in Figure 7.6.7. Note that the BRDF values away from the specular bump have a value of about 0.01.

Figure 7.6.8 shows that there is only a very small difference between the directional-hemispherical reflectance measured by the OL-750 instrument with and without the light trap. This implies that the energy content of the specular peak in Figure 7.6.7 is minimal. However, in Figure 7.6.8, the spectrum correction applied to the measured Gonio data does not appear to significantly improve the accuracy of the directional-hemispherical reflectance. Note that the reflectance values are sometimes very low as compared to the Spectralon reflectance material (95%).

One possible source of the error may be the non-linear response of the Gonio detector at low signal levels. Figure 7.6.8 shows that the directional-hemispherical reflectance measured by the OL-750 instrument is about 6% over the wavelength range from 550nm

to 750nm. At such low signal levels, the signal readings of the Gonio detector for BRDF measurements at most of the sampling positions are as low as approximately 10 counts. In Section 3.3, we showed that the non-linear response of the Gonio detector can be observed at such low signal levels. Another possible source of error might be the apparent difference in the directional reflection characteristics of the reference sample (Spectralon) and the Krylon blue paint.

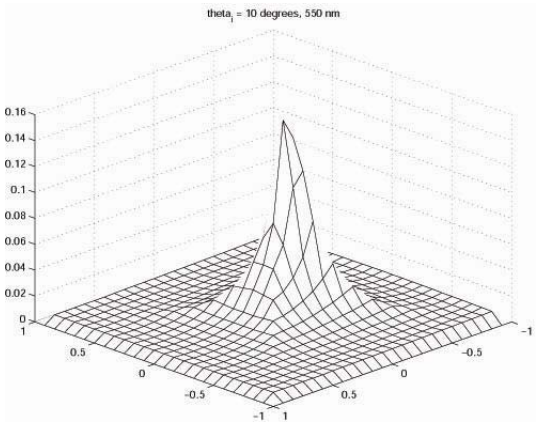

Figure 7.6.7 BRDF of Krylon blue paint over the mapped reflection hemisphere for θ_i=10 and λ=550nm

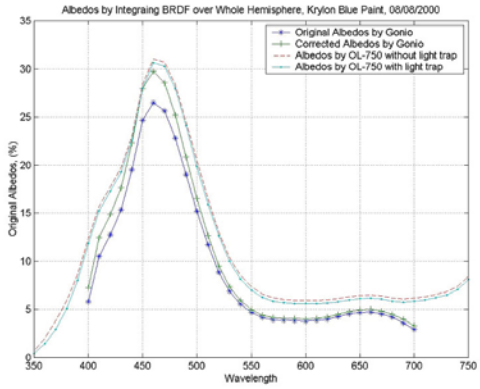

Figure 7.6.8 Comparison of directional-hemispherical reflectance of Krylon blue paint, as measured by two instruments; θ_i=10 and 0.28mm

7.6.4 Bristol Sample#4 (Light Gray):

The sample is a wood panel with light gray latex paint. The sample was sent to us by Ann McNamara, a doctoral student researcher at the University of Bristol, UK. She sent several samples, which were measured by us, and the results were used in her research.

The Bristol paint is very diffuse and the surface is rough. Apparently, the light reflection is quite diffuse, as shown in Figure 7.6.9. The light gray color implies a neutral reflectance spectrum.

The directional-hemispherical reflectance derived from the BRDF measurements is close to that measured by the OL-750 instrument. The error is very small, as shown in Figure 7.6.10. The spectral correction factor appears to accurately compensate for the spectral bias in the light source irradiance measurements.

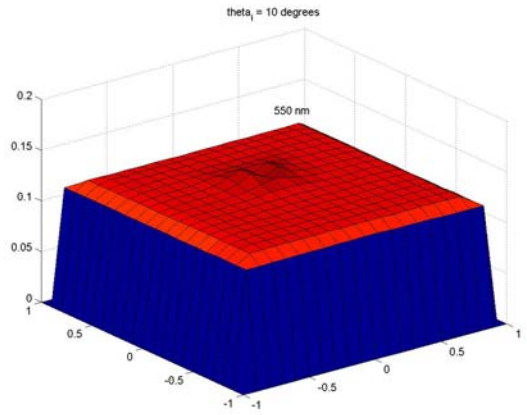

Figure 7.6.9 BRDF of Bristol Sample#4 over the mapped reflection hemisphere for θ_i=10 and λ=550nm

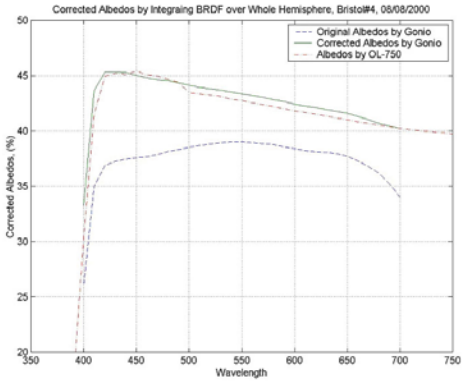

Figure 7.6.10 Comparison of directional-hemispherical reflectance of Bristol Sample#4, as measured by two instruments; θ_i=10 and 0.28mm slit

7.6.5 Ground plate glass (240 grit) with aluminum coating

The sample is a piece of ground plate glass with an evaporated-aluminum coating. The plate glass was ground by the lead author using 240 grit SiC powder. The evaporated-aluminum coating is glossy but the substrate surface is rough. The light reflection is directional-diffuse, as shown in Figure 7.6.11. The surface is not an ideal diffuse reflector, which would correspond to a constant value of the BRDF over the reflection hemisphere (the Bristol sample shown in Figure 7.6.9 is nearly ideal diffuse). A pure aluminum coating has a nearly neutral reflectance spectrum.

The directional-hemispherical reflectance derived from the BRDF measurements, and shown in Figure 7.6.12, is close to that measured by the OL-750 instrument. The error is very small.

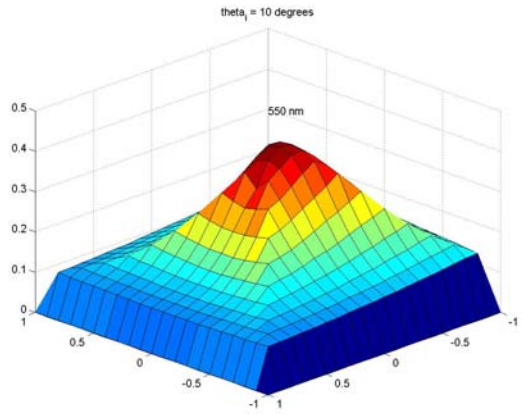

Figure 7.6.11 BRDF of ground glass (240grit) with evaporated-aluminum coating over the mapped reflection hemisphere for θ_i=10 and λ=550nm

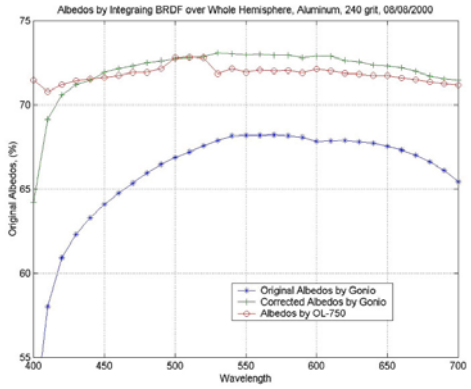

Figure 7.6.12 Comparison of directional-hemispherical reflectance of evaporated-aluminum coated ground glass (240grit), as measured by two instruments; θ_i=10 and 0.28mm slit

7.6.6 Ground plate glass (120 grit) with aluminum coating

The sample is a piece of ground plate glass with an evaporated-aluminum coating. The plate glass was ground by the lead author using 120 grit SiC powder. The evaporated-aluminum coating is glossy but the surface is even rougher than the one ground by 240 grit SiC powder. The light reflection is also directional-diffuse. The directional-hemispherical reflectance derived from the BRDF measurements, and shown in Figure 7.6.14, is close to that measured by the OL-750 reflectometer. The error is again very small.

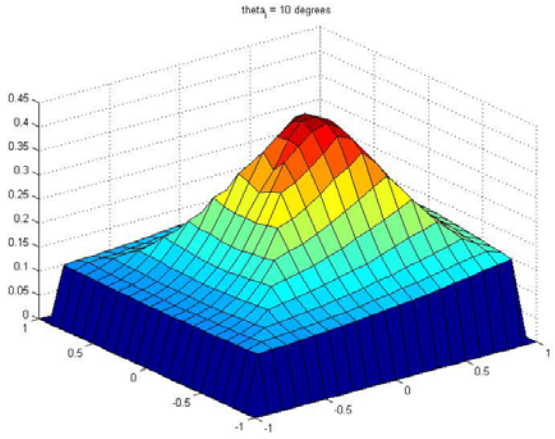

Figure 7.6.13 BRDF of ground glass (120grit) with evaporated-aluminum coating over the mapped reflection hemisphere for θ_i=10 and λ=550nm

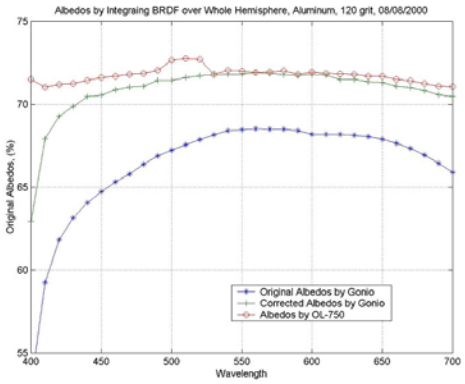

Figure 7.6.14 Comparison of directional-hemispherical reflectance of evaporated-aluminum coated ground glass (120grit), as measured by two instruments; θ_i=10 and 0.28mm slit

7.7 Conclusion

A relative BRDF measurement method is developed, discussed, and recommended. We applied the relative measurement method on a somewhat specular, but diffusing, sample (Ford metallic paint); a less-specular, diffusing sample (Q-panel); and five diffuse-like samples (Spectralon, Krylon paint, Bristol gray paint, two ground glass surfaces with aluminum coatings).

We examined both the directional BRDF and the integrated BRDF. The latter was compared with hemispherical measurements by an OL-750 reflectometer. The best agreement between the integrated BRDFs and the OL-750 measurements occurs for diffuse samples with a high hemispherical reflectance: Spectralon, Bristol light gray paint, two aluminum ground glass surfaces. We could reduce the error to 1% in these cases. There was a larger error for the dark blue Krylon paint.

For more strongly-specular samples, we have to scan the specular direction to find the maximum BRDF and the lateral shape of the specular lobe. By combining the diffuse

and specular region measurements, we could obtain the whole BRDF with good accuracy. This was demonstrated for the samples with some specular reflection on top of diffuse-like scattering: Ford metallic paint and the Q-panel. For pure mirror surfaces with negligible diffuse scattering, we recommend the absolute specular measurement method of Chapter 6.

The present study aims to achieve accurate and efficient BRDF measurements with our Gonioreflectometer. We achieve this goal by carefully re-tuning the instrument, improving the measurement procedures, and proposing a new relative measurement method. With the recommended relative method, the BRDF measurements can cover the entire visible wavelength region with better wavelength accuracy. The resulting BRDF values are believed to be accurate and adequate for computer graphics applications.

Appendix

Alignment Procedure for the Gonioreflectometer

By Stephen Westin

The Gonioreflectometer needs to be aligned very carefully, before any measurement is conducted. The following is a tentative procedure of aligning the instrument.

A. Laser setup

A cylindrical red HeNe laser with a $1/e^2$ beam diameter of 0.6mm is used to provide the reference beam needed in alignment. Most alignments in this alignment procedure require the laser, and need it aligned very carefully. The goal is to have the beam exactly parallel to the optical table, at the height of the center of rotation axis of Motor 2 (which is the height of the center of the whole optical system.), and to align it with some reference, often a row of holes in the table.

Alignment tools

We use a few simple tools to measure alignment of the beam. First, we use a post with a horizontal wire (actually a straightened paperclip) attached to the top (see Figure A.1). Since we can't guarantee that the wire is exactly horizontal, be careful to use only the tip for height measurement. The post is installed on a height-adjustable base, to adjust the height of the wire tip easily.

Next we have two cross-hair reticules, shown in Figure A.2. These are made from simple lens mounts that can be attached to a normal 1/2'' post. One is etched on a piece of Mylar overhead transparency film, the other is an actual human hair carefully taped in place.

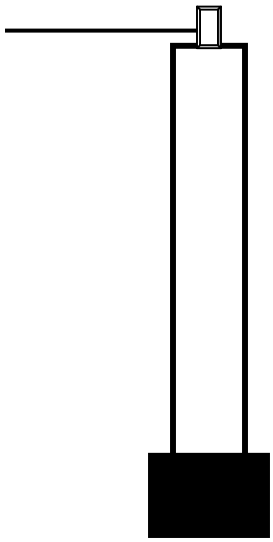

Figure A.1: Horizontal reference

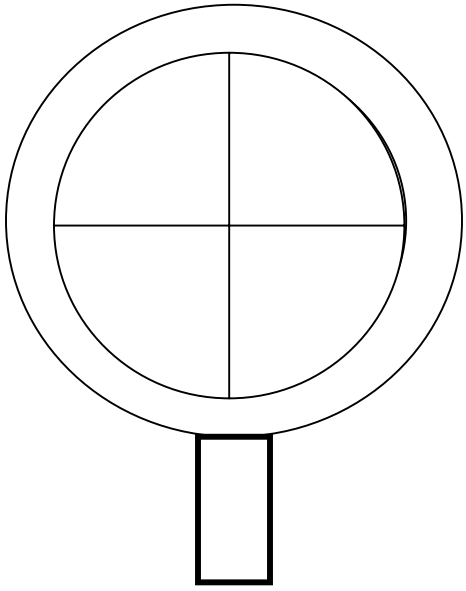

Figure A.2: Cross-hair reticule

Leveling and height

To get the beam level and at the proper height, the laser is setup on a magnetic base with posts including one of our height-adjustment post holders. The laser was put on the table in the region shown in Figure A.3, and was aimed to the beam into the machined cavity, as shown in Figure A.4.

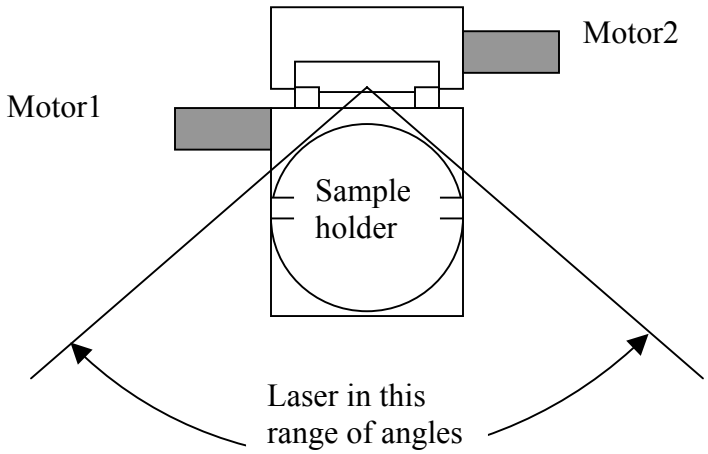

Figure A.3: Laser position for height and level adjustments

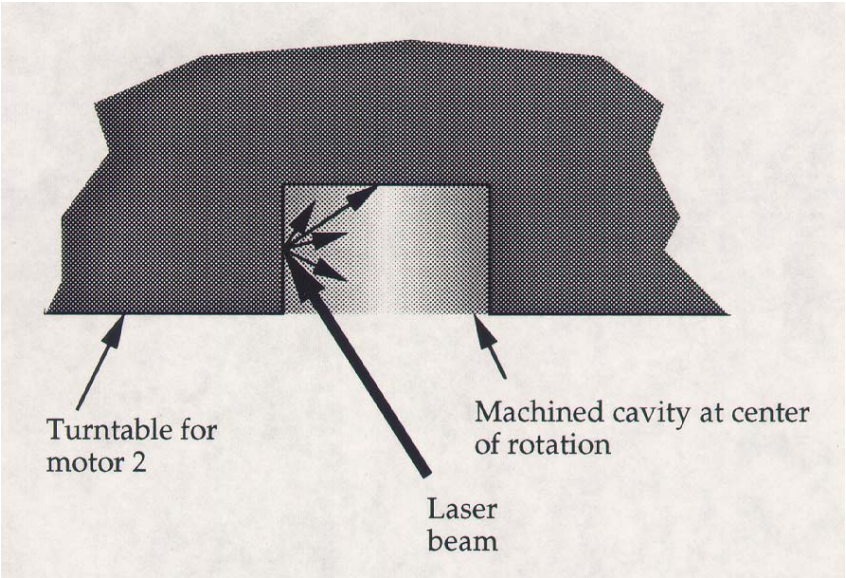

Figure A.4: Aiming the beam into the machined cavity (top view, cut away)

Procedures:

a. Aim laser at the machined center of the table of Motor 2;

b. Adjust the height of the laser to make the beam hit at the exact vertical center. This is visible by the reflection pattern; a good pattern is shown in Figure A.5;

c. Put the wire pointer as close as possible to the machined cavity, and adjust it carefully to intercept the beam at its center;

d. Move the wire pointer very near the front of the laser, and adjust the laser's height so that the beam is intercepted at dead center. This puts the nose of the laser approximately at the level of the machined cavity.

e. Move the wire pointer out of the way and adjust the laser's angle to correct the angle of the beam to strike the vertical center of the machined cavity. This is done by loosening and tightening the three screws at the back of the laser mount. There are two sets of screws: one at the front of the laser, the other at the back. A set of screws is shown in Figure A.6. To raise the back of the laser (i.e. to steer the beam downward), loosen the top screw and tighten the two lower screws. To lower the back of the laser, loosen the two bottom screws and tighten the top screw.

f. Go back and do it again: adjusting the wire pointer, raising or lowering the laser, and adjusting the vertical angles of the laser. Do this until the beam is level and at the correct height. This means that the pointer intersects the beam at dead center, both near the laser's front and near the center of Motor 2, and that it intersects the center (vertically) of Motor 2.

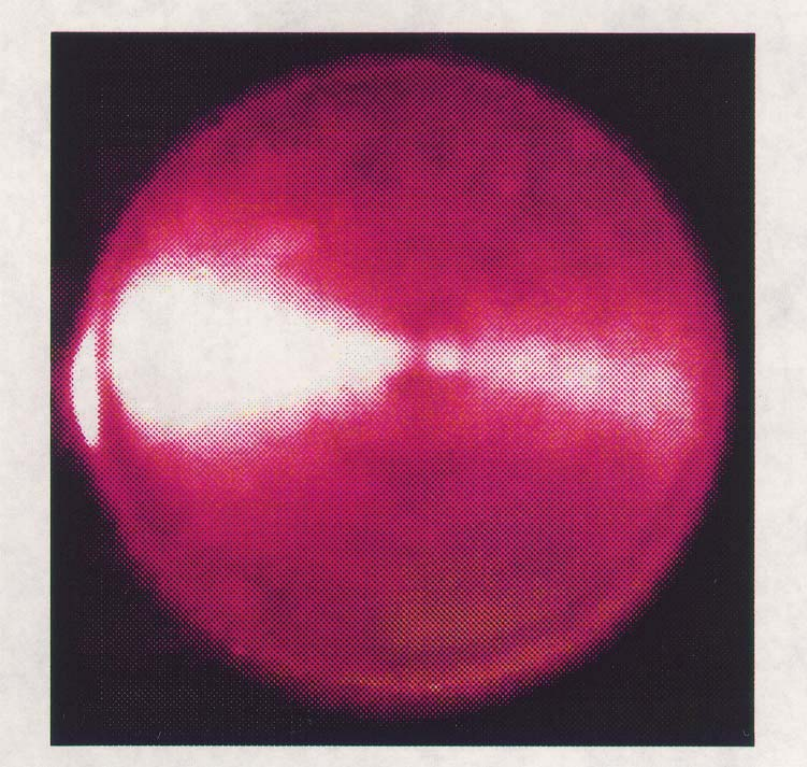

Figure A.5: Reflection of beam at correct height

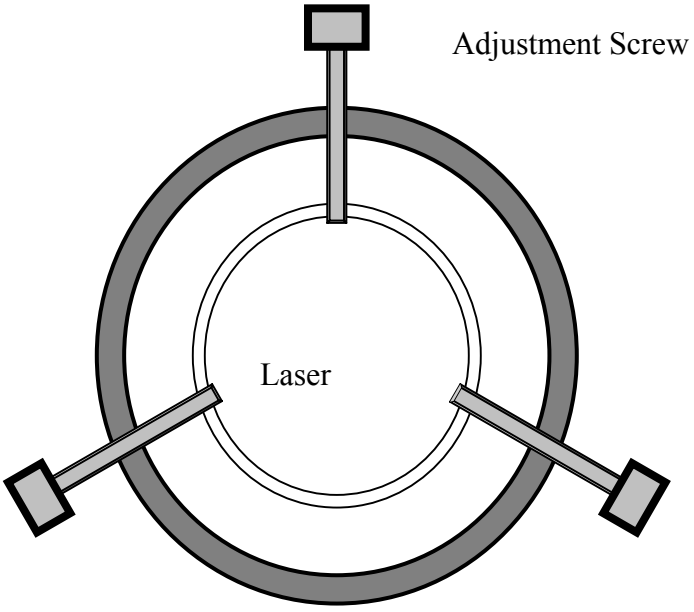

Figure A.6: Laser adjustment screws

B. Detector optics alignment

To begin, I move the source arm out of the way (say, to 150 degree) and move the laser carefully to look into the source optics. The laser should point directly down one row of holes: That intersects the center of rotation of Motor 3. It still must be level and at the correct height. The setup is shown in Figure B.1.

Horizontal alignment of laser beam

To align the laser horizontally, first set up the two cross-hair reticules in post holders screws into the table along the correct line of holes. To screw these in, don't tighten the screw in the bottom of the post holder, and then screw the assembly into the table. As shown in Figure B.2, the screw should be a bit loose with respect to the post holder, then the post holder must be tightened down the last millimeter or so. This makes sure that the post holder is seated well, rather than trusting to the screw for angular alignment. Be careful to align the reticules perpendicular to the beam, as rotating them translates the cross-hair reticule slightly.

Next, move the laser so that the first cross-hair intersects the beam. Diffraction pattern like that shown in Figure B.3 should be apparent. Move the laser and rotate it about its vertical axis so that the beam is centered on both the near and far cross-hairs. You should be able to see the diffraction pattern from the near cross-hairs, move the cross-hair out of the way, and see a second diffraction pattern from the far cross-hair.

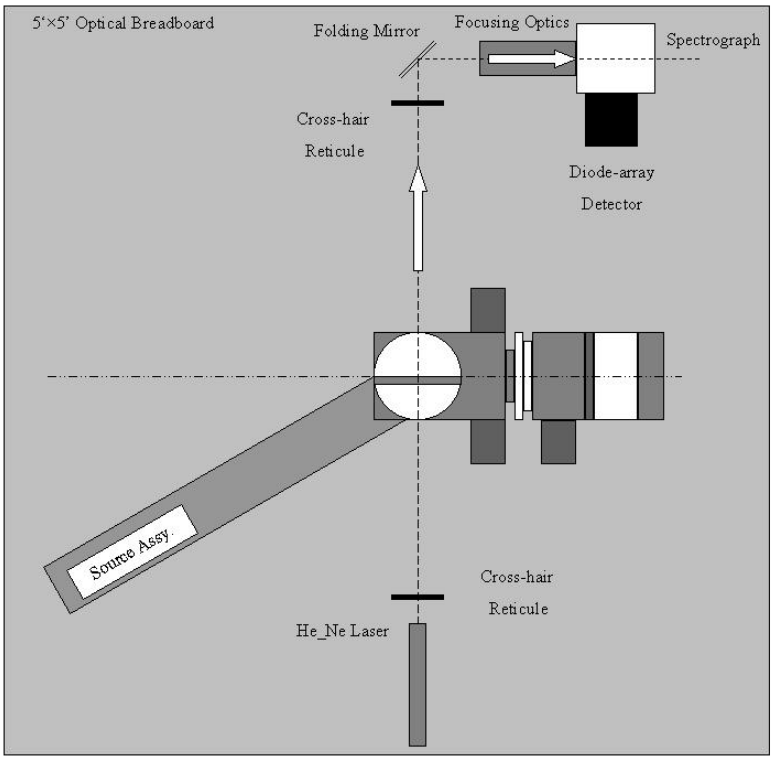

Figure B.1: Bird view of the setup of detector optics alignment

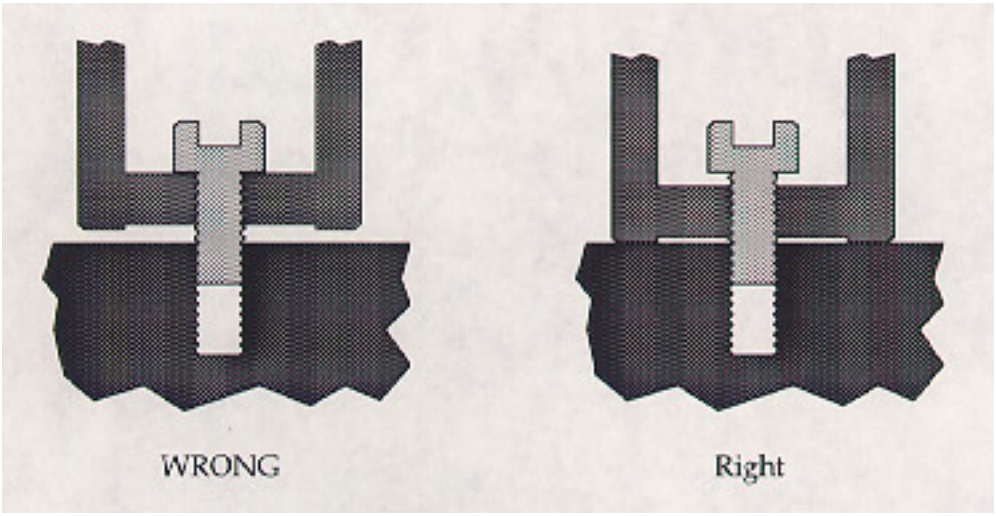

Figure B.2: Attaching post holder to table

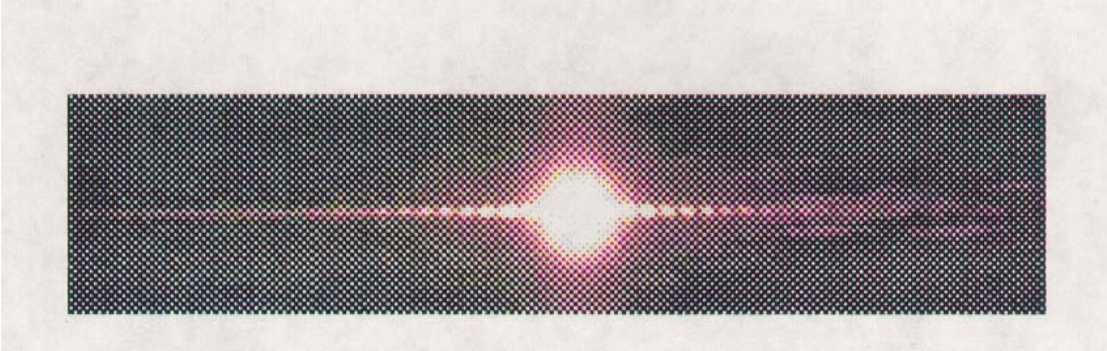

Figure B.3: Diffraction pattern from cross-hair

Folding mirror alignment

Next, we need to align the folding mirror so that the laser hits the center of the mirror and is deflected exactly 90° to pass down the exact center of the detector rail. The folding mirror is mounted to a double-sliding base plate to allow this. To move the post along one axis, loosen the hex screws holding the plate to the screw holding it to the plate.

Procedures:

a. Adjust the mirror so that it is about 45° from the laser beam and the beam hits its center. Remove all lenses, polarizer, etc. From the detector rail so there's nothing to deflect the beam.
b. The beam should be leveled. Use the wire pointer along the detector rail. Put it close to the detector slit and adjust the screw on the mirror mount so that the pointer intersects the beam in its exact middle.
c. Align the beam for angle and position so that it passes down the exact center of the detector rail. You can mount one of the cross-hair reticules to a baseplate that fits exactly in the detector rail; this will serve as a reference for the center of the beam. The beam, must be centered along its whole length; this will require a combination of

translating and rotating the mirror. Slide the reticules along the rail to check the beam at both ends.

The wire pointer is almost exactly half the width of the detector rail, so it may be used as an alternate reference to center the beam on the rail. First align the pointer at one side of the rail, being careful to seat the magnetic base against the side of the rail. Note where the pointer intersects the beam, and then move the pointer to the other side of the rail. If the beam does not intersect at the same point along the wire pointer, either slide the mirror post or adjust the angle of the mirror to make it do so.

Detector positioning and alignment

Once the beam is level and passes down the center of the detector rail, it can serve as the reference to align the rest of the detector optics. The detector should be aligned so that the beam enters the slit perpendicular to its face, and in the center of the slit.

- Angular alignment of detector

To align the detector, I hold a front-surface mirror against the mounting flange around the slit. This should reflect the beam back onto the exit port of the laser, showing a somewhat fuzzy spot on the front surface of the laser housing. If the spot is off laterally, loosen the clamp screws on the mount and rotate the entire detector slightly. If the spot is off vertically, loosen the mounting bolts and insert shims to align the detector. This is actually not a critical adjustment: the detector should be forgiving of a slight angular misalignment.

- Positional alignment of detector

The detector is easily adjusted in two axes: vertical and lateral. The lateral adjustment is through the micrometer just above the rail, and the vertical adjustment is a knob on the bottom of the fat vertical post supporting the detector. Use the software "Instasp2" to monitor the output of the detector in real time. Mount the smallest slit (50μm), and adjust the detector in each axis to maximize the signal. You will probably have to use a neutral-density filter, such as ND2 or ND3, in the beam to reduce intensity to avoid saturating the detector.

Alignment

After you are sure that the detector itself is properly aligned, mount the lens. Note that the direction matters: the lens is asymmetric and correction is only valid in one direction. In other words, the lens is fuzzy if you put it in backward.

Wavelength calibration of detector

The angle of the grating in the detector can be adjusted with the micrometer on the front of the detector itself. Use the laser with a neutral density filter, fire up Instasp2, and adjust the grating to center the spectrum on pixel 772 of the detector. Use the locking ring on the micrometer to keep the alignment from drifting or being bumped accidentally.

C. Source optics alignment

The source optics includes a PAR16 tungsten-halogen lamp (type ELH or FXL), an opal glass diffuser (to depolarize the light), a condenser lens, a variable aperture, and a Nikon camera lens.

Laser setup

With the source arm swung out of the way (say to 90), set up the laser between the folding mirror and the sample holder, pointing through the sample holder, as shown in Figure C.1. Just as in setting up the laser to align the detector optics, use two crosshairs to align the laser laterally to match a row of holes on the table. Level the laser as before.

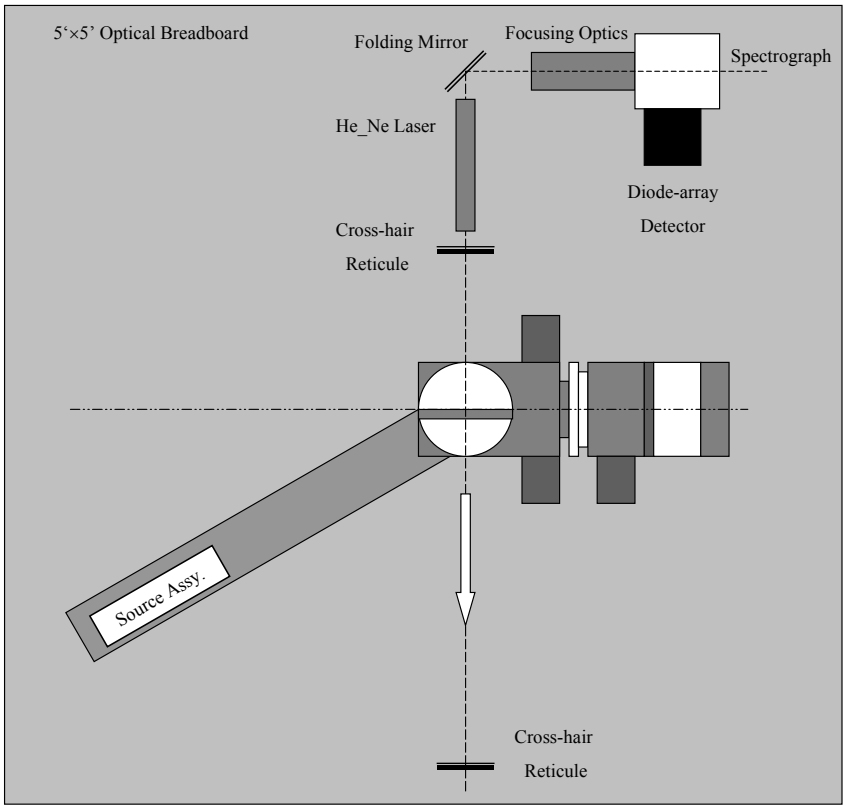

Figure C.1: Setup of laser alignment for light source alignment

Variable aperture

Next, we take the cross-hair reticules off and rotate the source arm to 180°. To align the optics of light source, the cardboard-made shade and Nikon lens should be taken off. The variable aperture has the least opportunity for adjustment, so it will serve as the reference to which the entire source assembly is aligned. Close the iris so the beam is visible around its edge, and then use Motor 3 to center the beam laterally. Loosen the screw and adjust the iris's height so the beam passes through its center. The beam should be visible as an even, bright fringe around the iris.

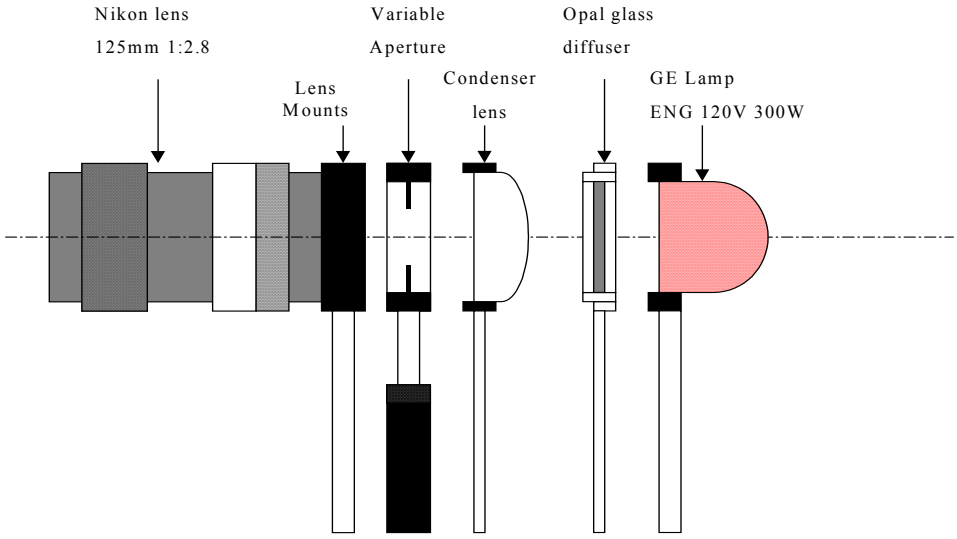

Figure C.2: The optics of the Gonio light source

Opal glass diffuser

a. Open the iris so that it doesn't block off the laser beam.

b. The condenser lens should be taken off.

c. The position of opal glass diffuser is adjusted so that the beam hits it in the center. This should not be a very critical adjustment. Then the diffuser and its post are adjusted so that its reflection hits the center of the front of the laser.

Condenser lens

a. The condenser lens is put back on the post;
b. A black card board is put between the condenser lens and Opal glass diffuser, to block off the laser reflection form the diffuser;
c. Looking at the font of laser and the half-open aperture, we should see two reflection patterns. One is from the flat side of the lens, which looks like a bright spot. The other is from the curved side of the lens, which looks like a larger and dimmer spot. Adjust the position of the lens in all the dimensions to make these two reflection patterns centered at the same point, the laser exit port. This is not easy, because we can only adjust the height easily.

Camera lens

The alignment of Nikon lens is actually to align the lens mount. The distance between the variable aperture and the Nikon lens is very important. The focus of the lens at this side should overlap the aperture center. A green tape was used to mark the correct position of the lens. So do not remove the tape.

(1) The Nikon camera lens is mounted on the lens mount, The lens aperture is set to full aperture and the focus is set to infinity;

(2). A black card board is put between the condenser lens and variable aperture, to block off the laser reflection form the condenser lens;

(3). Looking to the front of the laser, we should be able to see a complex interference pattern, which come from the internally well-aligned lens inside the Nikon lens. Then we should adjust the position of the lens mount to make it satisfy the following requirements: (a) The beam going through the lens should go through the variable aperture center as before; (b) All the reflected pattern must be centered to the laser exit port. This is a very challenging task, because we can only adjust the height of the lens mount easily.

After we align the detector and the light source, usually we have to conduct the following calibration and check-up.

(a). Use ‘Gonio’ program to align the motors;

(b). Check-up the reciprocity;

(c). Use ‘Gonio’ program to get the new calibration parameter, record it on the instrument log.

References:

1. S. C. Foo, "A gonioreflectometer for measuring the bidirectional reflectance of material for use in illumination computation," M.S. thesis, Cornell University, Ithaca, New York, 130p., July 1997.
2. A. W. Springsteen, J. Leland, and T. M. Ricker, "A guide to reflectance materials and coatings," Labsphere Corporation, North Sutton, New Hampshire, 1990.
3. X. Feng, J. R. Schott, and T. Gallagher, "Comparison of methods for generation of absolute reflectance-factor values for bi-directional reflectance-distribution function studies," Appl. Opt., **32**, pp.1234-1242, March 1993.
4. H. Li and S. H. Westin, "Measurement report of paint samples of Bristol University," unnumbered report, Program of Computer Graphics, Cornell University, Ithaca, New York, 52p., 1999.
5. Optical density measurement data, provided with Neutral Density Filter Set 03FSQ015, Melles Griot Company, Irvine, California, 1995.
6. S. F. Chen, W. C. Li, K. E. Torrance, and S. N. Pattanaik, "Preliminary calibration of the Photometrics PXL1300L CCD camera," Technical Report PCG-96-1, Program of Computer Graphics, Cornell University, Ithaca, New York, 102p., 1996.
7. E. D. Palik, *Handbook of optical constants of solids* (Academic Press, London, 3440p., 1998).
8. ASTM Standard E 1392-96, "Standard practice for angle resolved optical scatter measurements on specular or diffuse Surfaces," American Society for Testing and Materials, West Conshohocken, PA, 11p., 1996.

9. P. Shirley and K. Chiu, “Notes on adaptive quadrature on the hemisphere,” Technical Report 441, Department of Computer Science, Indiana University, Bloomington, Indiana, 1994.
10. J. C. Zwinkels, M. Noel, and C. X. Dodd, “Procedures and standards for accurate spectrophotometric measurements of specular reflectance,” Appl. Opt., **33**, pp. 7933-7944, December 1993.
11. T. Early, “Reflectance Comparison,” Physics Laboratory, National Institute of Standard and Technology, Gaithersburg, Maryland, 1999, http://physics.nist.gov/Divisions/Div844/facilities/ref/rc.html.